SEMMELWEIS EGYETEM

DOKTORI ISKOLA

Ph.D. értekezések

2411.

DEÁK GÁBOR GYÖRGY

Szemészet

című program

Programvezető: Dr. Süveges Ildikó, professor emerita

Témavezető: Dr. Resch Miklós, egyetemi docens

In vivo examination of laser induced retinal changes in patients with diabetic retinopathy

PhD thesis

Gábor György Deák MD

Clinical Medicine Doctoral School

Semmelweis University

Supervisor: Miklós Resch, MD, PhD

Official reviewers: Eszter Vizvári, MD, PhD
Anna Bakos-Kiss, MD, PhD

Head of the Complex Examination Committee: Judit Fidy, MD, DSc
Members of the Complex Examination Committee: Katalin Gombos, MD, PhD
Antal Szabó, MD, PhD

Budapest

2020

1 Table of contents

2 List of abbreviations

BCVA	Best corrected visual acuity
BM	Bruch's membrane
CCD	Charge-coupled device
CFP	Color fundus photography
CRT	Central retinal thickness
CRVO	Central retinal vein occlusion
CSME	Clinically significant macular edema
DM	Diabetes mellitus
DME	Diabetic macular edema
DR	Diabetic retinopathy
DRCR.net	Diabetic Retinopathy Clinical Research Network
DRS	Diabetic retinopathy study
ELM	External limiting membrane
ETDRS	Early treatment diabetic retinopathy study
FA	Fluorescein angiography
FAF	Fundus autofluorescence
GCL	Ganglion cell layer
GLD	Greatest linear diameter
ILM	Internal limiting membrane
INL	Inner nuclear layer
IPL	Inner plexiform layer
IR	Infrared
IRMA	Intraretinal microvascular abnormalities
IS/OS	Inner segment / outer segment *
LogMAR	Logarithm of the minimal angle of resolution
Nd:YAG	Neodymium-doped yttrium aluminum garnet
NPDR	Non-proliferative diabetic retinopathy
OCT	Optical coherence tomography
OCTA	Optical coherence tomography angiography
ONL	Outer nuclear layer

OPL	Outer plexiform layer
PASCAL	Pattern scanning automated laser
PDR	Proliferative diabetic retinopathy
PRL	Photoreceptor layer*
PRP	Panretinal photocoagulation
RCT	Randomized clinical trial
RF	Red free
RNFL	Retinal nerve fiber layer
ROI	Region of interest
RPE	Retinal pigment epithelium
SD	Standard deviation
SD-OCT	Spectral-domain optical coherence tomography
SS-OCT	Swept-source optical coherence tomography
SLD	Super luminescent diode
TRP	Thickest retinal position
VA	Visual acuity
VEGF	Vascular endothelial growth factor
*	IS/OS and PRL can both be used to describe the same layer in OCT

3 Introduction

3.1 Laser therapy

3.1.1 The physics of laser

The word laser is an acronym for Light Amplification by Stimulated Emission of Radiation.[1] The first publications mentioning an amplification chamber resulting with the emission of electromagnetic waves (microwaves) were published in the late 1940s simultaneously by two groups, Townes and Schawlow in the USA, and Prokhorov and Basov in the Soviet Union.[2–4] Later the American group of physicists continued their experiments with amplification cavities to produce infrared and visible light. The diligent work of both groups has paid off as they were jointly awarded with the Physics Nobel Prize in 1964 and in 1981. The first description of a ruby solid state red light emitting laser was made by Maiman in his 1960 publication in Nature.[5] The development of different laser "masters" has picked up pace in the following decades, and many of these laser types are still in use, such as gallium-arsenide phosphide laser diode in 1962 which is used in LEDs, CD and DVD players.[6] Carbon dioxide laser and the neodymium-doped yttrium aluminum garnet (Nd:YAG) laser were both published in 1964 and are both used in medicine for surgery and the later used in ophthalmology and dermatology for multiple indications.

The theoretical principals of lasers were described by Einstein in 1917, based on the quantum theory of Bohr and the hypothesis of de Broglie that light has a dual nature of wave and particle.[7] In Bohr's theory every material has a ground state energy. If this material is influenced by an external energy i.e. light, material can absorb energy and its molecules enter in an excited state. Usually after a short period of time these molecules return in to their ground state, and during this they emit a photon with the same energy as the energy difference between the molecules excited and ground states. This process is called a spontaneous emission (b). In Einstein's hypothesis if a molecule in an excited state is irradiated by a photon it can force a transition to ground state, and the resulting excited photon will have the same energy, the same direction and the same phase as the irradiating photon. This was called a stimulated emission (c).

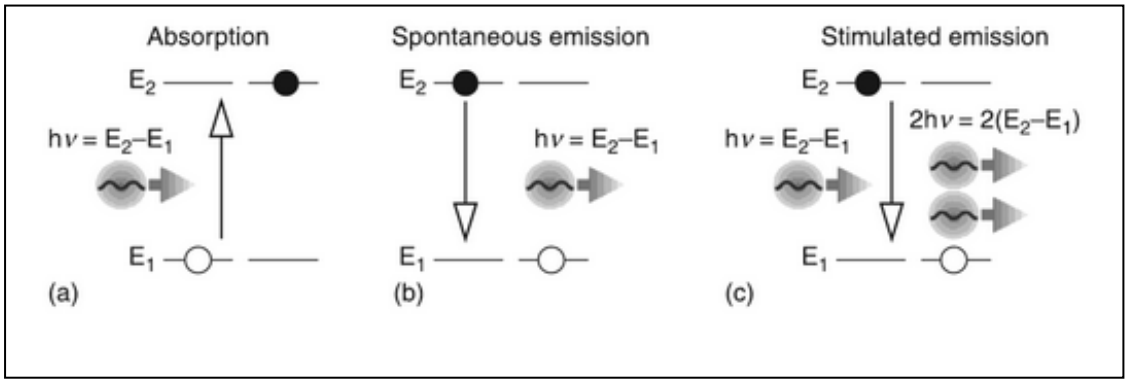

Figure 1.: Changes in quantum systems after an interaction with electromagnetic radiation. a) material absorbing the energy of a photon (E=hv (h Planck constant, v frequency)) moves from its ground state (E_1) to an excited state (E_2). b) spontaneous emission occurs after the lifetime of the excited material expires. The material returns to its original ground state, and a photon is emitted with the same energy as the difference between the excited and ground states of the material (E_2- E_1). c) Stimulated emission happens when a photon irradiates material already in excited state. During stimulated emission the material returns to its ground state, and in the mean while two photons with the same energy (E_2- E_1), same direction and same phase is emitted. [8]

In general lasers work the following way: A cavity is filled with a material that can be excited with a so called pump (which can be a flash lamp or some electric discharge). The material than enters in a "population inversion" state, where more molecules/atoms are in excited state than in their ground state. The two ends of the cavity are closed with two mirrors. One of these mirrors is a semi-reflective mirror, so that a light beam can escape the cavity. Inside the cavity photons are emitted as the excited material returns to its ground state. These photons which are in different polarization circulate in all directions inside the cavity, causing more and more stimulated emissions. Coherent light with the same wavelength, phase and directions escapes the cavity through the aperture of the semi-reflective mirror forming a laser beam (Figure 2.).

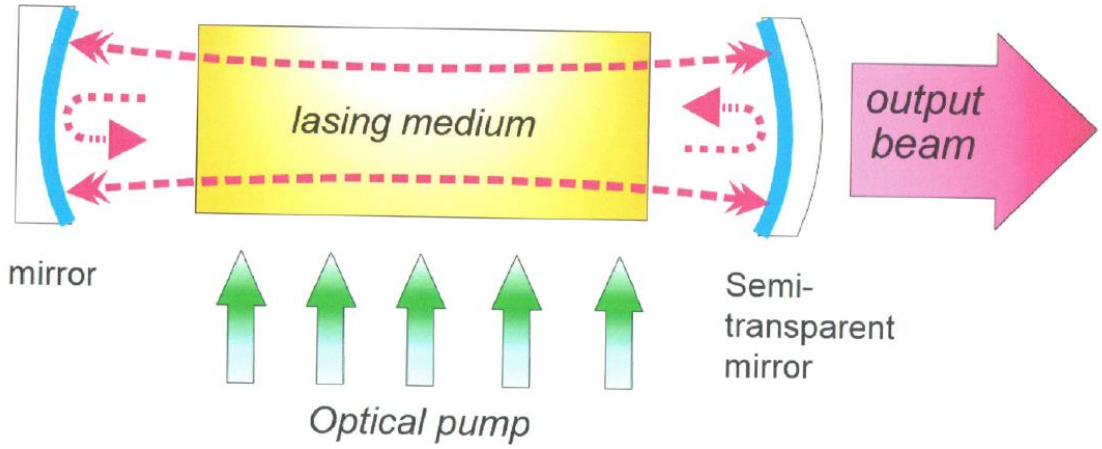

Figure 2.: Schematic drawing of a laser cavity or optical (open) resonator.[1]

3.1.2 Laser properties and radiation parameters

The properties of a laser light can be described by the same characteristics as any other light type or electromagnetic radiation. These characteristics are directionality, coherence monochromaticity and high brightness. Laser beams are very well collimated meaning that the spread of the beam stays very small even when projected over a long distance. This enables that high fluences can be achieved by laser beams compared to other light sources. The light waves in a laser beam are coherent meaning that they are in the exact same phase when they exit the optical resonator, and stays this way for an extended travel length. Most of the laser systems used generate a light beam with a very narrow wavelength. This property is called monochromaticity. Although some laser systems offer the possibility to change the wavelength produced such as tunable lasers, still the wavelength window of these devices is so narrow that they can still be called monochromatic. Finally, since lasers generate light with very high energy with high directionality they can achieve high brightness compared to other light sources.

The main parameters a laser beam can be described are the following: wavelength, pulse width or duration, repetition frequency, pulse energy of or mean power (depending on temporal characteristics of the laser), spot size and energy density or power density.

Wavelength can vary on a broad spectrum from infrared through the visible spectrum to UV and X-ray, and is generally dependent on the laser medium used. The optimal type of laser system for a specific use is mainly affected by the absorption characteristics of the target medium. The wavelength of a laser depends on the photon energy generated by the laser medium when it re-enters its ground state. Thus it has to be taken in to account, that photons of different wavelengths carry a different amount of energy, and therefore cause different effects on the target medium.

Regarding temporal characteristics, lasers can be divided in two groups: continuous lasers and pulsed lasers. A continuous laser emits a continuous beam of light as long as the laser medium is excited, whereas in pulsed laser the laser emits pulses of energy. There are three typical regimes how lasers can produce both continuous and pulsed light. Free-running regime means that the amplification process in not blocked and radiation amplifies freely within the laser resonator as long as the pumping is active. Depending upon whether the pumping is continuous or in pulses the laser emitted will also be continuous or pulsed. Q-switched lasers have a special shutter inside the resonator that prevents oscillation. The laser medium is activated by pumping, and when it reaches certain energy the shutter is opened and a very intense pulse is generated with a duration in the range of nanoseconds. If the pumping is continuous, a train of pulses is generated as long as the pumping continues. This is called a quasi-continuous Q-switched regime. Mode-locked lasers work similarly to Q-switched, but here the shutter causes the coupling of the longitudinal modes in the resonator so that their phases are locked. The beam created by mode-locked lasers is also similar to those of a Q-switched, but the pulse duration is even shorter in the range of pico- or femtoseconds.

Energy and power of a laser are the most important parameters steering what effect the laser beam will have on the tissue. Energy –measured in Joules (J)- is usually used to characterize radiation in pulsed lasers, and power (average output power measured in watt (W)) is used to characterize radiation in continuously running lasers. In medical application the most important parameter to describe a laser radiation is fluence or energy density. It describes the total sum of energy delivered to a specific area of tissue. It is calculated by the division pulse energy with laser spot size and is expressed as J/cm^2.

3.1.3 Tissue laser interactions and their implications in ophthalmology

Laser can induce a wide variety of reactions in human tissue ranging from photochemical changes to instant vaporization of the material. The qualities of laser that determine what happens with the irradiated tissue are wavelength, fluence and irradiation time. In general the higher the absorbed photon energy and the shorter the timespan the energy is delivered the more tissue disruption is generated.[9]

3.1.3.1 Photochemical interaction

Photochemical interactions are usually induced with light sources that emit light that is not absorbed by the target tissue itself, but the effect is mediated by an exogenous agent instead. To avoid tissue heating the exposure times are generally much longer (multiple minutes), and the irradiance is usually very low. Here the laser is only used to activate the exogenous material, and the tissue changes are mediated by this agent.[10] The two modalities using photochemical interaction that are currently performed are photodynamic therapy and corneal crosslinking. In the prior verteporfin is administered intravenously, and then the region of interest is irradiated with a low energy continuous laser with 689 nm wavelength. There is no thermal reaction involved, but the photoactivation of verteporfin that binds to low density lipoprotein (LDL)-receptors found on the endothelial cells of choroidal vessels cause vasoocclusion of choroidal vessels in the irradiated area. Retinal vessels that lack LDL-receptors are spared.[11] In corneal collagen crosslinking riboflavin is applied locally on the corneal surface (after abrasion), and is than irradiated with a low intensity (3mW/cm^2) UVA light for 30 minutes. It has been shown, that corneal collagen crosslinking is able to prevent progression of corneal ectatic diseases.[12]

3.1.3.2 Photothermal interaction

Photothermal interaction can cause a broad range of tissue alterations depending on the amount of heat generated. Such alterations range from minor changes in cell metabolism such as cytokine expression to apoptosis and necrosis of the cell. Chromophores such as water, hemoglobin, melanin, xanthophyll and other pigments absorb the light in tissues, and their absorption spectrum defines which wavelength of light is necessary for an optimal laser effect. The amount of tissue damage is defined by the amount of intracellular proteins denaturized. This changes exponentially depending on laser power and linearly

depending on exposure time as described by the Arrhenius integral. The most common form of photothermal laser interaction is retinal photocoagulation.

Laser wavelength used for retinal photocoagulation varies between 488 and 694 nm (argon and ruby laser respectively), but most commonly frequency doubled Nd:YAG lasers or semiconductor lasers with 532 nm (green) or 577 nm (yellow) respectively are used. In this wavelength spectrum the two chromophores absorbing laser energy are hemoglobin and melanin in the retinal pigment epithelium (RPE) and in the choroid. During a laser pulse application heat is generated at the level of the RPE. Depending on the power and the pulse duration this access heat diffuses to the adjacent tissue in 360°. This phenomenon is called thermal blooming. When a laser pulse with 100 ms duration is applied to the retina, heat diffusion can reach up to 200 μm meaning not only that the tissue at the lateral edges of the lesion will be affected (and with that the effective lesion size will be larger) but also the inner retinal layers including the retinal nerve fiber layer (RNFL) will be affected causing more widespread damage as the size of the lesion alone.[13] With the reduction of the pulse duration the amount of thermal blooming can be reduced, but to achieve the same visible threshold laser effect the laser energy has to be increased. After a certain reduction of the pulse duration unwanted photomechanical interactions might occur.

3.1.3.3 Photomechanical interaction

If a high energy laser with a very short exposition time (tens of ns) is applied on a tissue it causes a photoablation as the temperatures achieved are higher than the vaporization threshold. The gas bubbles created by the vaporization create small explosions that rupture nearby tissue with very high precision and only minimal tissue damage at the edges of the treatment zone. Photodisruption and dielectric breakdown happen when the pulse duration is even shorter (in the nanosecond-femtosecond region). If the energy is applied in such a short pulse plasma develops and mediates rapid explosive vaporization to the tissue. Photoablation is used in ophthalmology in laser mediated corneal surgery where nanosecond pulses of 193 nm wavelength laser irradiation causes extremely precise ablation of stromal tissue. With such short pulse duration the residual tissue damage is extremely low. Plasma mediated photodisruption is used to perform laser capsulotomies and laser iridotomies. Nd:YAG lasers cause explosive vaporization of the

liquid medium causing tissue rupture. With pulse durations in the femtosecond range photodisruption is used to perform the precise dissection of the corneal stroma, lens capsule and crystalline lens during femtosecond assisted cornea and cataract surgery.

3.1.4 The brief history of retinal photocoagulation

Ophthalmology is an ideal field for the use of lasers both in the treatment and in the diagnosis of diseases, since the eye is mainly built by tissue with clear optical properties. The first description of "laser" coagulation of the retina was actually light photocoagulation developed by a German ophthalmologist Meyer-Schwickerath.[14,15] He developed an elaborate conception on the roof of the Department of Ophthalmology in Hamburg-Eppendorf in the late 1940s to collect sunlight, and used a series of mirrors to bring the light ray in to the operating theater. Later in the 1950s he deployed a high pressure xenon arc lamp as light source, thus eliminating the need of direct sunlight.[16] The same year Meyer-Schwickerath failed with the first attempts of light coagulation, Kettesy the chair of the Department of Ophthalmology in Debrecen performed the first successful light coagulation in a patient with a retinal tear by having the patient look in to the sunlight.[17] Among others retinal detachments and diabetic retinopathy were among the first diseases to be treated with light and photocoagulation.[18–20]

The first truly "modern" concept of how to perform laser therapy in patients with proliferative diabetic retinopathy was described by Beetham et al in 1969.[21] The first randomized clinical trial examining the beneficial effects of laser was the diabetic retinopathy study (DRS). The DRS study started in 1972 and showed that panretinal photocoagulation (PRP) reduced the risk of severe visual in loss in 4 years both in the severe nonproliferative (NPDR) as well as in the mild and high-risk proliferative diabetic retinopathy (PDR) groups, with achieving a 24% reduction in the latter group.[22] The early treatment diabetic retinopathy study (ETDRS) was one of the most important landmark studies in diabetic retinopathy. It not just evaluated the effect of macular and panretinal laser treatment but also laid down the basis how we measure functional outcomes like visual acuity, how to analyze morphologic endpoints, and how to classify diabetic retinal disease.[23,24] In respect of laser treatment the ETDRS study examined the effect of macular and panretinal laser therapy in patients without high risk characteristics. It showed that macular grid and focal photocoagulation reduced the loss of VA after 3 years significantly

in patients with clinically significant macular edema with or without macular involvement.[25] Regarding PRP showed that it is safe to defer treatment in patients with severe NPDR or non-high-risk PDR until high-risk characteristics are seen.[26] In the 1980s laser therapy was examined in the indications for all major retinal diseases. The branch vein occlusion study showed, that in patients with macular edema due to branch retinal vein occlusion macular grid photocoagulation treatment resulted in better visual outcomes (65% vs 37% of eyes with 2 line VA improvement laser vs sham respectively) than observation. Furthermore the study showed that sectorial PRP reduced the risk of severe VA loss in patients with retinal or iris neovascularization.[27,28] The central vein occlusion study however showed that grid photocoagulation provided no benefit to patients with macular edema due to central retinal vein occlusion, but prompt panretinal photocoagulation was necessary and beneficious if neovascularization on the retina or iris occurred.[29] In age-related macular degeneration the macular photocoagulation study laid out the basis of performing laser therapy in patients with choroidal neovascularisations.[30]

3.1.5 Current challenges of laser therapy in diabetic retinal disease

Since the results of the DRS and ETDRS studies were published laser photocoagulation was the only approved and effective therapy for patients with diabetic macular edema and proliferative diabetic retinopathy.[31] This changed with the advent of novel pharmacological therapeutics in the late 2000s and early 2010s. Multicenter randomized clinical trials like the Ride/Rise, Vivid/Vista and Restore studies showed that intravitreal anti-vascular endothelial growth factor (anti-VEGF) therapy is more effective in improving visual acuity, reducing macular thickness and preventing sever visual loss than macular laser therapy in patients with diabetic macular edema (DME).[32–34]

The Diabetic Retinopathy Clinical Research Network (DRCR.net) conducted multiple studies regarding diabetic eye disease. In Protocol I they compared the efficacy of ranibizumab with prompt (at time of initiation of treatment) and deferred (≥24 weeks) focal/grid laser treatment. The 3-year results of the study suggested that focal/grid laser treatment at the initiation of intravitreal ranibizumab therapy was not better, and possibly worse for vision outcomes, than deferring laser treatment for ≥24 weeks in eyes with DME involving the fovea. The 1-year results showed that intravitreal ranibizumab with

prompt or deferred laser was more effective through 2 years compared with prompt laser alone for the treatment of DME involving the central macula.

Another landmark study from the DRCR.net -Protocol S- compared the effectiveness of panretinal photocoagulation vs. anti-VEGF therapy for proliferative diabetic retinopathy.[35,36] In this randomized, multicenter, noninferiority trial, 394 eyes of 305 adults with PDR were randomized to receive either PRP or anti-VEGF therapy (pro re nata). Eyes in both groups were allowed ranibizumab if DME was present. The study showed that rates of active neovascularization or rates of regression of neovascularization were similar between the two groups. Ranibizumab was not inferior to PRP in terms of visual acuity outcomes at 2 years (+2.8 letters vs. +0.2 letters respectively $P<0.001$). In the ranibizumab group there was less mean reduction in peripheral visual field (-23 dB vs. -422 dB; $P<0.001$) than with PRP treatment. The rates for vitrectomy (15% vs. 4%; $P<0.001$), and DME development (28% vs. 9%; $P<0.001$) was more frequent in the PRP group than in the ranibizumab group.

PRP has known side effects, most of all loss of visual field, worsening of night vision, but also reduced color vision and reduced contrast sensitivity.[37] Furthermore small case series reported loss of accommodation, and atonic pupils following PRP:[38,39] Despite these known side effects the DRCR.net study and its post-hoc analysis concluded, that although anti-VEGF therapy for the treatment of PDR is as good as panretinal photocoagulation, PRP is still a viable therapy option for this condition due to its long lasting effect, cost effectiveness, and less time burden due to less follow-ups on the patients and the health care system.[36,40]

Current guidelines rely on the clinician's decision on how they manage PDR. Anti-VEGF therapy might be a good option for patients with simultaneous DME, while patients with historically bad compliance might benefit more from PRP.[41,42] Data shows patients with poor compliance treated with anti-VEGF monotherapy often return after falling out of regular checkups with advanced PDR complications.[43]

In order to minimize side effects associated to PRP and to maximize patient and physician comfort a number of novel technological advances have been introduced. One of these methods is to deploy laser systems that can deliver high laser energy with shorter pulse

duration. Animal model studies showed that with reduction of the laser pulse duration the acute damage of the inner retinal layers can be significantly reduced (Figure 3).[13,44] Furthermore when only the outer layers of the retina are acutely damaged with shorter pulse durations a considerable amount of regeneration and remodeling was observed in the retina. The continuity of the RPE monolayer was restored through RPE migration and proliferation within 1 week compared with damage of longer-duration pulses of 100 ms.[45] The damage zone in the photoreceptor layer is initially filled with glial tissue, but over time, the photoreceptors from the adjacent retina shift into the damage zone, thereby reducing its size. With lesion size of 200 mm and below, and with no damage to the inner retinal layers, photoreceptors can completely refill the damage zone and rewire to local bipolar cells over time, thereby restoring retinal structure and function and avoiding the extensive glial scarring and neuronal loss associated with longer-duration retinal burns.[45] Another advantage of such a laser system, that it allows the subsequent placement of multiple laser burns in predefined pattern within a short period of time in order to reduce the time needed to perform the laser procedure.

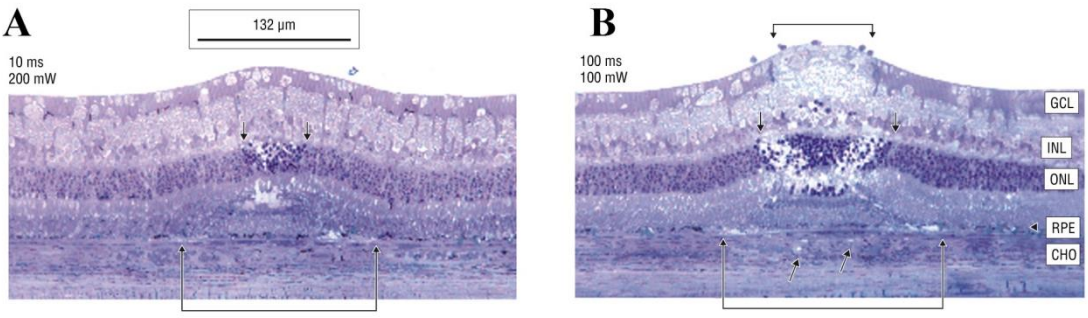

Figure 3.: The acute phase pf A) 10 and B) 100ms laser burns. A) Damage after 10ms laser pulse duration is limited to the RPE and photoreceptors. The inner retinal layers are intact. B) There is a considerable amount of damage to the choroid as well as the inner retinal layers in the acute phase. [44]

Creating funduscopically and/or instrumentally non-visible subthreshold laser burns using micropulsed diode lasers is another method to reduce laser side effects. In micropulsed laser the laser pule is not applied in a continuous wave, but in trains of laser bursts (usually 100-300µs) with predefined duty cycles. The pulses are divided by regular

off-times. This fractioning of the laser energy enables better heat diffusion in the tissue, and therefore the RPE is treated with a sublethal effect.[46] The hypothetical endpoint of subthreshold micropulsed laser therapy is not the destruction of the RPE but its modulation, to change its cytokine expression.[47,48] Early retrospective and prospective studies with small patient numbers showed promising results with micropulse laser in the treatment of DME and in PDR.[49–53] Randomized clinical trials to confirm these findings are currently under way.[54] In other diseases such as central serous chorioretinopathy subthreshold micropulse laser was found inferior to current standard of care (halved fluence PDT), although some authors question the results due to the laser protocol used.[55,56]

Navigated lasers use fundus tracking technology in order to find regions of interests, and deliver laser radiation to the exact location selected by the operator. Pre-treatment planning of the treatment is possible either from fundus photography or even from fluorescein angiography (FA) images. FA images captured can be registered to the real-time fundus image, and regions of interest such as microaneurysms can be treated even if they are not visible on fundus examination. Navigated lasers promise higher accuracy when aiming at small lesions due to the eye movement tracking, and also higher safety as predefined safety zones are constantly monitored, so that inadvertent treatment of these is not possible.[57] Large randomized studies like the Restore trial and Protocol I did not show benefit in combining anti-VEGF therapy with conventional ETDRS macular laser therapy for achieving better visual acuity or reducing the number of injections.[33,58] Some authors suggested, that the heterogeneity in the quality of how macular laser was performed limited the additional beneficial effect. A small randomized prospective study comparing anti-VEGF therapy with either navigated laser or conventional laser did not find a statistically significant difference in the number injections nor in VA improvement and central retinal thickness loss after 12 months.[59] Another study compared anti-VEGF in monthly versus treat and extend regiment versus treat and extend anti-VEGF plus navigated focal laser therapy. At 2 years the study found no significant difference between anti-VEGF alone vs. navigated laser plus anti-VEGF in terms of VA gain, central retinal thickness loss, or in the number of injections needed.[60]

In summary novel laser technologies may provide potential benefits for the patients, but these have to be confirmed in randomized clinical trials.

3.2 Optical Coherence Tomography

Optical coherence tomography (OCT) is a novel and emerging imaging modality in medicine, and in its short existence of roughly 30 years became a major diagnostic tool in everyday clinical life especially in ophthalmology. The basic functionality of OCT is somewhat similar to ultrasound, but instead of sound it uses light to penetrate and backscatter from biologic tissues. It does not possess the high penetrance of ultrasound, but has a much higher resolution than that. Although OCT had a slow start, and the first commercial instruments were difficult to use and were not widely used and accepted, as soon as more practicable instruments were presented they became widely popular in the field of ophthalmology.[61] Today OCT is among the most commonly performed ocular examination, and became standard of care in the diagnosis and management of retinal diseases. The fact that it is noninvasive, quick, and extremely reproducible it became the ideal diagnostic tool to monitor patients treated with intravitreal injections, where controls are frequently necessary, and treatment decisions have to be made based on only slight changes. Further developments of OCT technology such as OCT angiography (OCTA) promise to aid an even broader spectrum of clinical decisions with valuable information.

The physical background of optical coherence tomography, low-coherent of white light interferometry was first described by Sir Isaac Newton. The fist instrument that used interferometry to measure distance was constructed by Michelson who used it to measure the diameter of stars in 1921.[62] A schematic drawing and description of a Michelson interferometer is shown in Figure 4. In 1988 Fercher et al. reported the first biological (and ophthalmological) use of interferometry, when they used it to measured axial length of eyes.[63] This sort of interferometry is still used, and became standard of care in modern cataract surgery for measuring axial length for calculating intraocular lens power preoperatively.

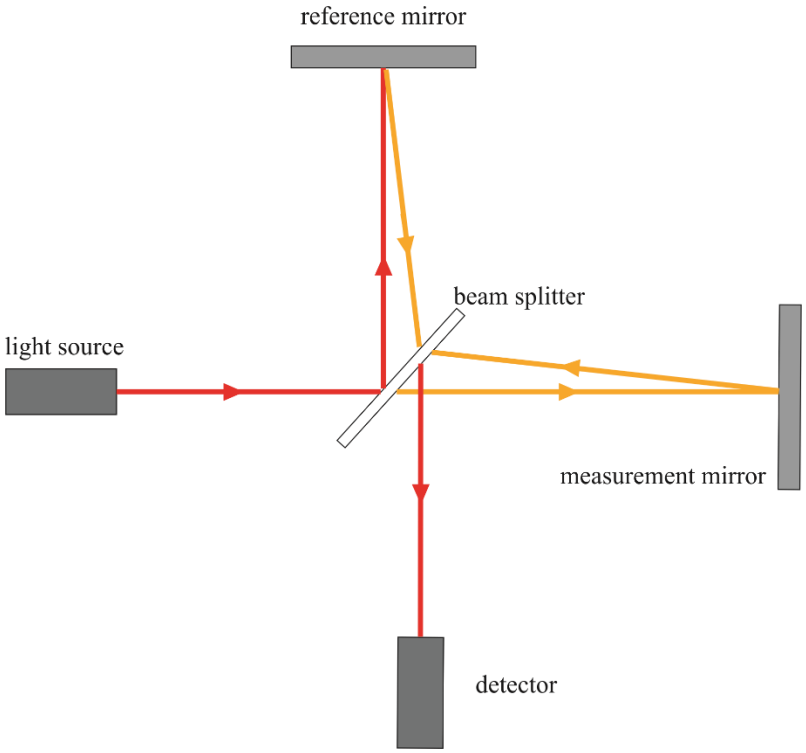

Figure 4.: Schematic drawing of a Michelson interferometer. A light source emits a low coherent light passes through a beam splitter (half-silvered mirror). One light beam is projected on a mirror at a known distance (reference arm). The other beam is measured at the test object with unknown distance. Both reflected beams pass through the beam splitter again and the created interference is captured by a detector. (Authors own image)

The first ever OCT image was published in 1991 by Huang et al.[64] These early images demonstrated that OCT image although not completely identical, showed very high resemblance to histological sections (Figure 5). The development of OCT technology progressed rapidly, the first in vivo images were published by Fercher and Swanson in 1993, and the first commercially available OCT device was introduced in 1996 by Carl Zeiss Meditec.[65,66] Although the first two generations of OCT devices, the OCT1 and OCT2 sold only a few hundred pieces, the introduction of the StratusOCT in 2001 with its enhanced handling and faster scanning times brought a breakthrough in OCT technology.[61] In Hungary a fair amount of publications were published with early experience with OCT technology.[67–69]

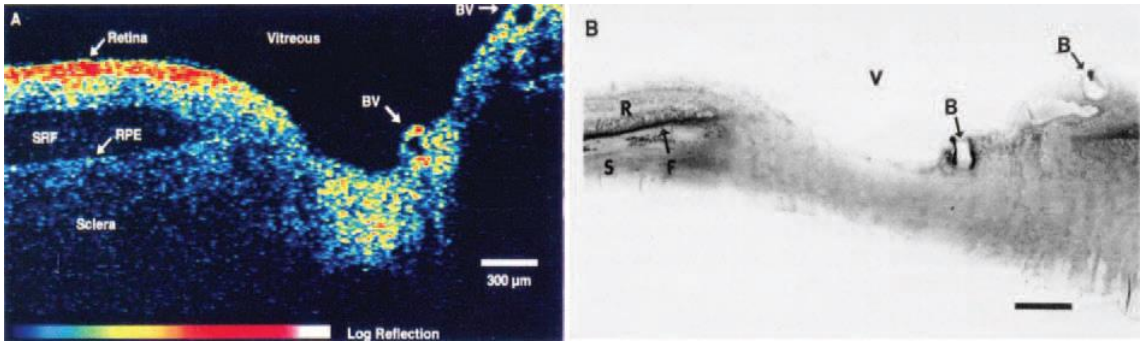

Figure 5.: Right: The first ever OCT image published by James Fujimoto's lab at the Massachusetts Institute of Technology of an ex vivo human retina and optic nerve head. The axial resolution of the scan is 15 µm. Left: the corresponding histologic image.[64]

The most important parameters in OCT imaging are: axial image resolution to enable the detailed visualization of retinal layer architecture. Axial resolution is determined by the wavelength and bandwidth of the light source. Transverse resolution is determined by the spot size of the focused light beam. The smaller spot size (larger numerical aperture) the finer the transverse resolution will be. On the other hand the smaller the spot size is the lesser the depth of field will be. In ocular media transverse resolution is mainly limited by optical aberrations of the eye. The advent of adaptive optics technologies will help overcome these limitations.[70] Data acquisition time is also an important factor, and is something that developed rapidly in the last decade with the introduction of Fourier domain detection, high speed detectors and swept light sources. Detection sensitivity determines the ease to capture a good-quality OCT scan and together with penetration depth is dependent on the wavelength of the light source, but also have an inverse relationship with acquisition speed.

3.2.1 Time-Domain OCT technology

The first three generations of OCTs were based on time-domain detection (TD-OCT) technology. In order to map the depth of different reflexes from the detector this technology uses a moving mirror in the reference arm of the interferometer. This moving mirror moves between its endpoints once for every A-scan performed (Figure 6). As light source a super luminescent diode (SLD) with a wavelength near 800 nm with a bandwidth of ca 30 nm was employed and reached an axial resolution of around 10-15 microns. This

axial resolution was enough to image most of the retinal layers, but the outermost retinal layers and the retinal pigment epithelium (RPE) were only displayed as a single hyperreflective band (Figure 7.). Research instruments with broad bandwidth titanium-sapphire laser were able to achieve approximately 3 µm axial resolution.[71,72] The main limitation of TD-OCT technology was acquisition speed. The StratusOCT the fastest commercially available TD-OCT had 400 A-scans per second acquisition speed.[61] Although this was enough to capture detailed images of the macula it was prone to image artefacts due to eye movements that would limit interpretation. Furthermore due to the slow acquisition speed it could only perform line scans, and radial patterns scans. Retinal thickness measurements that were introduced to aid clinical decision making relied on the segmentation of the innermost border of the retina the vitreoretinal interface, and the outermost part of the retina the inner border of the hyperreflective RPE band. Since large areas of the retina were not scanned between the radial scans these thickness values were interpolated. Thus segmentation errors in one of the line scans would affect a large area of the macular thickness profile. [73]

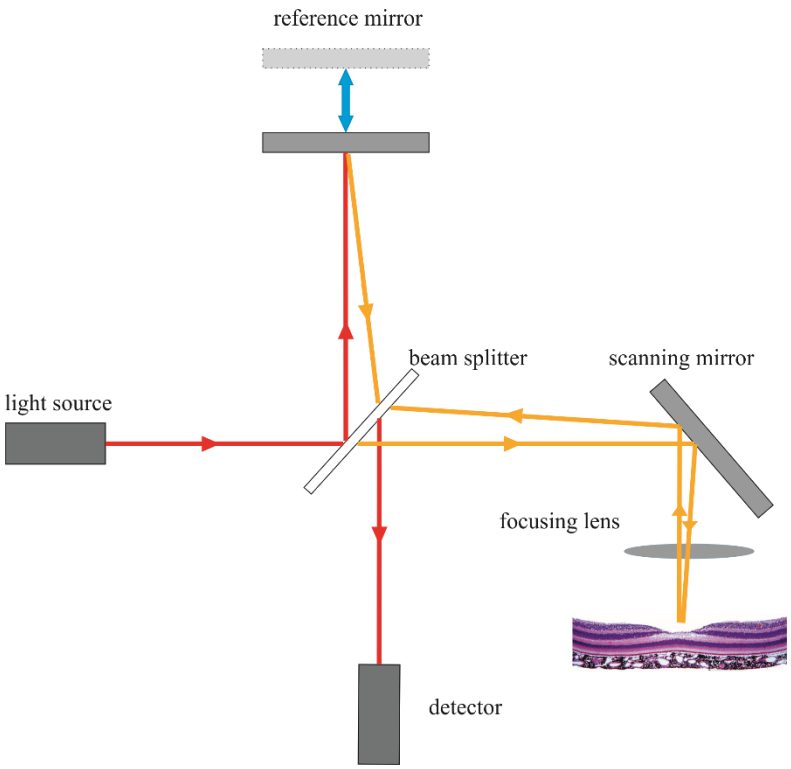

Figure 6.: Schematic drawing of a time domain optical coherence tomography. (TD-OCT) The reference mirror moves back to forth at every A-scan captured. Once an A-scan was captured the scanning mirror moves to the next retinal location to capture the next A-scan. (Authors own figure)

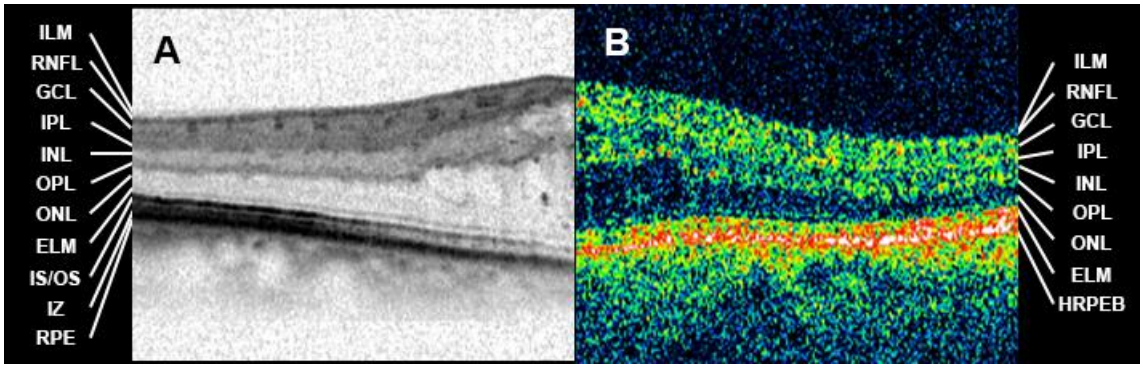

Figure 7.: Layers of the retina. A) Image captured with an SD-OCT device. B) Image captured with a TD-OCT device. ILM: internal limiting membrane, RNFL: retinal nerve fiber layer, GCL: ganglion cell layer, IPL: inner plexiform layer, INL: inner nuclear layer, OPL: outer plexiform layer, ONL: outer nuclear layer, ELM: external limiting membrane, IS/OS: inner segment / outer segment junction, IZ: interdigitation zone, RPE: retinal pigment epithelium, HRPEB: hyperreflective RPE band. (Authors own figure)

3.2.2 Spectral-Domain OCT Technology

In conclusion the greatest drawback of TD-OCT technology was slow acquisition speed. The answer to that came when a mathematical formula the Fourier transformation was applied in OCT technology. Instead of measuring optical echo signals sequentially as in time domain detection, Fourier/spectral domain OCT measure the entire optical echo signal simultaneously by using a spectrometer and a high-speed charge-coupled device (CCD) camera to detect interferometric information for the depth-resolved reflectivity profile (Figure 8.).

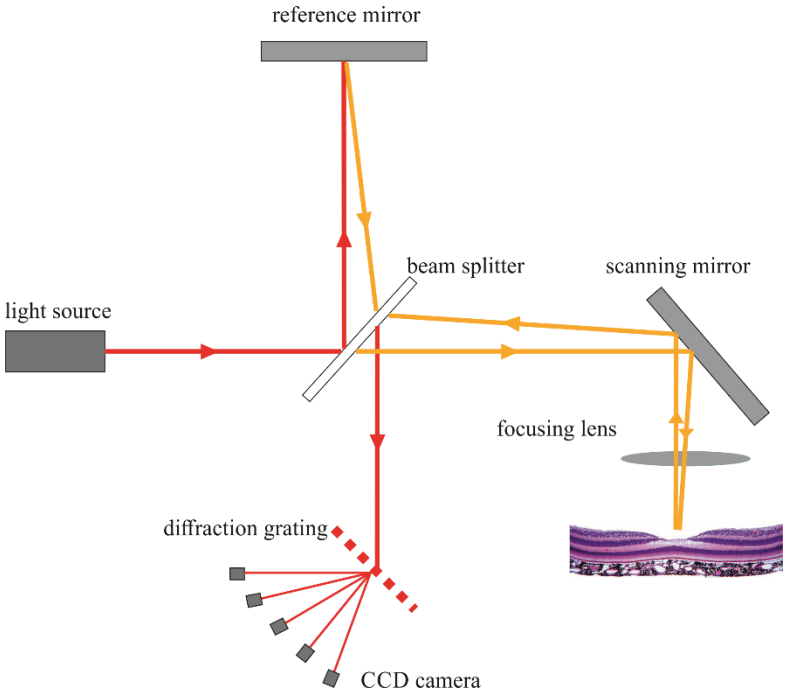

Figure 8.: Schematic drawing of an SD-OCT device. In comparison to TD-OCT (Figure 6) the mirror in the reference arm is stationary. The reflected beam of the measurement and reference arm reaches the CCD camera through a diffraction grating. (Authors own figure)

Since a constantly moving reference mirror is not necessary, image acquisition is faster, and only limited by the speed of the CCD camera. Thus commercially available SD-OCT devices can achieve acquisition speeds ranging from 20 000 to 100 000 A-scan per second. Increased speed has many advantages, first of all much more B-scans can be captured in the same time period as with TD-OCTs, thus new volumetric scan patterns imaging the complete macular or even the complete posterior pole became feasible. Motion artefacts can still occur between individual B-scans, but not within B-scans, and this decreases the chances of false or missed diagnosis due to artefacts.[74] This enables more precise thickness measurement as well. Secondly, higher acquisition speed together with advanced eye motion tracking technologies enable the capturing of multiple B-scans at the exact same retinal location. This on one hand makes image averaging to enhance signal-to-noise ration possible, and on the other hand enables the comparison of B-scans repeated within a fraction of time, and extraction of pixels with changes in reflectance or phase change between the two scans. This technology is called OCT angiography (OCTA) and is detailed later in section 3.2.4. The third advantage of higher acquisition

speed is that even with more B-scans to be taken the examination is still shorter than with TD-OCT, thus making the examination easier for both the patient and the examiner.

Of course there are also drawbacks of SD-OCT technology. The greatest drawback is the reduced depth measurement range. In SD-OCT technology the number of axial pixels in an A-scan is limited by the number of pixels in the CCD camera of the device. Fourier transformations halves the number of the axial pixels, meaning that there is a tradeoff between axial resolution and depth range. Due to limitations in current spectrometer resolution and pixel crosstalk effect in CCD cameras there is also a significant loss of sensitivity with increasing depth range. Post-processing algorithms can help reduce this, but depth range remains still an issue with SD-OCT technology.[75]

3.2.3 Swept-source optical coherence tomography

Swept-source OCT (SS-OCT) takes another approach to Fourier transformation. Instead of using a broad spectrum SLD light source and using a spectrometer to extract spectral information, SS-OCTs use a tunable laser light source with a narrow band that sweeps over the optical bandwidth and interferometric information is detected by a single photodetector.[76] This eliminates the speed limit that SD-OCTs have with currently available CCD technologies, and results in a much simpler system setup (Figure 9). Thus SS-OCT systems can achieve even higher acquisition speeds than SD-OCTs with commercial devices already in the 200 000 A-scans per second range, and research devices in the MHz range.[77] Higher speeds allow for even higher quality and even wider fields of view than before. Furthermore most SS-OCT devices use 1050 nm wavelength lasers. Compared to the most commonly used 800-820 nm used in SD-OCT SLDs this wavelength penetrates better and is less attenuated by optical opacities or the RPE, and has an enhanced depth range. As a downside axial resolution is somewhat less than what is achievable with 800 nm SD-OCTs. Another more practical downside of SS-OCTs is that their light sources are currently extremely costly, and their life span is limited.

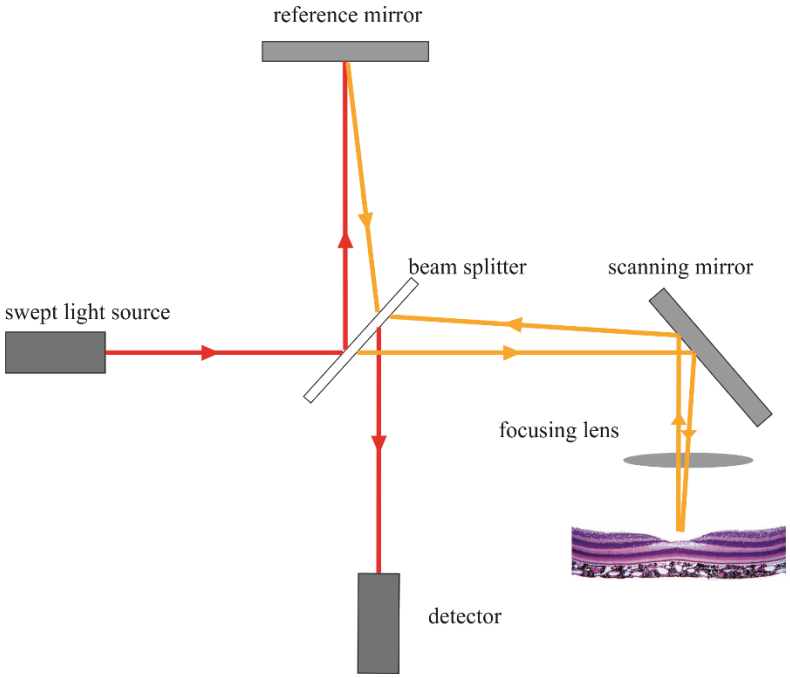

Figure 9.: Schematic drawing of a swept-source OCT device. The light source here is a laser sweeping through the optical bandwidth with extremely high speed. This eliminates the need of a spectrometer, and a single photometer is used as a detector. (Authors own figure)

3.2.4 OCT angiography

One of the most exciting new innovation in OCT technology was the introduction of OCT angiography.[78,79] On the basis of SD and SS-OCT technology OCTA enables the indirect visualization of retinal and choroidal vessels, and that in a non-invasive and three dimensional way. As briefly mentioned earlier in OCTA two OCT B-scans are taken from the same exact retinal location with only a few millisecond delay in-between. The only movement to be expected in the retinal tissue in this short time period is the flow of blood cells within retinal (and choroidal) vessels. The two most commonly used method to visualize flow are amplitude decorrelation and phase variance detection.[78,79] In the former, the amplitude change between subsequent B-scans is analysed, in phase variance the change in the phase of the light reflected from moving objects in respect to the emitting light source are analysed in the repeated B-scans. Proprietary algorithms developed by different OCT companies are based on these two methods.

On OCTA flow information is usually presented by highlighting pixels where movement i.e. flow was detected. The main advantage of OCTA over conventional fluorescein

angiography (FA) is that the flow information on OCTA is 3 dimensional and with appropriate layer segmentation the different vascular plexuses of the retina such as the superficial, middle and deep capillary plexus can be separated and presented individually in a 2D en-face projection image that is very similar to the images ophthalmologist are used to when examining FA images (Figure 10). These deeper plexuses are not visible on FA, so with OCTA new information can be gathered about the retinal circulation.[80–82] Another major difference between FA on OCTA that since no dye is used, there is no dye leakage to be seen. This has the advantage, that there is no masking effect from the leakage, but on the other hand the source of fluid accumulation cannot be so easily detected as in FA. This information can be indirectly gathered by analysing the normal reflectance OCT images, but there is still a lot to learn about the correct interpretation of OCTA images.

OCTA is a very promising modality as it is quick to perform, non-invasive, and as such repeating examination frequently is less burden to the patients as conventional FA. Unfortunately, current OCTA technology is very prone to artefacts and this limits the interpretation of the images greatly. The most commonly seen artefacts are motion, shadowing and projection artefacts (Figure 10). Although all OCTA devices are equipped with an eye tracking hardware or software algorithm, bulk eye movement can still present in motion artefacts. They increase background noise and reduce the signal to noise ratio necessary to detect flow. Shadowing is also a known artefact in SD- and SS-OCT technology. If a lesion in the inner layers of the retina has a very high reflectivity the light that passes through it will not be enough to reflect the signal of layers beneath this object back to the detector. This will result in a darker appearing area (shadow) beneath the reflective lesion. In OCTA even a minor shadowing –where reflectance information of the outer layers can still be gathered- can reduce the signal enough that no flow information can be extracted. Such a lack of flow information can be mistaken for real lack of flow. The most dreaded and most commonly misinterpreted artefacts are projection artefacts. Since retinal vessels cast shadows to the deeper layers (especially the highly reflective RPE layer) the flow movements in the retinal vessels will cause the same amplitude and phase changes in their shadows, and will be picked up by the algorithms as flow in the deeper layers. Thus flow information of the superficial layers will be projected to the deeper layers. There are numerous software algorithms currently used to

reduce projection artefacts. Simpler options are to simply subtract flow information of the inner layers form outer layers. This comes with a loss of information of the flow in the outer layers. More sophisticated algorithms are being developed and show promising results in making OCTA images more easily interpretable.[83,84]

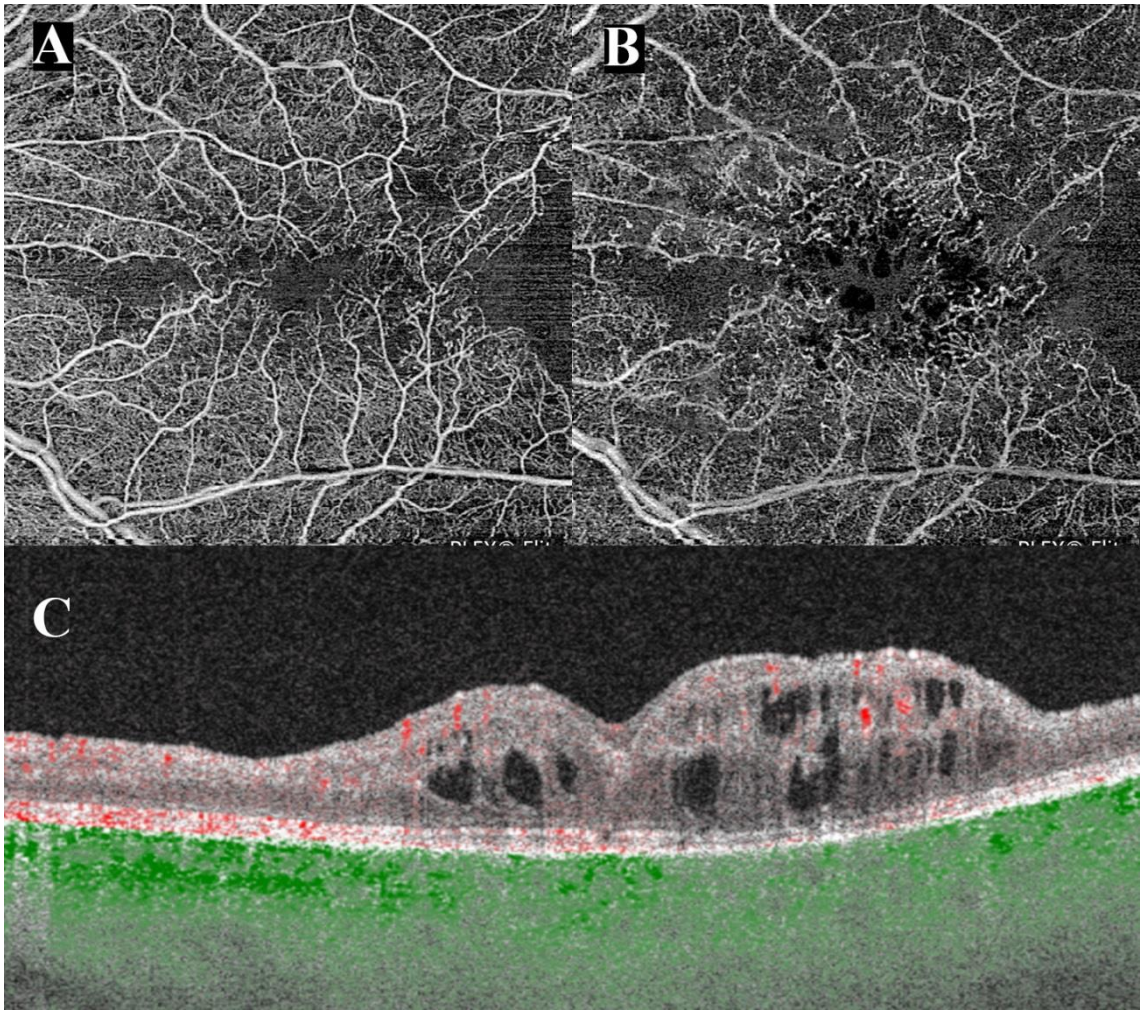

Figure 10.: OCT angiography of a patient with central retinal vein occlusion captured with an SS-OCTA system. A) En-face projection of the superficial capillary plexus. The foveal avascular zone is irregular, the perifoveal capillaries are dilated and intercapillary spaces are widened. Nasal and temporal to the fovea confluent areas without flow i.e. ischemic areas. B) En-face projection of the deep capillary plexus, the perifoveal capillary bed is severely damaged, the ischemic areas seen in the superficial plexus are even more pronounced. Dark round areas in the center represent cystic spaces. Large and medium vessels seen in A) are projected to the deeper layer. C) B-scan through the foveal center cystoid macular edema with disorganisation of the inner layers in the center, and marked thinning and loss of inner retinal layers nasally and temporally. Red dots represent flow in the retina, green dots represent flow in the choroid. (Authors own figure)

3.3 Diabetic retinal changes

3.3.1 Diabetes mellitus

Diabetes mellitus (DM) is a heterogenic group of metabolic diseases affecting the body's carbohydrate, fat and protein metabolism.[85] There are two main forms of diabetes. Type 1 is characterized by the cellular mediated autoimmune inflammation and destruction of the insulin secreting β-cells of the pancreas. This form was formally known as juvenile-onset DM or insulin-dependent DM as in most of the cases (although by far not in all cases) the disease develops in younger patients, and they need insulin substitution for survival. Type 1 DM constitutes 5-10% of all diabetes cases.[85] Type 2 DM is a group of diseases characterized by either increased insulin resistance or an insulin secretory defect combined with some degree of insulin resistance. In the past type 2 DM was referred to as noninsulin-dependent DM, as patient do not need insulin to survive, but still many patients with type 2 DM will need to take insulin to achieve good glycemic control. Obesity is a major risk factor for type 2 DM as it increases insulin resistance. Type 2 DM is by far the more common disease as it comprises 90-95% of all diabetes cases. [85]

A calculation based on epidemiological studies from 91 countries estimated a 6,4% prevalence of diabetes mellitus worldwide affecting 285 million adults in 2010. They predicted an increase of prevalence to 7,7% (affecting 439 million adults) by 2030, where the increase in prevalence in the developing countries will be 69% and in the developed countries around 20% in this time period.[86] In the USA according to the 2017 report of the Centers for Disease Control and Prevention 9,4% of American adults (30,2 million) are affected with DM and an additional 79 million have impaired fasting blood glucose levels.[87]

In summary the number of patients with diabetes is constantly and rapidly rising with the population growth of developing countries and the aging of western countries.[88] Health care systems must prepare for the management of these patients especially their late sequelae like diabetic retinopathy.

3.3.2 Diabetic retinopathy

Diabetic retinopathy (DR) is the most common ocular sequelae of diabetes mellitus, and one of the leading causes of blindness in the working age population worldwide.[89–94] The prevalence of diabetic retinopathy worldwide is estimated to affect around 93 million adults and vision threatening diabetic retinopathy worldwide is estimated to affect around 28 million adults with around 50% of these patients coming from the Asia-Pacific region.[95,96]

The most important risk factor for the development of diabetic retinopathy is duration of diabetes. In the Wisconsin Epidemiologic Study found that the after 5, 10 and 15 years of type 1 diabetes 25%, 60% and 80% of patient will develop diabetic retinopathy respectively.[97,98] In type 2 diabetes depending whether the patients required insulin to manage their diabetes 24% or 40% (no insulin, with insulin respectively) developed DR after 5 years, and 53% or 84% (no insulin, with insulin respectively) developed DR after 19 years of DM duration.[97] A study of 1433 young patient with DM showed, that diabetic retinopathy is more common and usually more severe in patients with type 1 DM than in type 2 DM (20% vs 4% respectively). In real life since there are much more patients with type 2 diabetes, most of the patients seen in the clinics with ocular complications are in fact type 2 DM patients.[99] A recent study conducted in Hungary in 50 years and older population showed that the prevalence of DM was 20%, and in the patients with DM the prevalence of DR and/or diabetic maculopathy was 20.7%.[100]

Regarding modifiable risk factors blood sugar, blood pressure and blood lipid levels seem to be the most important. The importance of glycemic control in the development of DR and especially on the severity of DR after development have been confirmed in multiple studies, and although blood pressure and blood lipid control is beneficial in diabetes mellitus its impact on diabetic retinopathy is still to be confirmed.[101–104]

The most commonly accepted theory is that diabetic retinopathy is a microangiopathy caused by the hyperglycemia induced cellular changes in retinal capillaries leading to the formation of capillary occlusions and microaneurysms.[105,106] There is growing evidence that parallel to these vascular changes, or even proceeding these there is a neurovascular component as well.[36,107,108]

Clinically diabetic retinopathy can be divided into two stages. Nonproliferative diabetic retinopathy (NPDR) is characterized by microaneurysms, intraretinal hemorrhages, venous dilatations and in later stages cotton wool spots, hard exudates, venous beading and intraretinal microvascular abnormalities (IRMA) (Figure 11).[109]

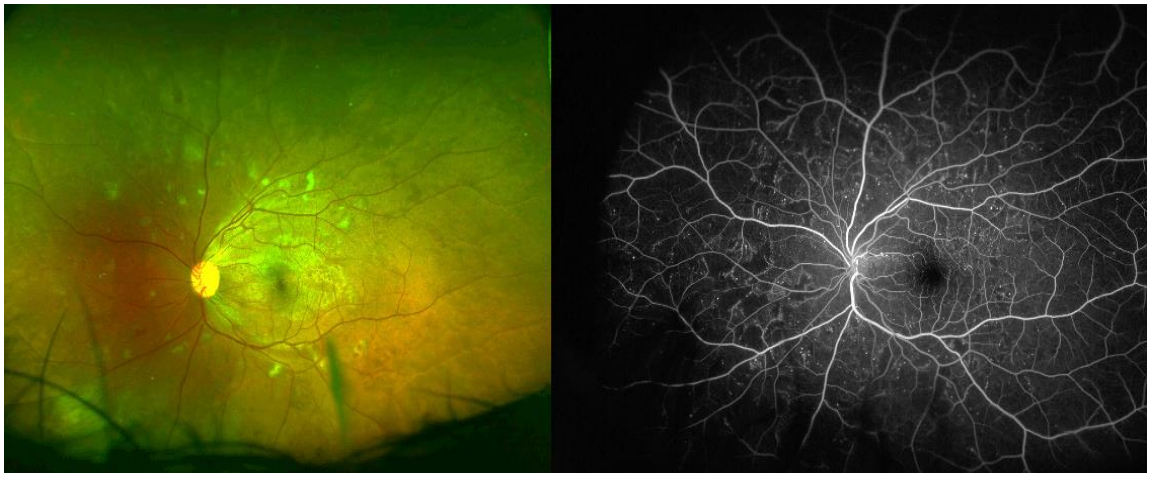

Figure 11.: Wide-field fundus photography (CF) and fluorescein angiogram (FA) of a patient with moderate nonproliferative diabetic retinopathy (NPDR). CF shows numerous microaneurysms in the posterior pole and outside the vessel arcades, as well a multiple cotton wool spots and intraretinal hemorrhages. Signs of severe NPDR such as extensive intraretinal hemorrhages in 4 quadrants, venous beading in 2 or more quadrants or prominent intraretinal microvascular abnormalities (IRMA) are not seen. FA shows the extensive amount of microaneurysms and focal areas of capillary nonperfusions.

Diabetic retinopathy progresses gradually with the increasing amount of retinal capillary occlusion. These occlusions promote the expression of various cytokines among them the most important VEGF. VEGF induces to vascular remodeling seen in the form of shunt capillary formations (i.e. IRMA), increased vascular permeability (i.e. diabetic macular edema formation), and the formation of new vessels either on the inner surface of the retina or in more severe cases in the anterior segment. Such neovascularization either on the optic nerve head, around retinal vessels or on the iris are the leading signs of a proliferative diabetic retinopathy (PDR) (**Figure 12**)

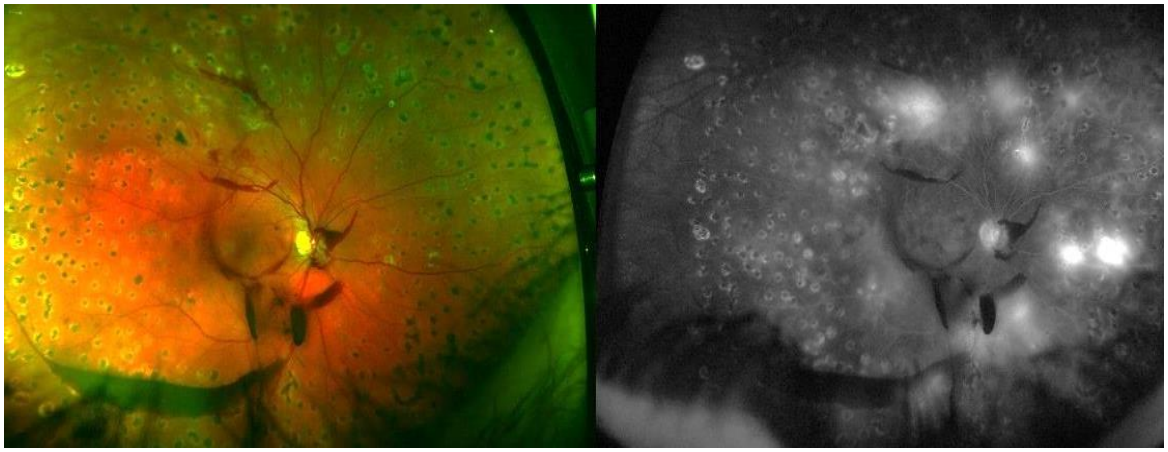

Figure 12.: Wide-field fundus photography (CF) and fluorescein angiogram (FA) of a patient with proliferative diabetic retinopathy (PDR). Neovascularizations elsewhere (NVE) are readily seen on CF as well as preretinal and intravitreal hemorrhages. The middle periphery is covered with pigmented panretinal photocoagulation (PRP) scars. Late phase FA shows even more leaking NVEs as well as ischemic areas already covered by the PRP. The macular area shows diffuse and focal leakage.

3.3.3 Diabetic macular edema

Diabetic macular edema is sequel of diabetic retinopathy, and can develop both in NPDR as well as PDR stages. It is characterized by the increased inflow of fluid, proteins and lipids from the retinal vasculature -due to increased vascular permeability- into the extracellular space of the retina. This causes thickening of the retina, formation of intraretinal cystoid spaces, subretinal fluid accumulation, and the formation of hard exudates (**Figure 13**). Although retinal thickening does not directly correlate to visual acuity it is still the main cause of visual impairment in patients with diabetic retinopathy.[90,110]

Before the advent of OCT technology, DME was detected based on fundus examination (or fundus photography in clinical trials) aided by fluorescein angiography. The ETDRS study divided DME into clinically significant macular edema (CSME) and non-CSME based on the location and extent of the retinal thickening and hard exudates on fundus exam or fundus photography. OCT made the detection and quantification much simpler, and it made possible to detect DME before it causes obvious clinical sings or functional

symptoms. Randomized clinical trials (RCTs) in the OCT era usually define DME using central subfield thickness, and the presence of fluid compartments on OCT (**Figure 13**).

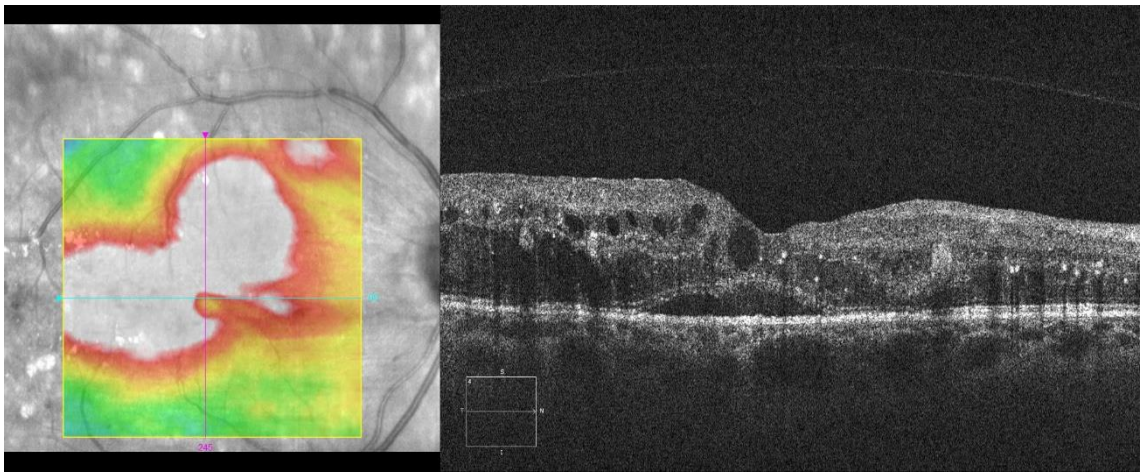

Figure 13: Infrared image with retinal thickness heat map and OCT image of a patient with center involving DME. On the heat map warmer colours represent thicker retina. OCT shows intraretinal cystic spaces in the outer and inner nuclear layers (ONL and INL), subretinal fluid accumulation under the fovea, multiple hyperreflective foci at the apical border of the ONL, and an incomplete posterior vitreous detachment. (Authors own figure)

4 Purpose

Although in indications such as diabetic macular edema novel therapeutic approaches became the standard of care grid and focal laser therapies can still have their value in the armamentarium of therapies.[31–33,42,111–114] In other indications like proliferative diabetic retinopathy retinal photocoagulation is still the preferred way of treatment due to its long lasting effect.[35,36,115] Although the timely execution of laser therapy can save the patient from profound visual loss due to vitreous hemorrhage or tractional retinal detachment, it is well known, that panretinal laser photocoagulation has a number of side effects such as peripheral visual field loss, night blindness or central visual decrease.[36,116] These side effects can have a major impact on the quality of life of patients with PDR, since many of these patients are still in the working age group, whose daily job and living might depend on their eyesight.

Novel developments in laser technology showed promising results in animal models in reducing collateral damage when performing laser therapy.[13,45] It is a well-known feature that laser scars grow with time, and cover larger and larger areas of the peripheral retina further reducing the already impaired peripheral retinal function. Furthermore animal model studies confirmed, that laser burns applied with standard laser pulse durations cause disruption of the RNFL causing further functional loss.[13,44] It is imperative for the wellbeing of our patients to develop and apply the most beneficial therapeutic approach with the least amount of collateral damage.

The aims of our research were the following:

1. examine the in vivo effects of a short duration continuous thermal laser onto the human peripheral retina using optical coherence tomography
2. examine the longitudinal healing process of laser burns, and quantify laser scar size changes over time
3. examine the immediate in vivo morphologic changes after macular grid photocoagulation using a short duration continuous thermal laser
4. examine the immediate and long term in vivo effects of non-visible sub-threshold laser burns applied by a short duration continuous thermal laser on retinal morphology

5. to describe a novel potential biomarker seen in patients with diabetic macular edema, and observe in vivo its behavior in respect to changes in macular thickness after macular photocoagulation.

5 Methods

To answer the clinical questions described in the purpose section we performed four separate studies. In the following section we present the methods used in each of these studies separately.

All four studies were conducted at the Department of Ophthalmology at the Medical University of Vienna. The protocol followed the tenets of the Declaration of Helsinki and was registered at www.clinicaltrials.gov (NCT00682240) as well as approved by the responsible ethics committee of the Vienna University. In a personal interview, the interventional study design, investigations for scientific purposes, and imaging procedures were explained in detail to each patient before obtaining informed consent.

5.1 In vivo examination of retinal changes following panretinal photocoagulation

5.1.1 Patients

Ten consecutive patients (9 men, 1 woman) assigned to PRP due to proliferative diabetic retinopathy were enrolled in a prospective, interventional, and open-labelled trial.

5.1.2 Examination and documentation

Before laser treatment, each patient underwent a complete baseline evaluation, including slit-lamp examination, ophthalmoscopy, visual acuity testing, fluorescein angiography, fundus photography, and SDOCT imaging. Follow-up visits were performed at 1 day and 1 week after PRP, and at monthly intervals thereafter until month 6. The standardized examination procedures were repeated according to protocol at each follow-up visit, except fluorescein angiography, which was performed every 3 months.

5.1.3 Retinal Photocoagulation

A photocoagulator offering a fully integrated pattern scan laser system designed to treat retinal diseases using a single spot or a predetermined pattern array of up to 56 spots was used (PASCAL Pattern Scan Laser, OptiMedica Corporation, Santa Clara, CA).[117] This

laser instrument is capable of delivering high laser powers during short laser exposure times (10-20 ms) achieving similar fluences as conventional laser settings. This faster laser application allows that a large number of identical spots can be applied by a single foot-pedal depression, which allows for constant treatment parameters to be maintained during the entire laser procedure at each spot location. For spot size uniformity and precise spot placement, identical and reproducible laser power settings were needed to obtain reproducible morphologic effects at all spot locations. Photocoagulation was performed via irradiation with a frequency doubled neodymium: yttrium-aluminium-garnet (Nd:YAG) laser diode with a 532-nm wavelength.

Before the laser procedure, pupillary dilatation was induced by the topical application of 1% tropicamide (Mydriaticum "Agepha") and 2.5% phenylephrine hydrochloride eye drops. Topical oxybuprocaine 1% (manufactured by the institutional pharmacy) was instilled immediately before treatment initiation. Carefully maintaining a safe distance from the optic disc of 1 disc diameter, a sufficient number of laser burns were applied, to cover the retinal periphery beyond the limits of the upper and lower arcades as close to the pars plana as possible.[118] A 20-msec burn duration and a 200 μm diameter laser spot size were chosen as standard laser settings.[44] An Ocular Mainster wide-field contact lens (magnification 1.5; Ocular Instruments, Bellevue, WA) was used to focus the laser beam on the retina, magnifying the 200 μm diameter laser spot to approximately 300 μm on the retinal plane. The laser power (mean, 588 mW; min, 300; max, 1025) was determined based on ophthalmoscopic visibility of the treatment spot and adjusted until a distinct grey spot was observed clinically.

5.1.4 Retinal Imaging Using Spectral Domain-Optical Coherence Tomography

A novel generation SD-OCT was used (Spectralis, Heidelberg Engineering GmbH, Heidelberg, Germany), combining high-resolution OCT and fluorescein angiography in one instrument, which was useful in our diabetic study population where both diagnostic procedures had to be performed. The instrument enables 40.000 A-scans per second. A super luminescence diode implemented as the light source in the system radiates an 870-nm laser beam, which confers improved light penetrating properties to the system compared with other systems and provides an axial resolution of 7 μm and a transverse resolution of 14 μm. Such optimized image quality was needed for precise identification

of the tissue effects at the level of individual retinal layers and for distinct delineation of the thermal damage zone. Another technologic feature relevant to the study purpose and superior to other OCT devices is the specific image alignment technique of this device for locating, tracking, and constantly aligning retinal locations. Tracking laser tomography (TruTrack) enables real-time, simultaneous imaging while tracking eye movements. Utilizing this image alignment software, the instrument continuously monitors the position of the eye using a beam of light. The tracking system enables the scanning of the same exact b-scan multiple times and averaging the images further increasing signal to noise ratio. Additionally it allows for the identification of the same retinal location throughout each follow-up visit for a precise evaluation of progressive changes during the healing response. To reproducibly identify an image location, an area closely adjacent to the upper or lower vascular arcades, which was identified by the image tracking system, was selected. This location was close to the posterior pole and provided a consistent central retinal anatomic structure.

5.2 In vivo examination of retinal changes following macular grid and focal photocoagulation

5.2.1 Patients

Thirteen consecutive patients (9 men, 4 women; mean age 58±10 years) with diabetic maculopathy showing generalized clinically significant macular edema associated with diabetes mellitus type 2 were included in the study. All patients were treatment naïve or had not received any treatment for DME at least 3 months before inclusion.

5.2.2 Examination and documentation

Color fundus photography and SD-OCT examinations for imaging structural and biometric retinal changes secondary to macular grid laser treatment with time and biomicroscopy were performed at baseline and day 1. In addition, patients were examined using a standardized protocol (ETDRS) for the assessment of best-corrected visual acuity and by fluorescein angiography at baseline.

5.2.3 Retinal photocoagulation

In all patients, the PASCAL system was used, which is designed to treat retinal diseases using a single spot or a predetermined pattern array of up to 56 spots.[117] Procedures before the laser procedure were discussed in detail in chapter 5.1.3.

As recommended for the modified ETDRS grid laser treatment, patients with DME received a predetermined grid pattern laser treatment of the edematous perifoveolar region in this study setting consisting of 56 laser lesions performed in a homogenous ring pattern after energy titration using the PASCAL® Pattern Scan Laser System (OptiMedica Corporation, Santa Clara, CA) laser system.[25,119] In addition, single microaneurysms were coagulated with single laser lesions. In 1 patient, the grid laser treatment was performed using a single spot laser treatment. A 10-ms burn duration and a 100-µm diameter laser spot size were chosen as standard laser settings, and the treatment was performed using an Area Centralis Laser Lens (Volk, Mentor, OH). In all patients, the laser power was determined on the basis of ophthalmoscopic visibility of the treatment spot and adjusted to a spot of light greyish color observed clinically.

5.2.4 SD-OCT Imaging

SD-OCT imaging was performed using the Spectralis OCT (Heidelberg Engineering GmbH, Heidelberg, Germany) described in detail in chapter 5.1.4. Retinal thickness measurements by SD-OCT were defined as a thickness change in the central millimeter of the ETDRS grid. Examination were performed at the same time of the day (late morning) based on the possible diurnal fluctuation of the extent of DME.[120]

5.3 In vivo morphology of retinal changes following sub-threshold panretinal photocoagulation

5.3.1 Patients

Ten consecutive patients with retinal or anterior segment neovascularisation due to diabetic retinopathy (8 patients) or central retinal vein occlusion (2 patients) were enrolled in this prospective cohort study.

The main inclusion criterion for the study was the need for scatter laser photocoagulation because of retinal neovascularisation (neovascularisation on the disc or elsewhere), or neovascularisation on the iris caused by type 1 or 2 diabetes mellitus or retinal vascular occlusion. Further requirements were no prior laser photocoagulation, no indication for intravitreal drug injection and clear optical media.

5.3.2 Examination and documentation

Prior to laser treatment, each patient underwent a complete baseline evaluation including slit lamp examination, ophthalmoscopy, best corrected ETDRS visual acuity testing, FA, color fundus photography, fundus autofluorescence and SD-OCT imaging. Follow-up visits were performed at day one, three and seven following laser treatment, and monthly intervals thereafter until month 3 with a final visit at 6 month. The standardized examination procedures were repeated according to protocol at each follow-up visit, except FA, which was performed only at baseline.

5.3.3 Retinal photocoagulation

All laser treatments were performed using the PASCAL® Pattern Scan Laser System (OptiMedica ® Corporation, Santa Clara, CA, USA), and the Mainster PRP 165 laser lens (Ocular Instruments Inc, Bellevue, WA, USA, laser spot magnification 1.96x). A study area was selected beside the superior or inferior temporal vessel arcades. After titrating the laser power to produce the typical grey- white lesion, the first 2x2 pattern was applied in the study area. Afterwards the laser power was decreased to halve the laser irradiation fluence (J/cm2) and a second 2x2 pattern was placed adjacent to the first pattern. The same process was repeated another two times to produce four group of laser spots from threshold to 1/8 fluence. Following the completion of the study zone a standard scatter laser therapy was applied in 2 or 3 sessions using standard threshold fluence laser spots.

5.3.4 SD-OCT Imaging

SD-OCT evaluation was performed using the Spectralis© OCT system (Heidelberg Engineering GmbH, Heidelberg, Germany), that was described in detail in chapter 5.1.4. Thirty minutes after laser therapy the patients were imaged using single line scans aligned to fit at least 2 laser spots of the study area.

5.4 Hyperreflective foci on OCT in patients with diabetic macular edema and their response to macular photocoagulation

5.4.1 Patients

Thirteen consecutive patients with CSME due to diabetic retinopathy were enrolled in this prospective interventional study performed by a single site (Department of Ophthalmology, Medical University of Vienna, Austria).

Inclusion criteria for the study was type 2 diabetes mellitus, the presence of a clinically significant macular edema, no prior laser photocoagulation, no pharmacologic intervention within three months prior to inclusion and clear optical media.

5.4.2 Examination and documentation

Prior to laser treatment, each patient underwent a complete baseline evaluation including slit lamp examination, ophthalmoscopy, BCVA testing, FA, CFP and SD OCT imaging. Follow-up visits were performed at day one, week one following laser treatment, and in monthly intervals thereafter until month 4. The standardized examination procedures were repeated according to protocol at each follow-up visit, except FA, which was performed at baseline and every three months.

5.4.3 Retinal photocoagulation

Retinal photocoagulation was performed following the modified ETDRS laser protocol.[118] In case of leakage in FA from microaneurysms, the laser therapy was aimed to coagulate the leakage origins. If no leakage source was detectable by FA, a grid pattern with barely visible laser burns was applied on the entire edematous area with a 500 micron safety distance towards the foveal center. All laser treatments were performed using the PASCAL® Pattern Scan Laser System (OptiMedica ® Corporation, Santa Clara, CA, USA).

5.4.4 SD-OCT Imaging

SD-OCT evaluation was performed using the Spectralis OCT system (Heidelberg Engineering GmbH, Heidelberg, Germany). This OCT system was described in detail in

section 5.1.4. The average thickness value of the central 1mm field of the ETDRS grid was used to measure changes in the central retinal thickness (CRT) with time. The thickest retinal position (TRP) was also defined at the baseline examination. Using the follow-up function, the thickness of the same location was recorded for the follow-up visits as well. At baseline one or more regions of interests (ROI) were defined by each patient. These ROIs consisted of such areas of the retina, where lipid micro or macro exudates were visible. In some cases showing new lipid exudates during follow-up outside of predefined ROIs, new areas were added retrospectively.

6 Results

The results of the four studies performed are presented below in separate sections.

6.1 In vivo examination of retinal changes following panretinal photocoagulation

6.1.1 Early Effects of Photocoagulation

Retinal images for each subject were analysed and revealed comparable results as follows. At 1 day after treatment, the focal tissue alteration owing to the applied thermal energy was clearly visible in the SD-OCT image (Figure 14.). The morphologic damage was characterized by an increased reflectivity and condensation of neurosensory elements localizing to the outer retinal layers. The upper margin was located at the level of the outer plexiform layer (OPL) and continuous throughout the outer nuclear layer (ONL) and the PRL, down to the RPE. The spots seemed to be distinct and were sharply delineated toward the adjacent unexposed area, demonstrating an intact layered architecture. No transition zone between damaged and undamaged structures was observed. Within the well-circumscribed laser burn, retinal striation seemed blurred as compared with untreated areas, but still distinguishable. The thickness and contours of the single layers remained unmodified; the layers seemed to be continuous, corresponding in orientation to the surrounding intact areas. Analysis of the laser spot by each separate layer revealed only marginal structural damage of the superficial layers. Manifest alterations began within the OPL, which became slightly indistinct and was characterized by structural irregularities and blurred borders. The laser tissue interaction extended toward the neighbouring ONL, where a pronounced hyperreflectivity of the otherwise hyporeflective internal signal was observed, with a sharp demarcation toward the ONL of the untreated space between the spots. Within the laser spot, a hardly recognizable hyporeflective line adjoining the lower limit of the ONL was interpreted to be the external limiting membrane, merging into the PRL. The inner photoreceptor segments seemed to be less reflective than their corresponding counterparts in the untreated areas, but the internal texture, as well as the layer delineation, seemed unchanged. The RPE revealed

signs of laser effects, identified as a reduction in overall reflectivity, together with a discrete thinning of all the layers. Light transmission underneath the laser spots was decreased. Limited OCT capacity to penetrate to layers below the RPE did not allow for an exact interpretation of the choriocapillary anatomy. A lower magnification overview clearly highlights the confinement of the laser effects to the outer retinal layers and the increased reflectivity, as well as the intact layer organization.

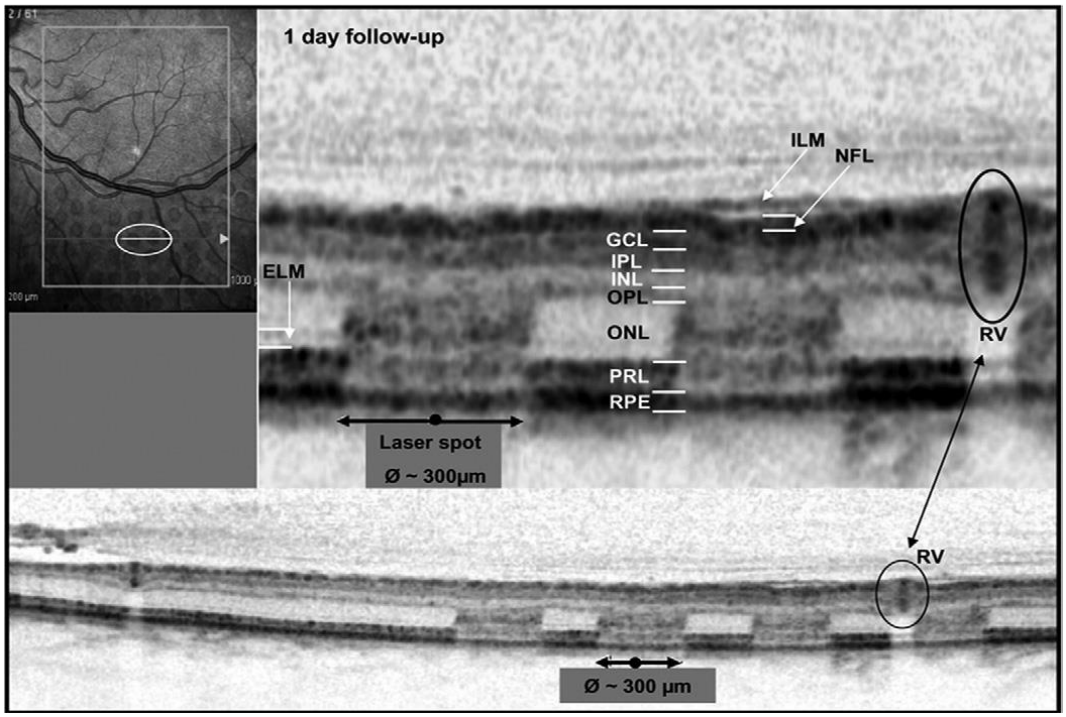

Figure 14.: Spectral domain optical coherence tomography (SD-OCT) image of laser spots 1 day after photocoagulation. The white circle on the red-free image on the left panel indicates the scanned retinal area. Right panel and lower panel: SD-OCT images of laser effects: The spots seem to be sharply delineated, uniformly spaced, and of similar morphology. Internal layers (inner limiting membrane [ILM], nerve fiber layer [NFL], ganglion cell layer [GCL], inner plexiform layer [IPL] and inner nuclear layer [INL]) are morphologically unaffected. Obvious structural alterations of the retinal tissue occur within the external layers at the OPL and extend through all outer retinal layers toward the retinal pigment epithelium [RPE]. ELM: external limiting membrane; ONL: outer nuclear layer; OPL: outer plexiform layer; PRL: photoreceptor layer; RPE: retinal pigment epithelium; RV: retinal vessel.[121]

6.1.2 Healing Response after Photocoagulation

At 1 week (Figure 15.), the laser spot had contracted in relation to its initial transversal as well as longitudinal diameter. The main difference in retinal morphology was the involution of the ONL, which was reduced to a thin layer that was most pronounced in the central portion of the laser lesion. The resulting narrowing of the ONL led to a distortion of the overlying inward layers and the OPL seemed to adhere directly to the hyperreflective layer of condensed, amorphous photoreceptor segment remnants. The shrinking of the ONL exerted traction through all overlying layers, from the OPL toward the ILM, almost causing a depression on the retinal surface. The contracting ONL and possibly the condensed PRL induced an outward displacement of retinal strata and as a consequence, dissolution of the inner nuclear layer (INL), which was markedly widened at the site of the lesion center. Delineated by the slightly hyperreflective OPL, these phenomena—ONL loss and INL widening—generated a pattern of "archways," extending from 1 spot to a neighbouring region. Within the lesions at the level of the PRL and RPE layer, a secondary tissue response was observed that seemed to be absent in earlier follow-up. At the margin of the lesion, and beyond the immediate treatment area, a sharply demarcated defect with a complete loss of the photoreceptor segment layer was noted. In the lesion center, however, the previous hypodense PRL seemed to be condensed and hyperreflective, suggesting that at this location the apoptotic photoreceptors were replaced by migrated RPE cells. As described, the atrophy of the PRL was not limited to the circumscribed laser burn, but extended in a ring like fashion into the surrounding area. Within untreated areas between the laser burns, the PRL and the RPE bands were clearly defined, whereas in the photocoagulated tissue it was not possible to differentiate between these 2 layers and the PRL and the RPE present as 1 solid layer with intensive RPE-like reflectivity.

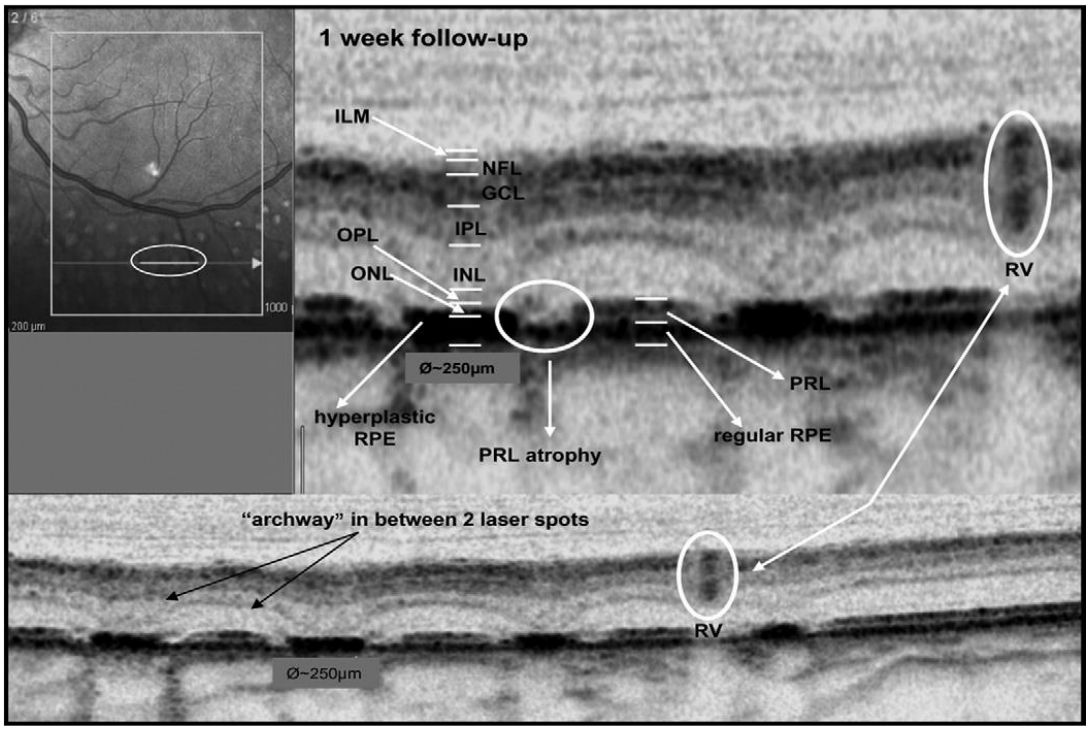

Figure 15.: Spectral domain optical coherence tomography (SD-OCT) image of laser lesions 1 week after treatment. The laser spots were smaller relative to their initial diameter and were no longer well-defined, with loss of the previous sharp demarcation. Substantial thinning of the outer nuclear layer (ONL) leads to expansion and outward displacement of inner retinal layers, but most obviously of the inner nuclear layer (INL), which generates the impression of archways connecting neighboring laser burns. The photoreceptor layer (PRL) seems to be eliminated, leaving a distinct atrophic zone around the spot margins. In the lesion center, the damaged PRL seems to be invaded and partially replaced by retinal pigment epithelium (RPE), forming a solid, hyperreflective scar. The diameter of the laser scar has reduced to approx.. 250 µm (including the atrophy ring (noted erroneously on the published figure))[121]

During the following weeks (Figure 16.), the hyperdense amorphous material in the lesion center underwent progressive resolution and decomposition. The central area of the laser spot imposed a circumscribed hyperreflective irregularity with an RPE-like consistency. The peripheral defect in the original PRL, however, seemed to be enlarged. The ONL, on the other hand, seemed to have recovered partially and could be identified as a separate hyporeflective layer between OPL and the damaged PRL. It had not, however, completely re-established its original condition. The "archway"-like distortion (INL, ONL) remained visible, but was less pronounced than earlier. At 3 and 6 months, the nature of the lesions did not change. The ONL remained thinned at the lesion center, which was characterized

by a focal, amorphous, hyperreflective scar surrounded by a zone of persistent, but not further enlarging, defect in the RPE and PRL (Figure 17.). The greatest linear dimension of the lesions decreased from the 300 μm seen at day 1 after treatment to approximately 250 μm at 1 month, and stayed like that until the end of the follow-up period. No scar enlargement was observed.

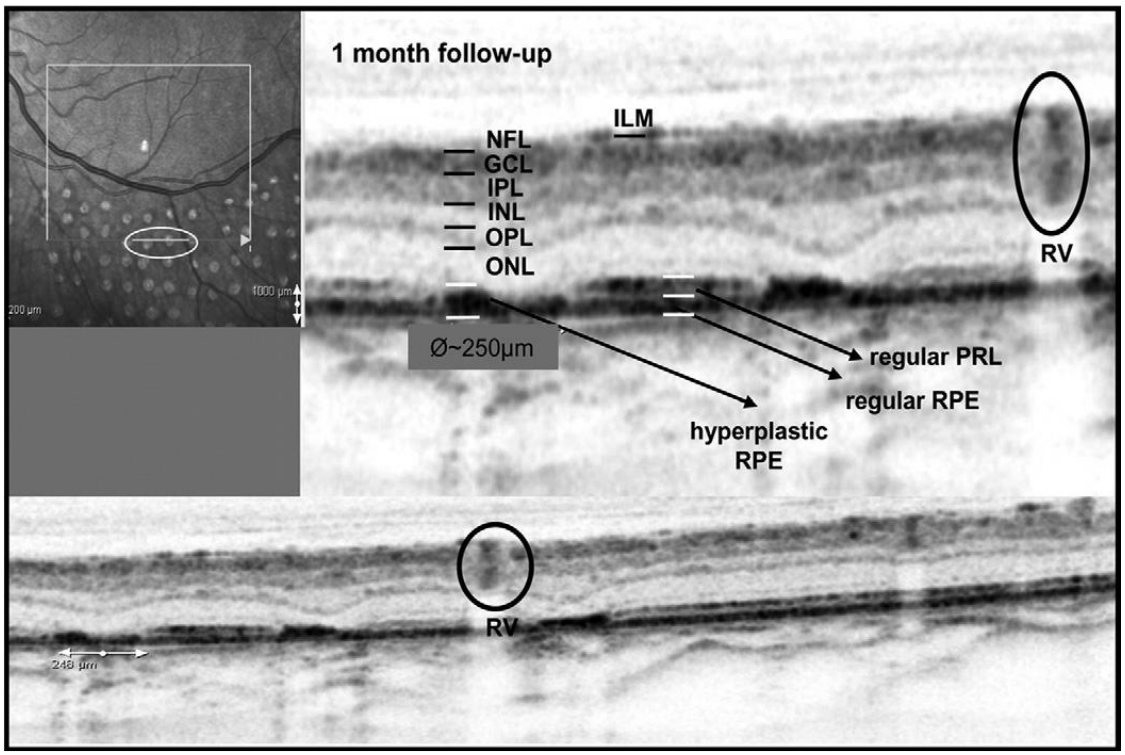

Figure 16.: Optical coherence tomography (OCT) image of lesions 1 month after treatment. Owing to beginning regeneration of the ONL, the retinal anatomy partially normalizes, but the outward distortion and subsequent archway architecture remain unchanged. The central hyperplastic scar has contracted, whereas the photoreceptor layer (PRL) with inner and outer segments and the external limiting membrane (ELM) is absent throughout the entire exposed area.[121]

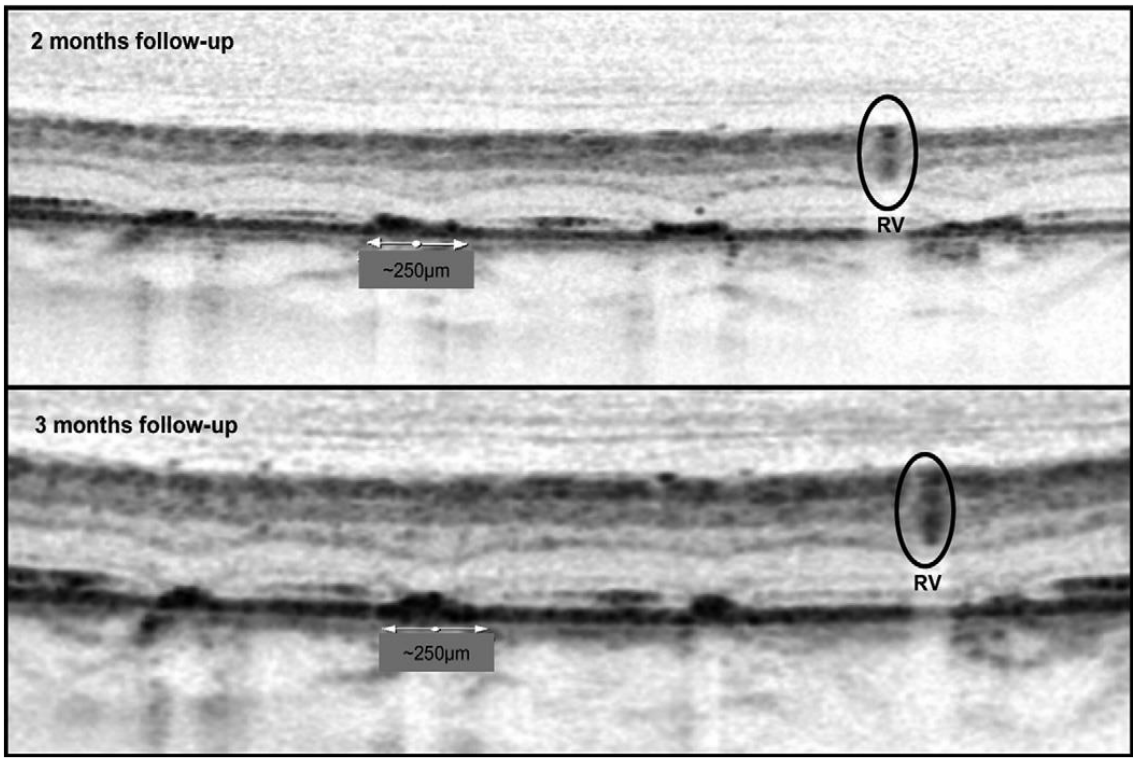

Figure 17.: Optical coherence tomography (OCT) images at 2 (top) and 3 months (bottom) after photocoagulation. The retinal morphology remains remarkably unchanged over time: The inner retinal layers from the inner limiting membrane (ILM) to the outer plexiform layer (OPL) seem to be intact. The outer nuclear layer (ONL) seems to be partially restructured, although thinned. The external limiting membrane (ELM) and photoreceptor layer (PRL) remain discontinuous at the lesion margins. The PRL band and the RPE layer have condensed and seem smaller, leaving a focal hyperreflective lesion in the center of each laser spot.[121]

6.2 In vivo examination of retinal changes following macular grid and focal photocoagulation

The mean ETDRS visual acuity score for the 13 patients was 74±8. All patients had generalized clinically significant macular edema secondary to type 2 diabetes mellitus.

6.2.1 Morphologic Retinal Changes

The characteristic changes typically seen in DME, such as cyst formation and diffuse swelling in the inner nuclear layer and outer nuclear layer (ONL), were observed in all patients.[122] Additional subfoveolar subretinal fluid was observed in 4 patients.

Morphologic changes secondary to the retinal grid photocoagulation were observed on day 1. In all patients, each laser lesion was visible as a clear alteration at the level of the RPE, the PRL, and to a lesser extent, the ONL. No specific changes of the inner retinal layers were observed. The shape of the laser lesions did not show a sagittal alteration pattern throughout the outer retinal layers as expected, but rather seemed to have an oblique pathway throughout the ONL, changing direction at the level of the external limiting membrane (ELM) and proceeding sagittally in the PRL and RPE.

A representative example of these characteristic effects is shown in Figure 18. Before laser treatment (image indicated as baseline), small areas of bleeding were observed in the Infrared image (left), and there were large intraretinal cystoid changes in the ONL and inner nuclear layer, as well as subretinal fluid beneath the fovea in the OCT image (right). One day after laser treatment (indicated as day 1), the laser lesions were slightly visible on infrared photography (left) and clearly visible in the corresponding OCT scan (right) as diagonal alterations of the ONL, changing their orientation at the border of the ELM. The red boxes indicate areas of magnification shown below. All lesions seemed to have followed a concentric pathway throughout the outer retinal layers, heading toward the center of the grid pattern. This characteristic oblique and concentric laser lesion pattern was observed in all patients on day 1. The infrared and OCT findings on day 1 of 3 other patients are shown in Figure 19.

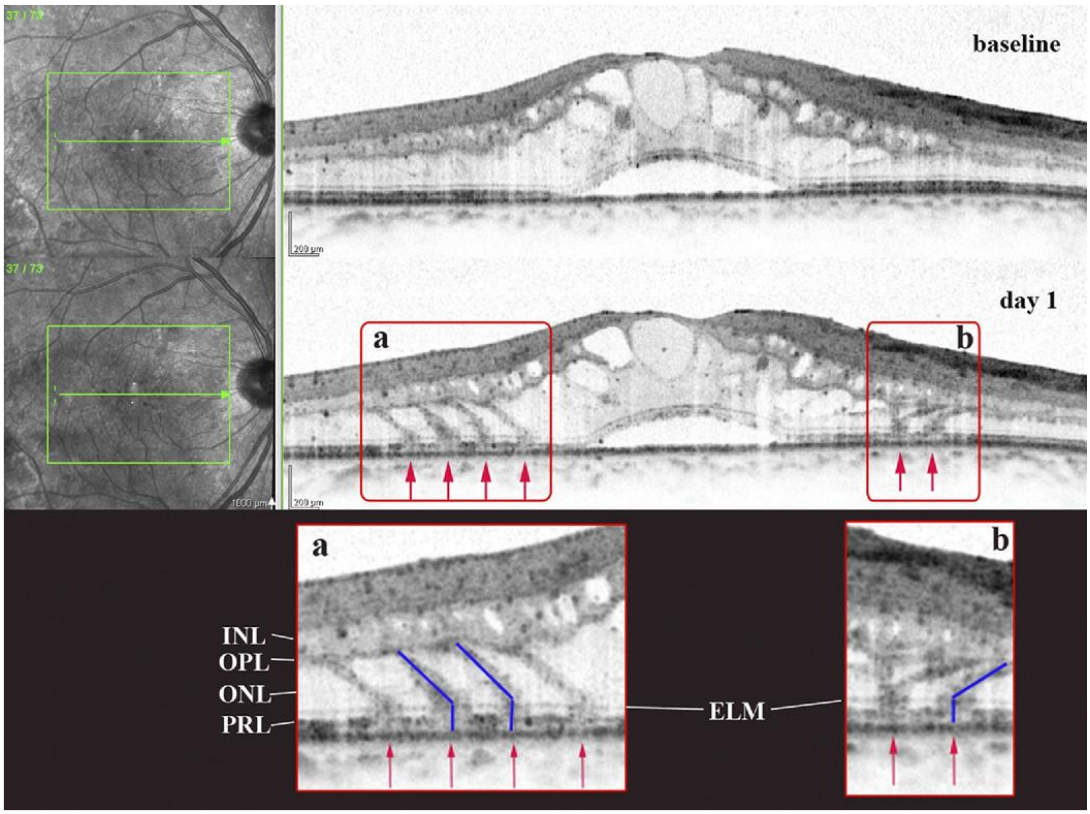

Figure 18.: Immediate morphologic changes after grid photocoagulation. Morphologic findings before (first line) and 1 day after (middle line) laser treatment are shown in infrared imaging (left) and OCT (right). The green line in the infrared image indicates the position of the scan performed exactly at the same position in both examinations. The red boxes indicate the areas (a, b) magnified in the lower line. Laser lesion site (red arrows) at the level of the pigment epithelium. The blue lines in the magnifications indicate the characteristic angulated alteration pattern in each single laser lesion.[123]

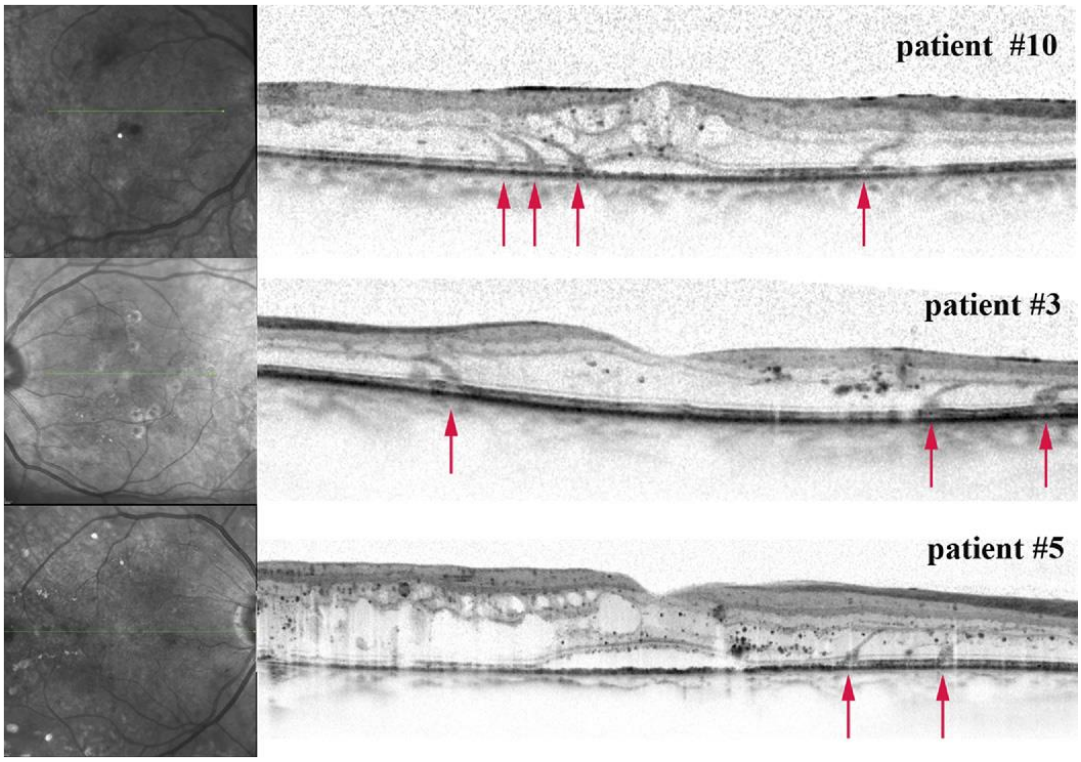

Figure 19.: Laser lesions 1 day after laser therapy in 3 different patients are shown in infrared imaging left and OCT (right). Laser lesion site (red arrows) at the level of the pigment epithelium[123]

Because it was not clear whether these unexpected changes were due to the specific PASCAL grid pattern used to perform several laser spots at nearly the same time, in 1 patient the laser grid treatment was performed with a single laser spot. In this patient as well, however, similar changes were observed (Figure 20.) Furthermore, it was not clear whether a single laser lesion would cause the same morphologic characteristics. Thus, in 2 patients the grid laser treatment was performed in 2 steps, first placing 1 single laser lesion and analysing its effects on morphology in OCT, and second completing the grid photocoagulation as explained above. The results showed that even a single laser lesion caused comparable intraretinal changes that did not change in size or position because of the grid completion (images not shown).

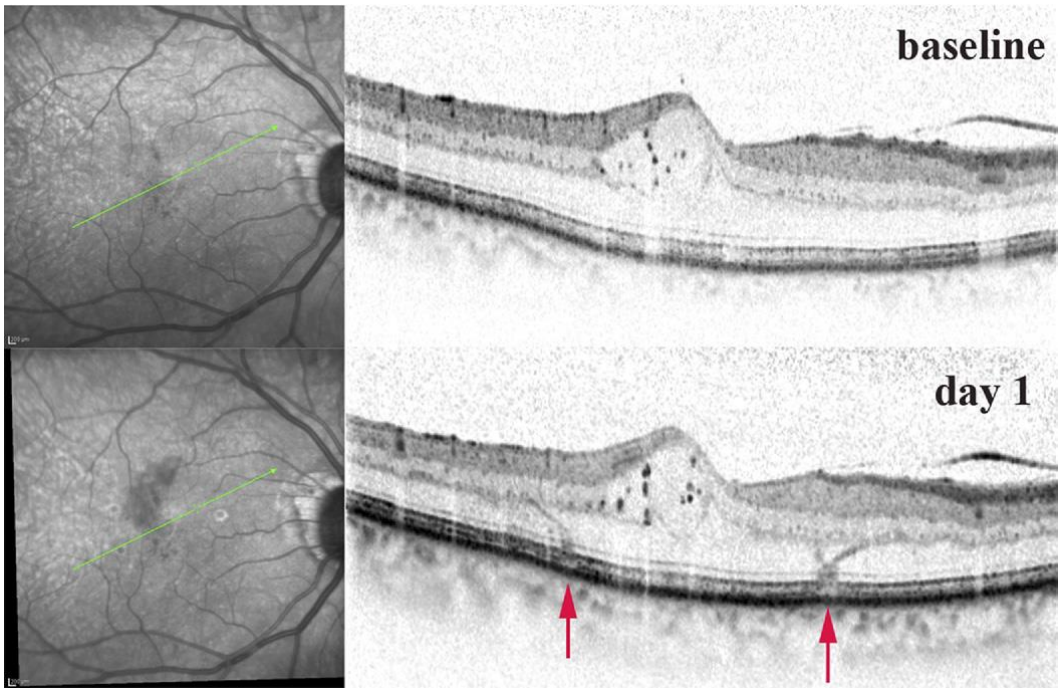

Figure 20.: Morphologic alterations after a single spot laser treatment in 1 patient. Comparable findings to those after grid pattern treatment were detected in infrared imaging (left) and OCT (right) before (upper line) and 1 day after laser treatment (lower line). Laser lesion site (red arrows) at the level of the pigment epithelium.[123]

6.2.2 Biometric Retinal Changes

At baseline, mean central retinal thickness measured in the central millimeter was 436±124 µm. On day 1, mean CRT was 434±119 µm (P = 0.7). The CRT was decreased in 7 patients (range, −3 to −34 µm) and increased in 6 patients (range, 1–40 µm). A decrease was observed specifically in 3 patients with subretinal fluid at baseline (−34 µm, −17 µm, and −21 µm).

In those patients with a decrease in CRT on day 1, local thickening was observed in the parafoveal area altered by the laser lesions. The scans of 2 patients on day 1 and the corresponding thickness profiles automatically generated by the Spectralis software are shown in Figure 21A and B. The black curve indicates the actual retinal thickness profile of the section shown above. The green area above the curve indicates a decrease, and the red area under the curve indicates an increase in the local retinal thickness compared with baseline. In both patients, there was a decrease in CRT indicated by the green area, but

also local swelling at the site of the laser lesions (indicated by the red area in the thickness profile).

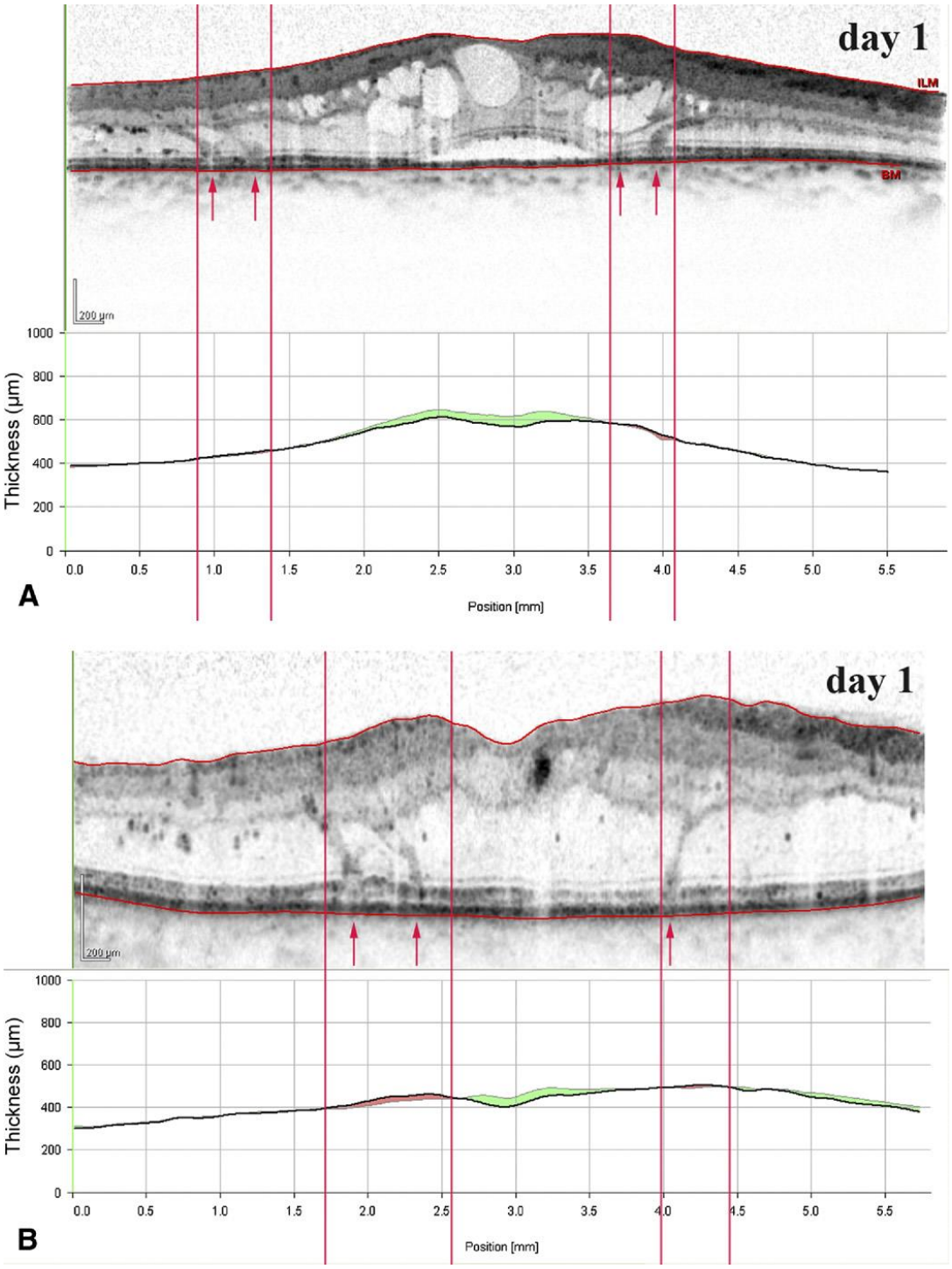

Figure 21.: Biometric changes 1 day after the laser treatment in 2 patients. The upper image shows the OCT scan at day 1; the lower image shows the thickness profile (see text). The vertical red lines indicate the laser lesion site in OCT and of retinal thickening

in the thickness profile. Laser lesion site (red arrows) at the level of the pigment epithelium.[123]

A comparison of the baseline and day 1 findings in the same patient shown in Figure 21B is shown in Figure 22. The laser lesions caused measurable local thickening at the level of the PRL. In this patient, the distance between the outer border of the RPE and the inner border of the inner and outer photoreceptor segment junction was 48 µm at baseline and 78 µm on day 1.

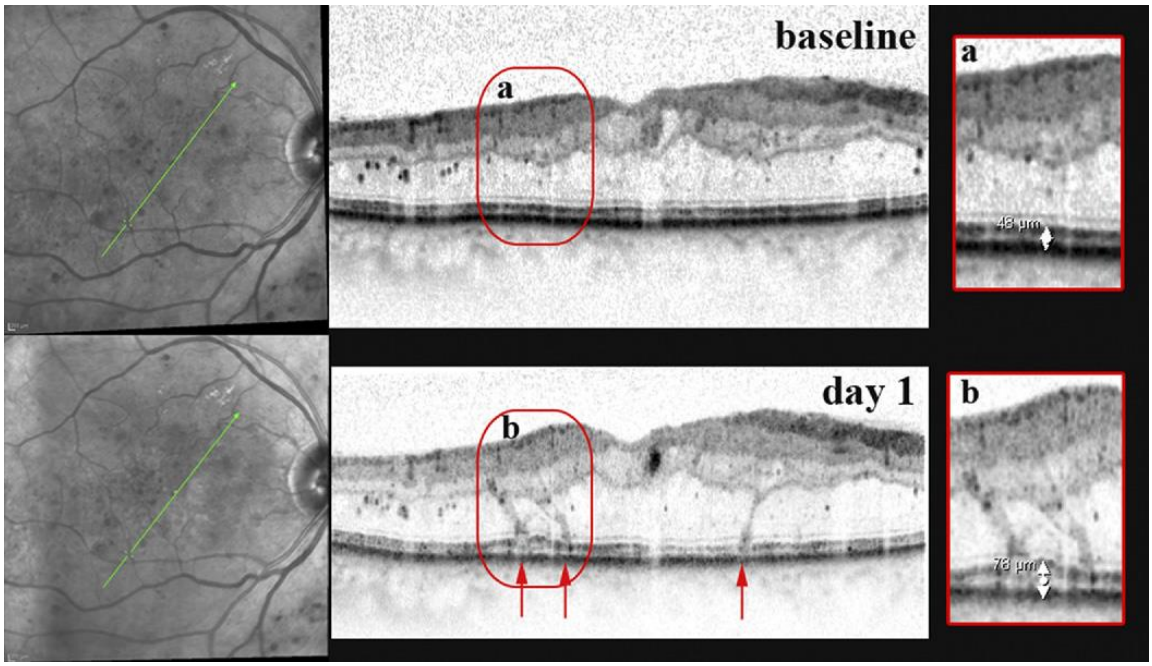

Figure 22.: Local retinal thickening at the laser lesion site. Infrared (left) and OCT (middle) findings in the patient from Figure 21B before (upper line) and 1 day after (lower line) grid laser treatment. The red box indicates the area of magnification shown on the right.[123]

6.3 In vivo morphology of retinal changes following sub-threshold panretinal photocoagulation

The mean age of the patients was 60.7 years (28-79 yrs.). 2 patients had type 1 and 6 type 2 diabetes mellitus. The mean duration of diabetes was 26 years. The duration of symptoms in the two patients with central retinal vein occlusion (CRVO) was 7 and 12 months. At baseline the mean visual acuity of all patients was 0.5 logMAR (SD±0.57), at the end of the study 0.68 logMAR (SD±0.62). Two patients developed a vitreous hemorrhage and were dropped from the study (both after month 3). The laser settings of the titration lesions and the fluences for each patient are shown in Table 1.

Table 1.: The mean laser parameters of the titration lesions.

	Threshold				1/2 Fluence			
Patient	**Power (mW)**	**Spot size (µm)**	**Time (ms)**	**Fluence (J/cm²)**	**Power (mW)**	**Spot size (µm)**	**Time (ms)**	**Fluence (J/cm2)**
1	1025	200	20	65	500	200	20	32
2	650	200	20	41	300	200	20	19
3	450	200	20	29	225	200	20	14
4	1300	200	20	83	650	200	20	41
5	625	200	20	40	325	200	20	21
6	1150	200	20	73	575	200	20	37
7	925	200	20	59	500	200	20	32
8	1900	200	20	120	950	200	20	60
9	875	200	20	56	400	200	20	26
10	1000	200	20	64	500	200	20	32
Mean (±SD)	990 ±409	200 ±0	20 ±0	63 ±26	493 ±207	200 ±0	20 ±0	31 ±13
	1/4 Fluence				1/8 Fluence			
Patient	**Power (mW)**	**Spot size (µm)**	**Time (ms)**	**Fluence (J/cm2)**	**Power (mW)**	**Spot size (µm)**	**Time (ms)**	**Fluence (J/cm2)**
1	250	200	20	16	125	200	20	8
2	150	200	20	10				
3	100	200	20	6				
4	325	200	20	21	150	200	20	10
5	150	200	20	10	100	200	20	6
6	300	200	20	19				
7	225	200	20	14	100	200	20	6
8	475	200	20	30				
9	200	200	20	13				
10	250	200	20	16	130	200	20	8
Mean (±SD)	243 ±107	200 ±0	20 ±0	16 ±7	120 ±21	200 ±0	20 ±0	8 ±2

6.3.1 Morphology of laser burns during the follow-up

6.3.1.1 One hour

On color fundus photography threshold laser burns were visible as light gray spots with blurry contour. Sub-threshold burns with halved fluence became visible in 20% of our cases one hour after treatment, and were seen as barely visible light gray spots. Otherwise they were not visible. Laser burns with lower fluence were never detectable on CFP. Fundus autofluorescence showed barely visible hypofluorescence of the RPE with the threshold and halved fluence burns while on infrared (IR) and red free (RF) images they were clearly visible. Lower fluences were not detectable with any of the mentioned imaging modalities. On SD-OCT threshold laser burns and halved fluence laser burns showed similar changes: hyperreflectivity in the outer nuclear layer (ONL), and relative hyporeflectivity in the photoreceptor layer (PRL). Irregularities in the retinal pigment epithelium (RPE) were also seen in both groups. Although during the laser treatment the same spot size setting was used, the halved fluence lesions had a smaller transverse diameter (Greatest linear diameter (GLD)) than threshold lesions (234±52 µm vs. 402±42 µm mean±SD respectively measured on SD-OCT). Laser burns created with quarter or lower energy flux were undetectable on OCT. (Figure 23. and Figure 24.)

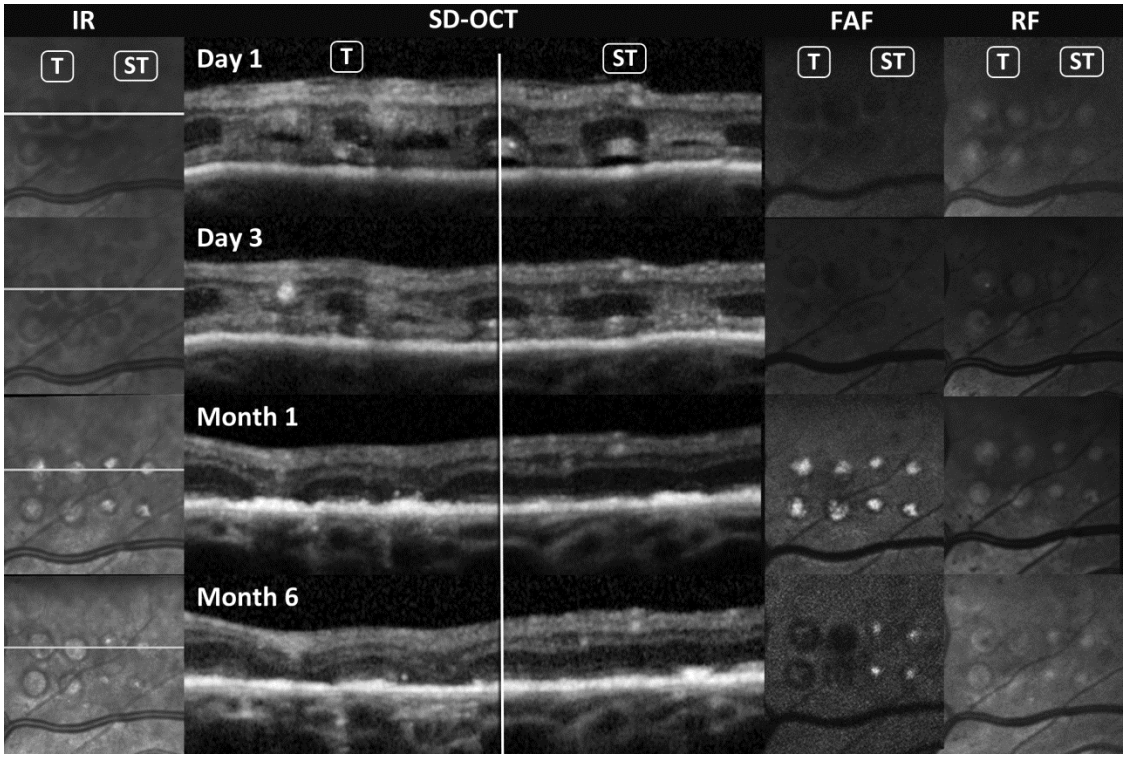

Figure 23.: The images of patient 4 during the 6 month follow-up. Left the Infrared reflection images (IR) showing the section of the OCT scan in relation to the laser lesions. Both the threshold (T) and halved fluence sub-threshold (ST) lesions gain reflectivity during the follow-up. The difference in the size of the lesions is clearly visible. SD-OCT images of the threshold and halved fluence lesions: at Day 1 the intraretinal vacuole formation and subretinal fluid accumulation between the burns is visible that almost complete resolves till day 3. The typical archway structure is seen in the threshold lesions at month 1 and 6 with a wide PRL defect an RPE loss. The halved fluence burn (the nasal one is not well centered on the scan) develops no ONL atrophy, and there is no sign of RPE loss around the central RPE/glial proliferation. Nevertheless the PRL only reaches the edge of the proliferative tissue, and no reorganization is seen in the central lesion area. On fundus autofluorescence the slowly developing central hyperautofluorescence is seen with the absence of atrophy ring around the halved fluence lesions. On the right side red free (R) images of the lesions are shown.[124]

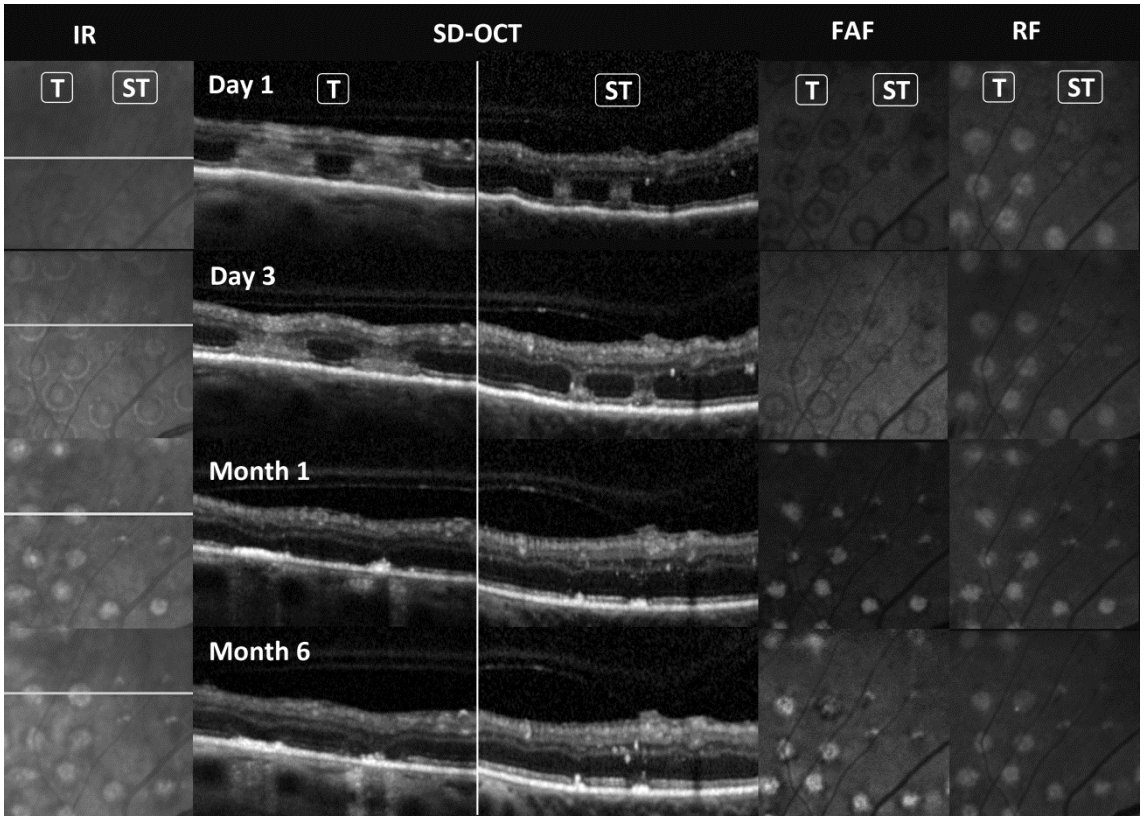

Figure 24.: IR and separate SD-OCT images of the threshold and sub-threshold laser spots accompanied by the FAF and RF images of a patient during the follow-up. At month 1 and six there is a centripetal reorganization of the PRL and external limiting membrane (ELM) in the halved fluence (ST) laser burns.[124]

6.3.1.2 Day one and three

On CFP threshold burns became more prominent. In 3 eyes sub-threshold burns were barely visible. On FAF both threshold and sub-threshold burns became less hyporeflective. On SD-OCT a discrete retinal thickening was observed on day 1 which lessened by day 3 and was more prominent at the site of threshold burns. The hyperreflectivity of the ONL was unchanged, but intra-retinal "vacuoles" developed between the ONL and the PRL in 4 of the eyes. Furthermore sub-retinal fluid (SRF) was observed in three eyes between the laser burns. In these cases an irregular thickening of the choroid around the laser burns was also seen. (Figure 23. and Figure 25.). All of these signs decrease by day 3.

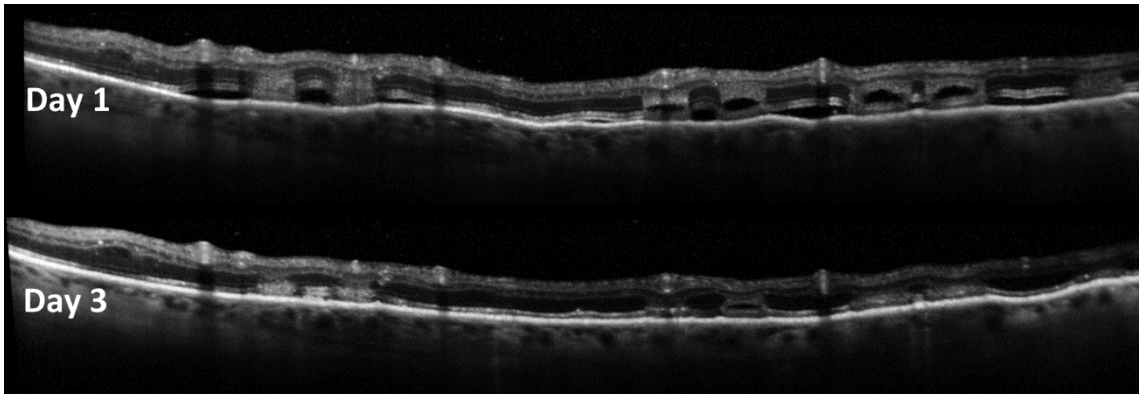

Figure 25.: SD-OCT image of sub-retinal fluid accumulation and intra-retinal vacuole formation 1 day following laser surgery.[124]

6.3.1.3 Week one

On CFP and biomicroscopy the acute whitening of the laser burns had begun to diminish and the burns were best seen in indirect light. The sub threshold burns became invisible at this time. On FAF a distinct hyperfluorescence surrounded by a hypofluorescent ring had begun to develop. On SD-OCT the intraretinal fluid (if previously present) together with subretinal fluid had disappeared, and the RPE had flattened out. Simultaneously the retinal thickness had decreased. The hyperreflectivity of the ONL was replaced with a downward shift of the inner layers forming the typical archway figure described in chapter 6.1.2.[121] This archway structure was either not present or only moderately visible in the halved fluence burns.

6.3.1.4 Month one

On ophthalmoscopy the threshold laser burns had started to pigment, and were surrounded by an atrophy ring. The sub threshold burns were either invisible or seen as small pigment irregularities. On FAF both threshold and sub threshold burns showed hyperfluorescence with surrounding hypofluorescence. The only difference was the size of the lesions, the sub-threshold burns being smaller, and often irregular. On SD-OCT in the threshold burns the archway configurations had stabilized or in some cases had lessened. In the PRL/ RPE layers a central hyperplasia of the RPE was seen surrounded by a ring of atrophy (window defects seen on OCT). The PRL was destroyed in the whole region of the laser burn. In case of the sub-threshold burns only a minimal thinning of the ONL layer was observed, and no archway configuration was present. The RPE had a

similar hyperplasia in the center of the burn, but the surrounding atrophy was much more discrete than for threshold burns. In some cases an impending closure of the defect of the PRL was seen as the PRL band together with the external limiting membrane (ELM) started to reappear at the edges of the lesions as seen in Figure 24.

6.3.1.5 Months two through six

During months 2 through 6 the changes seen on CFP and FAF at month 1 remained unchanged, and on SD-OCT the diameter of both threshold and halved fluence burns have further shrunk 295±63 µm (73,5% of original GLD), 147±81 µm (61,7% of original GLD) respectively. Both changes were statistically significant ($p<0.0001$). No changes were seen in the threshold laser burn morphology, but in 40% of the patients a further centripetal reappearance of the PRL and ELM was observed in the sub-threshold laser burns, as the PRL band reached and in some cases overlapped the central RPE hyperplasia/ glial proliferation (Figure 24.).

Furthermore as shown in Graph 1. and Graph 2. there was no significant correlation between the laser fluence used and the greatest linear diameter of the lesions at month 6 neither in the threshold nor in the halved fluence lesion groups ($r2=0.03$ $p=0.405$ and $r2=0.025$ $p=0.458$ respectively).

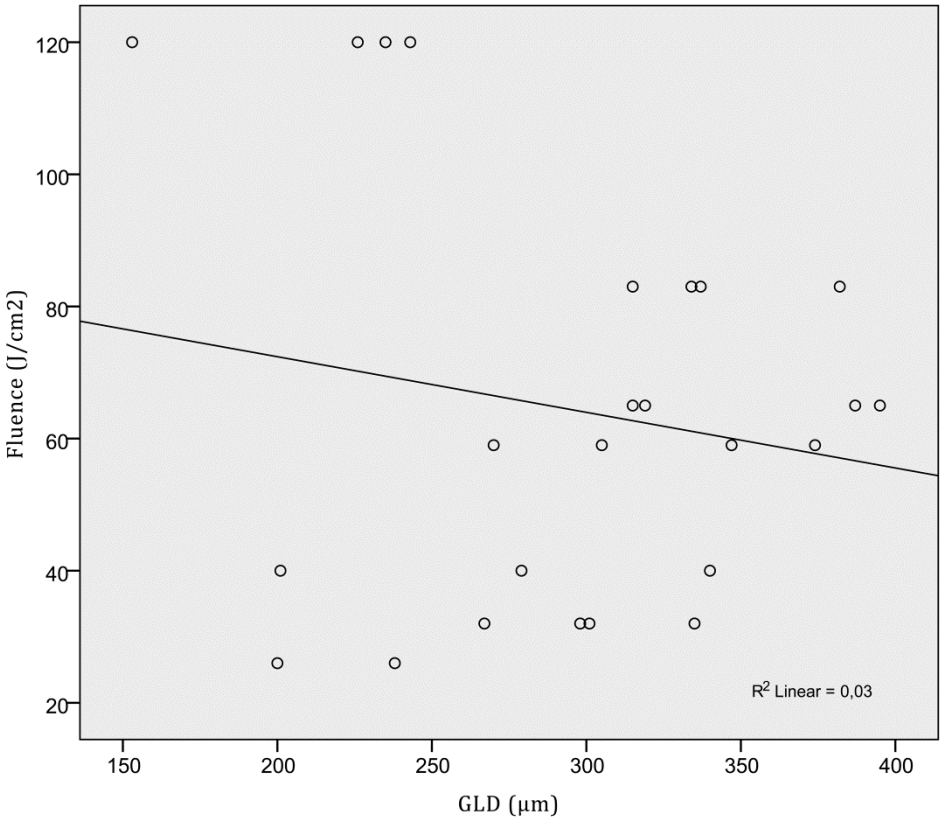

Graph 1.: Scatter plot diagram of the greatest linear diameter (GLD) measured at month 6 of the threshold laser burns in relation to the fluence used to create them.[124]

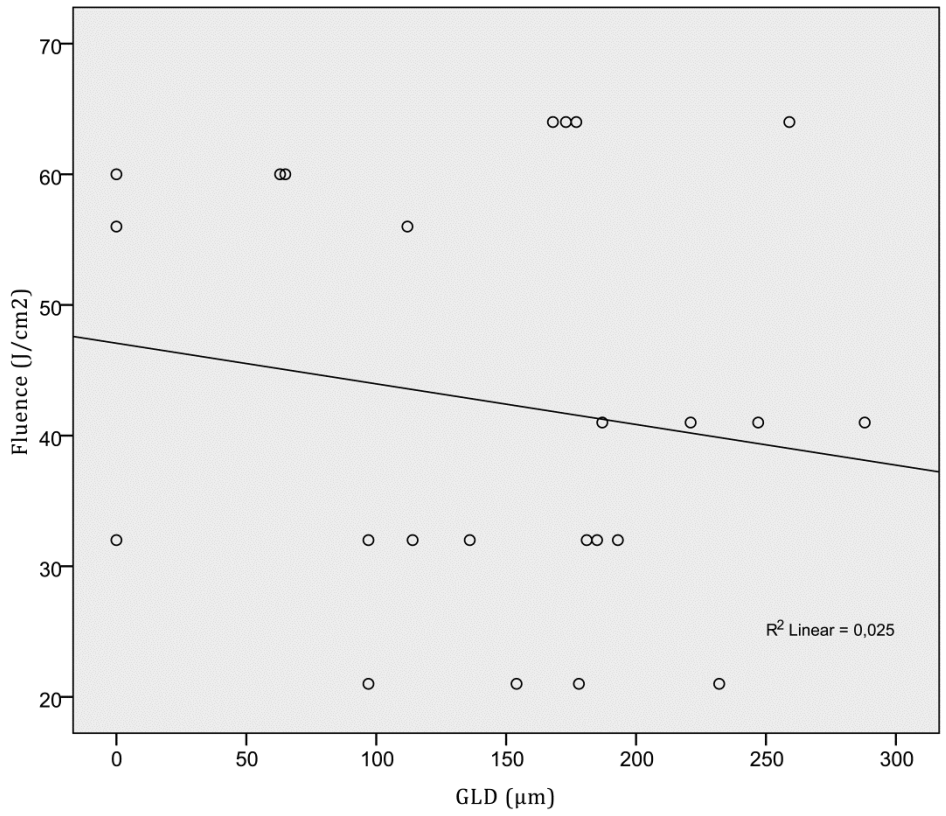

Graph 2.: Scatter plot diagram of the greatest linear diameter (GLD) measured at month 6 of the halved fluence laser burns in relation to the fluence used to create them.[124]

6.4 Hyperreflective foci on OCT in patients with diabetic macular edema and their response to macular photocoagulation

The mean age of the patients was 57 yrs. (range: 44-68 yrs.). All patients (6 male and 7 female) suffered from type 2 diabetes mellitus. At baseline, the mean retinal thickness in the central 1mm ETDRS field was 381µm ± 130µm (mean ±SD). At the end of the follow-up period, the mean central 1mm retinal thickness was 344µm ± 117µm (mean ±SD). The eye tracking system of the Spectralis OCT© enabled the capturing of SD-OCT images exactly with the same topography from baseline throughout the subsequent visits allowed to determine the thickness change at the thickest retinal position (TRP) (measured at baseline) throughout the study. The mean change of the TRP at the end of the four month interval was -55µm ± 117µm (mean ±SD) with an initial TRP value of 535µm±117µm

and a final TRP of 480µm±127µm. There was a one ETDRS line visual acuity improvement during the follow-up (baseline: 70±12, month four: 75±13).

At baseline, distinct hyperreflective foci representing early lipid deposits were evenly scattered throughout all retinal layers in eyes with DME. During follow-up, the localized resorption -therapy response- or the progressive accumulation of intraretinal fluid in localized non-responder areas had a major impact on the dynamics and amount of lipid foci in these areas. Four characteristic patterns were identified following photocoagulation, which are presented in Table 2.

Table 2.: Retinal thickness measurements and distribution patterns of the hyperreflective dots in Optical Coherence Tomography (OCT) at the baseline and final visits.

Patient No	ROI No	Baseline CRT	Baseline TRP	Baseline pattern of lipids	Final CRT	Final TRP	Final patter of lipids
1	1	364	524	Diffuse distributed dots with 1-1 larger foci	403	508	large conglomerate (hard exudate, HE) at the apex of the ONL
1	2			Diffuse distributed dots with 1-1 larger foci			Diffuse distributed dots
2	1	452	685	Moderate amount of small foci in the ONL and INL	259	625	Large number of foci in ONL
2	2			Large amount of dots in the ONL, INL and GCL			No foci visible
3	1	262	463	Large conglomerate	287	400	Larger conglomerates
4	1	550	575	Large conglomerate	707	809	Smaller dots in the ONL and INL
5	1	253	270	Small amount of foci in the ONL	210	300	No foci visible
6	1	266	465	Diffusely distributed foci	271	399	Diffusely distributed foci
6	2			No foci visible			Medium sized conglomerate
7	1	484	556	Diffusely distributed foci	432	446	Downward shifting of foci
7	2			Diffusely distributed foci			Diffusely distributed foci in different positions
8	1	414	640	Large conglomerate in the ONL	260	369	Smaller foci in the ONL
8	2			Large conglomerate in the ONL			Large conglomerate in the ONL
8	3			Diffusely distributed dots			Downward shifting of foci
9	1	667	713	Diffusely distributed foci	516	538	Diffusely distributed foci
9	2			Diffusely distributed foci			No foci visible
10	1	392	537	Diffusely distributed dots	360	471	No foci visible
10	1			Diffusely distributed dots			Diffusely distributed dots
11	1	275	559	Large conglomerate surrounded by diffuse foci	226	462	Large conglomerate surrounded by diffuse foci
11	1			Diffuse distributed dots with 1-1 larger foci			Downward shifting of foci
12	1	322	512	Diffusely distributed dots	297	442	Downward shifting of foci
13	1	251	475	Diffusely distributed foci	245	465	Diffusely distributed foci in different positions

(ROI= Region of interest, CRT = Central retinal thickness, TRP= Thickest retinal position, ONL= Outer Nuclear Layer, INL= Inner Nuclear Layer, GCL= Ganglion Cell Layer, HE= Hard Exudate)

6.4.1 Resorption of intraretinal lipids

A localized decrease in retinal edema was associated with a resolution and a decrease in the amount and density of foci (Figure 26. area marked with rectangle). The infrared (A) and color fundus images (B) demonstrate no hard exudates, or microaneurysms in the scanned area at baseline. In the baseline scan (C), marked hypo-reflectivity and cystoid swelling of the outer nuclear layer (ONL) can be observed. Multiple hyperreflective foci are present mainly in the ONL, but also in the outer plexiform (OPL) and inner nuclear layers (INL). One day after focal laser coagulation (D), an increase in the level of ONL thickening and in the number of hyperreflective foci in the ONL has occurred. Three months following treatment (E) the outer nuclear layer swelling gradually decreases. Hyperreflective microexudates resolved completely In the INL and OPL and partially in the ONL. One month later (F – month 4), focal retinal thickening has resolved completely together with the disappearance of hyperreflective dots in all retinal layers of the marked area.

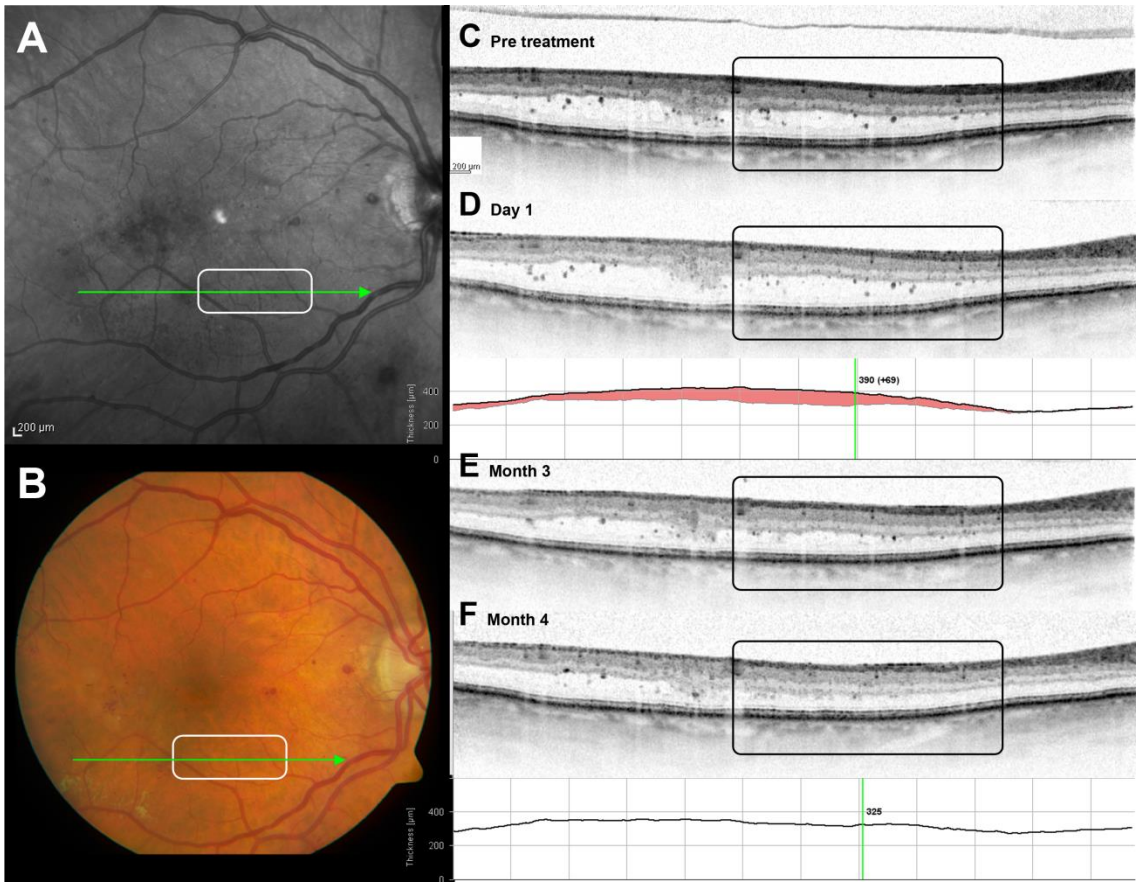

Figure 26.: The resorption of hyperreflective foci in a 4 month follow-up.[125]

6.4.2 Condensation of microexudates to clinically visible hard exudates

In case of decrease in local retinal thickness hyperreflective foci located throughout all retinal layers moved toward the apical region of the ONL, and formed condensed larger hyperreflective conglomerates. These conglomerates were identified as hard exudates in fundus photography. In Figure 27, the 4 month follow-up images of a 47 years old male patient are shown. In the fundus photography, a microaneurysm in the nasal inferior parafoveal region (center of the marked region) appears clearly visible on the pre-treatment images (A). During laser treatment, one laser spot was applied to this region to occlude the microaneurysm. By color fundus imaging, hard exudates are absent in the area of the microaneurysm at the baseline visit. Three month after laser treatment (B), focal thickening and appearance of hyperreflective dots at the level of the outer nuclear layer is seen in SD-OCT. The infrared image indicates the localization of the scan – slightly superior to the microaneurysm. On the color fundus image taken during the same visit, hard exudates are visible inferiorly to the microaneurysm, but not superiorly where the scan was taken. One month later (C), the focal retinal thickening has resolved, and the hyperreflective foci have accumulated and have become confluent in the apical zone of the outer nuclear layer involving the outer plexiform and inner nuclear layers. In the color photography hard exudates are visible in the scan area as well. A similar but more prominent process is seen in Figure 28. In the baseline image (A) circinate hard exudates are visible in the color and infrared images. In the corresponding areas (ellipse and right side of square) large hyperreflective conglomerates are present in OCT. Four month later (B) the hard exudates have partially resolved (encircled area) in OCT the corresponding hyperreflective conglomerates became smaller. In the area marked with a square the hard exudates flared out, and reached the scan line in a greater extent. In OCT it is clearly visible that the center area of the square where at baseline a cystoid swelling of the ONL and disseminated small hyperreflective foci were seen has thinned during the follow-up, and the ONL is filled with large hyperreflective conglomerates corresponding to the hard exudates seen in the infrared image.

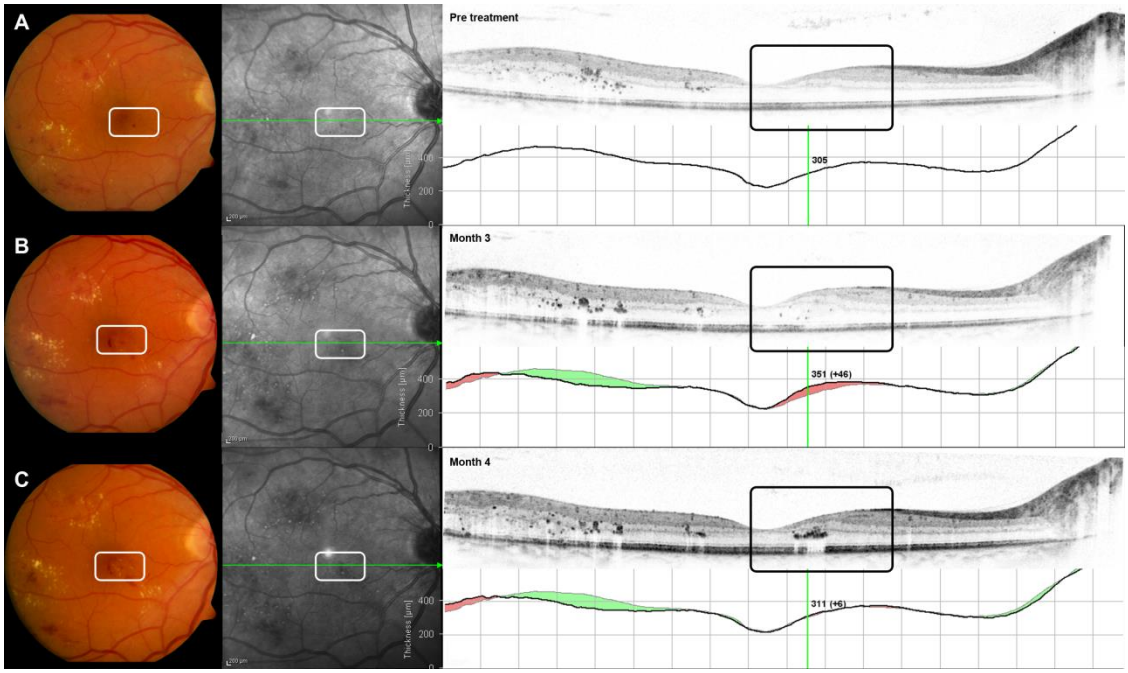

Figure 27.: Hard exudate formation.[125]

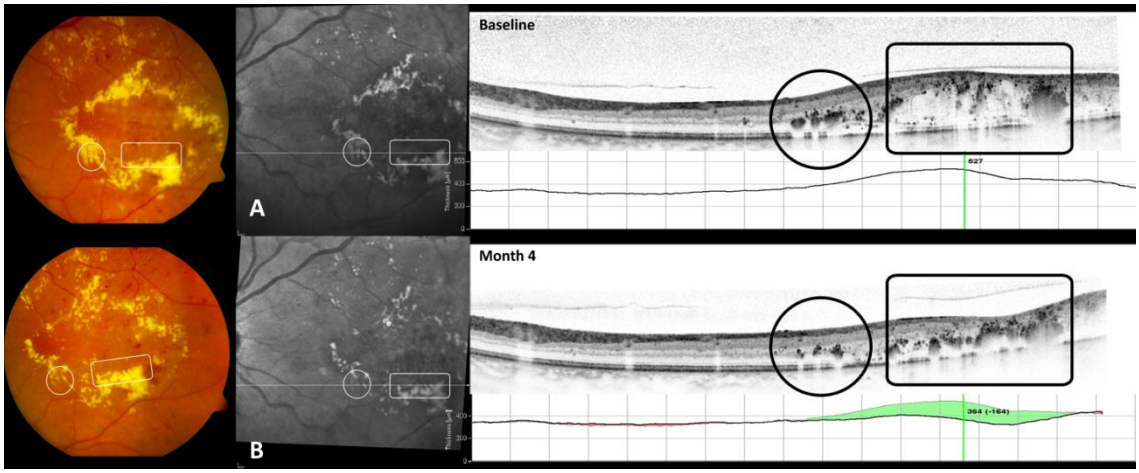

Figure 28.: Formation of hyperreflective conglomerates. (A) Baseline, (B) 4 months follow-up.[125]

6.4.3 Dynamic shifting of microexudates with persisting retinal swelling.

In the event of stable retinal thickness or further retinal thickening, hyperreflective foci were seen in multiple retinal layers throughout the follow-up period. Occasionally some foci stayed at the same location throughout the study, but mainly a dynamic shifting of

foci was seen. In the area marked in Figure 29. retinal thickness slightly increases throughout the 4 months associated with a various number and density of hyperreflective lesions seen in multiple retinal layers. Overall there is a marked fluctuation in the topography of these hyperreflective dots, although there are certain foci that appear to be unchanged in respect to location and shape during the entire study.

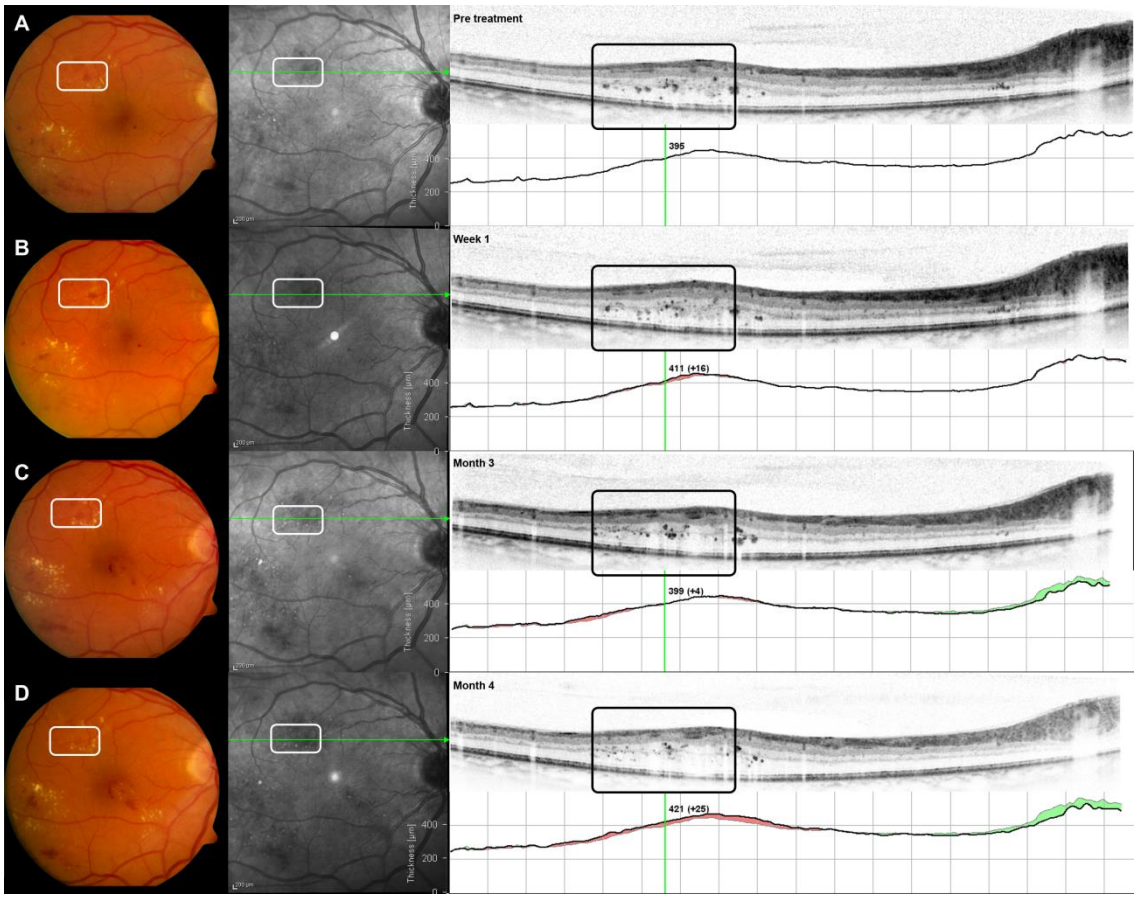

Figure 29.: Dynamic shifting of hyperreflective foci with persisting retinal swelling.[125]

6.4.4 Dissemination of clinical hard exudates into multiple hyperreflective foci

In case of continuous retinal swelling in areas where hard exudates were seen at baseline the disappearance of the hard exudates were seen on fundus photography. In these cases in OCT the dissemination of hyperreflective conglomerates in to multiple hyperreflective foci were seen. Figure 30 illustrates the retinal appearance and morphology of a 53-year-

old female patient showing clinically significant DME with hard exudates at baseline examination (A). The lipid exudates (marked area) are clearly visible in both, fundus photography and IR image. In the SD-OCT scan, a dense hyperreflective area is seen at the level of the outer nuclear/outer plexiform layer consistent with the location of the hard exudates ophthalmoscopically. There are several hyperreflective foci in this area spread out through all layers of the retina. One month after the laser treatment (B), there is an increase in retinal thickening. The hyperreflective area, however, remained unchanged in shape and location. The hyperreflective foci in the vicinity of the hard exudate moved towards the border of the outer nuclear/outer plexiform layer. Four months after treatment (C), there is further increase in the amount of intraretinal fluid, and an accumulation of subretinal fluid has occurred. The hard exudate disappeared ophthalmoscopically and in the infrared image. In the SD-OCT scan, the large hyperreflective deposit has dissolved into two smaller hyperreflective foci, located at INL and ONL. Most of the hyperreflective foci previously seen in the outer nuclear layer have disappeared, but there are numerous novel hyperreflective foci in the outer plexiform and inner nuclear layers.

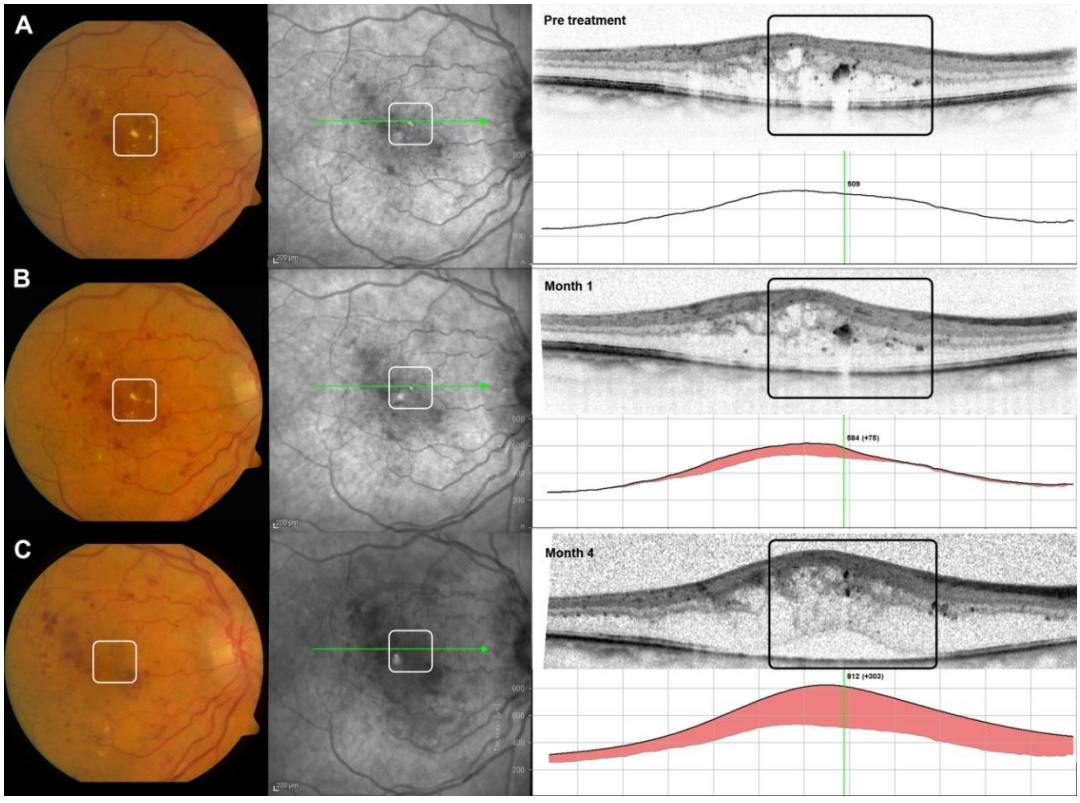

Figure 30.: The dissemination of a hard exudate into smaller hyperreflective foci.[125]

7 Discussion

Laser therapy has been the gold standard treatment for a number of retinal diseases until recent advents in intravitreal pharmacologic therapies.[25–29,118] Laser is still an important therapeutic procedure, it is performed every day in ophthalmic care centers around the world, and will be performed on millions of patients in the future.[35,36,113]. A novel laser improvement called short pule continuous wave lasers were recently introduced. These devices deliver laser energy in a ten times shorter time period than in conventional lasers. Animal models using this laser delivery method showed reduced collateral damage both in the inner retinal layers as well as around the laser spots. In our examinations provide evidence, that short pulse laser induces similar laser burn morphology in the human retina then in animal models. Our OCT results were very similar to the histological reports of Jain et al., that threshold laser lesions with created with 20ms pulse duration did not affect the inner retina, but confined in the outer retinal layers.[44] Furthermore follow-up examinations these lesions showed similar healing response as described by Paulus et al. in their animal studies.[13] They showed that light-moderate lesions with 20ms pulse duration showed focal swelling of the retina an hour after laser, which subsided at day 1, and damaged photoreceptors were replaced by hypertrophied glia and hyperpigmented RPE cells. Furthermore they described a significant reduction in spot size (40%). In case of barely visible and invisible laser lesions (produced with 7ms and 5 ms pulse duration) they found initial photoreceptor damage and glial proliferation, which was replaced with migrating photoreceptors form neighboring retinal areas, and retinal morphology normalized by 4 month post-laser. The results we observed on OCT in the human retina are very much in line with these animal model changes. Threshold laser lesions showed hyperreflective scars in the level of the RPE and photoreceptors, and the size of the lesions did decrease during the follow-up period (although not as much as in the animal models). Invisible sub-threshold laser burns showed even less damage in the retina, and with time the damage in the photoreceptor layer decreased in many cases resembling the photoreceptor shift seen in the aforementioned animal models.

A major shortcoming of our results, that we can’t draw conclusions about the clinical implications of short pulse lasers. Although there is a clear theoretic advantage in sparing

the inner retina (within the nerve fiber laser) in terms of collateral damage in visual field and night vision, our study design and cohort size did not allow to examine such effects. Muqit et al found favorable PDR regression with short pulse lasers, but more laser burns were necessary to control the disease than with conventional lasers.[126] The same group also examined central and peripheral visual fields after laser therapy and found improvements in central visual fields after panretinal laser photocoagulation.[127,128]

In the following chapters we will discuss our results, and review current relevant literature for each study separately.

7.1 In vivo examination of retinal changes following panretinal photocoagulation

Diseases of the modern "Western world" lifestyle, mainly diabetes and hypertension, the so-called diseases of civilization, affect a growing population worldwide. The consequences of these diseases have generated an immense demand for modern, effective therapy. In the field of retinal vascular disorders, laser photocoagulation is still considered to be a "gold standard" intervention for multiple different indications. Current scientific efforts are focused on improving laser therapies with regard to enhancing the therapeutic benefit, minimizing the negative side effects, as well as simultaneously improving patient and operator comfort and efficiency. The PASCAL laser system used in our study, fulfill the requirements for modern treatment, and enable the application of a large number of laser spots in 1 second, minimizing patient discomfort and pain by shortening the laser pulse duration and optimizing the treatment dose by providing identical laser parameters, leading to homogenous effects.[117] Because photocoagulation may be associated with negative side effects resulting in visual impairment, the aim of recent studies has been to determine the optimal treatment parameters required to achieve an adequate therapeutic benefit, but reduce unwanted damage.[37,47] This issue has been investigated in clinical trials comparing "light" or "subthreshold" versus "classic" photocoagulation with varying laser energies or laser exposure times.[44,129–131] In these studies, "light" photocoagulation was superior to classic treatment, showing good therapeutic efficacy and a lower rate of adverse effects. The most informative way to document the effect of laser energy on the

retina, layer by layer, is histologic evaluation of the photocoagulated tissue. In previous studies, animal models were routinely used to test different laser settings.[13,132–134]

Although these animal model studies provided essential basic information, the findings have limited applicability because the conditions in the animal models differ from the physiology in the diseased human eye, and, most important, preclude a continuous follow-up of lesions to examine the characteristic healing response. However, SD-OCT is an ideal tool to provide in vivo, high-resolution imaging of retinal tissue with repeated evaluation of identical spots over time. The Spectralis OCT system used in our study captures high-definition images with exceptional signal to noise ratio. Although the resolution is not the same as that of histology, it is sufficient to clearly distinguish the components of the retinal layers. Together with the PASCAL laser system, the Spectralis OCT offers ideal conditions for evaluating laser tissue damage and the healing response.

Our study characterized the effect of thermal laser energy on the human retina in vivo, observing early primary alterations and subsequent secondary changes. We defined laser power settings dependent on the ophthalmologic visibility of the laser burn, visualized as a grayish spot. The PASCAL system creates regularly spaced and evenly sized laser spots with a similar histologic appearance. Early after treatment (Figure 14.), there was no clear change in the inner retinal layers of the coagulated tissue, but structural disorganization was observed from the OPL to the RPE. These results are consistent with findings of histologic studies done on animal models. After application of laser energy comparable to the settings used in our study, alterations mainly appeared in the outer retinal layers with detachment of the PRL from the RPE with inward bulking of the neural retina due to extensive exudation.[13,133] This early localized destruction characterizes the primary photocoagulation effect. The SD-OCT images show hyperreflectivity and a granular appearance of the ONL, which likely corresponds with the focal necrosis and pyknosis observed in histologic preparations. Over time, the cellular swelling recedes and the edema is reabsorbed. The lesions shrank continuously and atrophic scarring occurred, most impressively at the level of the PRL and RPE (Figure 15.). After 1 month, however, the organization of the intraretinal layered pattern had partially recovered and continuous SD-OCT imaging revealed an unprecedented intraretinal pattern: owing to comprehensive shrinking of the ONL, the OPL and the INL formed archway-like

structures between the laser spots (Figure 16.). Over time, the layer structure partially recovered and the misalignment eased. Simultaneously, the atrophic PRL was invaded and replaced by tissue, which, on our high-resolution images had the reflectivity of RPE cells, resulting in a hyperreflective prominent scar with large pigment clumps. Realignment of the intraretinal layers, photoreceptor degradation, and replacement by migrating cells constitutes the active secondary healing phase. The present findings are consistent with the results of several histologic studies based on animal models.[13,131,133–135] Histologic analyses in several animal models have demonstrated a strong correlation between laser power and retinal damage, highlighting the importance of determining laser treatment parameters with maximum therapeutic benefit, but minimal collateral injury.[13,133] These findings, together with the results of several human clinical trials, suggest that "light" photocoagulation performed with a short duration continuous laser provide the necessary treatment effect on the retinal level. The combination of modern laser systems and high-definition OCT techniques providing superior image resolution offer the opportunity to monitor the therapeutic effects.

7.2 In vivo examination of retinal changes following macular grid and focal photocoagulation

The present study examined the immediate morphologic and biometric retinal changes secondary to macular grid laser treatment performed with a short duration continuous laser in patients with DME using SD-OCT. Characteristic morphologic alteration patterns were detectable in the outer retinal layers already at day 1. These alterations were visible as oblique hyperreflective changes in the ONL, changing their direction at the level of the ELM and continuing sagittally through the PRL and RPE. Clear biometric changes were also observed on day 1, indicating an immediate effect, although these changes were not statistically significant.

The characteristic intraretinal morphologic alterations after laser treatment observed in this study may be explained by several phenomena. The finding that the photocoagulation lesions were not sagittal might have been due to an imaging artefact.[136] In several OCT devices, scan images are aligned to a certain extent to improve morphologic or biometric analysis. This kind of post-processing could induce changes in the orientation of the

morphologic retinal details, such as laser lesions. However, this would not explain why the laser pathway changes its direction at the level of the ELM. Thus, this explanation seems rather unlikely.

It can also be discussed whether the central grid laser lesions penetrated the ONL in a diagonal manner rather than sagittally because of a change in the intraretinal refractive index caused by retinal swelling. This could also cause changes in the light and laser light pathway through edematous retinal layers. This explanation, however, also seems unlikely because the difference between the refractive indices of the vitreous and the retina, be it in edematous or physiologic condition, is not remarkably different.

There may be an immediate thermal photocoagulation effect. The grid itself consists of several homogenous single laser spots produced almost at the same time in a ring-shaped pattern. This could induce an immediate scarring reaction, leading to a centrifugal contraction at the level of the RPE and PRL in the area of the grid pattern. The oblique ONL lesions observed in OCT might emerge secondarily because the inner retinal layers do not follow this centrifugal outer layer shift. Bruch's membrane consists of not only collagenous but also elastic fibers, possibly inducing a shift of the RPE/PRL complex if coagulated. Accordingly, there was no significant transverse shift of the intraretinal structures in the inner retinal layers after laser therapy (Figure 18.), corroborating this theory. However, in SD OCT a transverse shift of distinct preexisting hyperreflective areas within the outer retinal layers (RPE or PRL) could not be identified either.

Another explanation for these results may be found in the physiologic retinal morphology. The shape of the laser lesions complies remarkably with the intraretinal orientation of sagittal rods and cones and the subsequent rather oblique inner part of the ONL the Henle's layer. Photocoagulation induces a thermic effect at the level of the RPE and PRL, possibly spreading retrogradely into the layers above according to the intraretinal cellular architecture. This has not been described in animal studies on histologic retinal changes after laser treatment, which again can be explained by differences in retinal architecture between, for example, rabbits (not having a foveal retinal excavation) and humans. Only in the human or primate fovea, rods and cones are oriented sagittally, and all subsequent layers are displaced laterally causing an oblique orientation. Even if the distinct intraretinal layer distribution can be analyzed in SD OCT in detail, until now the exact

cellular orientation in each layer itself could not because of a lack of imaging resolution. Thus, according to this theory, these early alterations secondary to laser treatment visualize the normal histologic architecture of coagulated photoreceptor complexes, beginning at the outer segment of the photoreceptors and ending in the ONL.

Nevertheless, these explanations are hypothetic and were not examined or authenticated in the present study. It does not seem to be a phenomenon typical to only the PASCAL laser grid pattern. Comparable results were also observed in a patient treated with a single spot photocoagulation (Figure 20.) In addition to the morphologic changes, at day 1 there were already clearly measurable biometric changes, although they were not statistically significant. It is not clear why there was local thickening in the PRL at the lesion sites (Figure 22.). This could be explained by a thermal effect or a transversal RPE/ PRL wrinkling according to the centrifugal outer retinal layer shift theory. Studies of how to analyze these morphologic changes over time and the impact of these morphologic changes on retinal function are in progress.

7.3 In vivo morphology of retinal changes following sub-threshold panretinal photocoagulation

In our study we demonstrated that laser fluence levels half of the level used to produce threshold laser burns produce distinct morphologic changes in the retina as imaged with SD-OCT, fundus autofluorescence and color fundus photography. The laser burns created with halved fluence showed similar characteristics to threshold burns, but were smaller in extent, and importantly showed less collateral damage to the surrounding neuroretina. Halved fluence sub-threshold burns had a smaller ring of RPE atrophy –seen as window defects surrounding the central pigment proliferation on SD-OCT, and as a hypofluorescent ring on fundus autofluorescence. Most importantly there was a tendency for photoreceptor layer reorganization (seen as centripetal reappearance of the IS/OS and ELM lines in OCT) at the edge of the halved fluence laser spots which was not observed in the threshold burns. Lower laser fluence settings did not produce detectable changes in the retina at any point during the follow-up. This PRL reorganization may have several explanations. It may be caused of sublethal thermal irradiation of the RPE/ PRL at the periphery of the lesions. This can be explained due to the Gaussian distribution of the

temperature profile during laser treatment which is present even if the laser energy is delivered homogeneously throughout the laser lesion.[137,138] A different explanation of the reappearance of the PRL line in the periphery of the lesions may be shrinkage of the laser lesion pulling the PRL towards the glial proliferation in the center of the lesions.

In their paper Muqit et al. described the morphology of sub-threshold, threshold, and supra-threshold laser burns with 20-200 millisecond irradiation times.[139] Their results are in agreement with our findings, but in our patients we demonstrated similar retinal changes with even lower fluence values than Muqit et al. used. Further we could demonstrate the photo receptors' tendency to shift into the direction of the lesion center which may be interpreted as a healing response. Inagaki et al also described similar morphologic changes following short pulse pattern scanning laser therapy in their paper where they compare different laser systems by macular grid laser.[140]

Sub-threshold micropulse laser has been examined in several studies in diseases such as diabetic macular edema, central serous chorioretinopathy, proliferative diabetic retinopathy or branch retinal vein occlusion, and has been found to be effective by some authors, whereas other studies found no benefit.[52–55,141–143] There is still some debate whether micropulse delivery has an advantage over continuous laser.[144]

When the Diabetic Retinopathy Study and the Early Treatment Diabetic Retinopathy Study first developed the recommended settings for scatter laser photocoagulation in patients with proliferative diabetic retinopathy, the aim was to produce "hot" white lesions. These standards were revised by several workgroups in order to reduce the intensity of the laser burns to the light gray lesions we use today.[145] These lesions are still clearly visible in the retina during the treatment and afterwards and leave atrophic scars. The fact that the gray laser lesions are visible during and after laser surgery means that the heat produced by the light absorption in the RPE layer reached the neuroretina through thermal diffusion, and was high enough to change its optical quality. This thermal diffusion is not just directed toward the neuroretina, but also to the surrounding RPE, and choroid causing late laser scar expansion.

Recent publications suggest that the beneficial effect of laser is not solely due to the reduction of ischemia, but also by up and down regulation of cytokines in sub-lethally

injured RPE cells.[135,146–148] This may mean that the endpoint of our current laser treatment strategy is potentially too intense, since destruction of the RPE cells may not be necessary to achieve our treatment goals.

7.4 Hyperreflective foci on OCT in patients with diabetic macular edema and their response to macular photocoagulation

The aim of this study was to examine the morphologic changes of intraretinal lipid exudates detected as hyperreflective foci by SD-OCT following retinal photocoagulation. SD-OCT images were correlated with color fundus photography and infrared imaging. The results show that the localization and movement of lipid foci greatly depend on the localized accumulation or resorption of intra-retinal fluid.

In the event of progressive fluid extravasation with persistent retinal thickening, lipid microexudates were constantly present in the retina throughout all layers. The topography of these individual microexudates appeared to undergo dynamic changes. On the other hand, in the event of localized resorption of intraretinal fluid following laser, the foci disappeared first from the inner retinal layers and later from the outer nuclear layer. Regarding the relationship of hyperreflective foci and hard exudates two characteristic features were identified: In the event of resolution of intraretinal fluid, hyperreflective foci formed confluent deposits in the inner part of the outer retinal layers and appeared clinically as hard exudates by color fundus photography and IR-imaging. If hard exudates were present in an area of persistent retinal thickening, in some cases, a resolution of hard exudates was observed by ophthalmoscopy. Independently, hyperreflective foci were still detectable by SD-OCT in the treated retinal area.

Since these hyperreflective foci represent extremely tiny particles in the retina a localized change in the amount of intraretinal fluid is enough to induce a change in the topography of these foci. This may result in that completely different change patterns are seen at different retinal locations of the same patient.

Since the Early Treatment Diabetic Retinopathy Study it is known that total serum cholesterol and LDL fraction cholesterol levels increase the risk of exudative diabetic maculopathy.[149] Superior outcomes following laser photocoagulation therapy for macular

edema have also been reported in subjects who have higher HDL cholesterol or normal total cholesterol serum levels.[150–156]

Although exudative diabetic maculopathy is currently not an indication for systemic lipid lowering therapy, growing number of evidence support that following such a therapy a marked reduction of hard exudates occurs in patients with dyslipideamia.[151–156] It is also known, that with the resolution of macular edema, hard exudates tend to grow in size and shift centrally. These subfoveal hard exudates can lead to severe visual loss. If further evidence is gathered through multicenter studies regarding the beneficial effect of systemic lipid lowering on the presence of retinal hard exudates, it would be most informative to evaluate the therapeutic effects using imaging modalities such as SD-OCT which is able to detect subclinical intraretinal lipids at their early formation as hyperreflective foci.

8 Conclusions

8.1 In vivo examination of retinal changes following panretinal photocoagulation

Panretinal photocoagulation using a short pulse laser with conventional threshold settings resulted in characteristic OCT findings both in the immediate post laser as well as the late follow-up period. These findings showed sharp bordered hyperreflective lesions in the outer retina at the site of laser irradiation with a transverse dimension comparable to the laser spot size setting used. In the reparative phase thinning of the ONL and PRL as well as RPE scarring was observed. These finding are very similar to those seen in histological animal model studies. We can conclude that the positive characteristics of short pulse lasers are also seen in OCTs of the human retina.

8.2 In vivo examination of retinal changes following macular grid and focal photocoagulation

Characteristic morphologic findings similar to those seen in patients undergoing panretinal photocoagulation were seen after macular photocoagulation as well. Disruption at the level of the RPE and PRL were evident right after photocoagulation. Hyperreflectivity in the ONL showed an oblique orientation with a tilt away from the foveal center, very similar to the physiologic orientation of photoreceptor inner segments and Henle's layer. Our theory is that this is evidence that the true thermal laser effect is only localized at the RPE/PRL level, and that the changes seen in the ONL are retrograde changes to the inner segments of the photoreceptors, and not direct thermal effects.

8.3 In vivo morphology of retinal changes following sub-threshold panretinal photocoagulation

Sub-threshold laser spots result in definitive changes in the outer retina, but with much less retinal pigment epithelium atrophy that enables a reparative mechanism in the photoreceptor layer. This suggests that treatment with a therapeutic effect and lesser

collateral damage may be possible by reducing the used laser fluence by half. With the recent development of pattern scanning laser technology, and fundus tracking imaging, it is possible, to deliver complete scatter laser treatments even if the surgeon doesn't actually see the laser lesions during the treatment session since the fundus tracking system records where the treatment was done. Recently introduced software algorithms allow the physician to easily set the level of sub-threshold fluence after the titration of the threshold power, and adjusts laser parameters automatically according to the desired level. This way the sub-threshold lesions described in the present paper can be delivered quickly and consistently during a panretinal scatter laser session. Limitations of our study are the relative low patient number, and that we cannot draw conclusions whether a PRP session done with halved fluence lesions is as effective as threshold laser is. Although these results are promising, further studies are necessary to assess the efficacy of these sub-threshold scatter laser treatments, in reducing the risk of developing severe visual acuity decrease comparable to standard threshold laser.

8.4 Hyperreflective foci on OCT in patients with diabetic macular edema and their response to macular photocoagulation

Our recent findings support our previous hypothesis that these hyperreflective foci may represent retinal microexudates composed of lipids, lipoproteins or lipid filled macrophages and that they are precursors and components of retinal hard exudates. Further evidence was supported that retinal hard exudates and microexudates represent a dynamic balanced system. The fact that these microexudates are clearly visible in SD-OCT long before any funduscopically detectable hard exudates appear, can be helpful in realistically determining the extent of lipid extravasation due to blood-retinal barrier breakdown. This SD-OCT based parameter may be useful in future studies providing new insight in patho-physiologic mechanisms of therapeutic agents for DME.

9 Summary

In summary our results showed that:

1)
   a) In vivo morphologic changes after panretinal laser therapy with a short duration continuous laser were comparable to result published from histological studies on animal models.
   b) Lesions were sharply demarcated, and showed no collateral damage at the edges of the lesions
   c) Laser lesions extended to the inner border of the outer nuclear layer, but the inner layers of the retina were not affected by direct thermal laser effect.

2)
   a) During their evolution a loss of PRL and ONL thickness -suggesting photoreceptor loss-, as well as RPE atrophy around the scar was observed.
   b) Laser lesions performed by a short duration continuous laser shrank considerably during the follow-up period and did not show lesion growth known to happen with laser scars of normal duration lasers.

3)
   a) Laser lesions of macular grid laser were similar in morphology to panretinal lesions. The oblique orientation of the lesions in the ONL suggest, that the true thermal effect of the laser is only limited to the RPE/PRL layers, and the involvement of the ONL is mainly a consequence of retrograde cellular changes.

4)
   a) Sub-threshold laser lesion created with halved fluence showed similar characteristics to threshold lesions, but were smaller in diameter, and showed less atrophic RPE changes.
   b) An inward migration of the photoreceptors is possible after sub-threshold laser, as the diameter of defects in the PRL layer reduced over time.

5)
   a) Intraretinal hyperreflective foci are a common finding on OCT in patients with diabetic macular edema, and show characteristic changes after laser therapy mainly influenced by the decrease or accumulation of intraretinal fluid.

b) Hyperreflective foci in diabetic macular edema may represent microexudates, and may serve as precursors of retinal hard exudates.
c) Hyperreflective foci might be an interesting biomarker in the detection of early increased lipid extravasation even before the development of macular edema or hard exudates.

10 Összefoglalás

Kutatási eredményeink alapján összefoglalhatjuk:

1.
    a. A rövid pulzusú folyamatos lézerrel végzett pánretinális lézerkezelést követően észlelhető in vivo elváltozások nagyon hasonlóak voltak a korábbi állatmodelleken végzett hisztológiai vizsgálatok eredményeivel.
    b. A lézerhegek élesen demarkálódtak, és a hegek közötti retinán nem látszódtak kollaterális károsodások nyomai.
    c. A lézerhegek a külső magvas réteg belső határáig nyúltak, de a retina belső rétegei nem mutattak direkt termikus lézer behatás nyomait.
2.
    a. A lézerhegek fejlődése során fotoreceptor veszteséget sugalló PRL és ONL vékonyodást, valamint retinális pigmenthám atrófiát észleltünk.
    b. A rövid pulzusú folyamatos lézerrel végzett lézerhegek jelentős zsugorodáson mentek keresztül, és a konvencionális lézerkezelésre jellemző heg megnagyobbodás jeleit nem mutatták.
3.
    a. A makuláris grid lézerkezelés hegei jelentős hasonlóságot mutattak a pánretinális lézerkezelésnél látott hegekkel. Az ONL rétegben látható ferde heg lefutás a direkt lézer effektus PRL/RPE rétegekre korlátozódását, és az ONL réteg inkább másodlagos a fotoreceptorok retrográd érintettségét sugallja.
4.
    a. A felezett energiasűrűséggel létrehozott „sub-threshold” lézerhegek morfológiájukban hasonlítottak a „threshold” lézerhegekre, de kisebbek voltak, és kevesebb RPE atrófiával jártak.
    b. A „sub-threshold” lézerkezelést követően a PRL rétegben észlelt sérülések csökkenése a fotoreceptorok migrációját sugallja.
5.

a. Az intraretinális hyperreflektív pontok gyakori elváltozások a diabéteszes makulaödémás betegek OCT felvételein, és lézerkezelést követően az intraretinális folyadék csökkenésének vagy gyarapodásának függvényében változnak.
b. Diabéteszes makulaödémában az OCT-n észlelt hyperreflektív pontok valószínűleg lipid mikroexudátumok, és a kemény exudátumok előjelei.
c. A hyperreflektív pontok a diabéteszes makulaödéma és kemény exudátumok kialkulását megelőző korai lipid extravazációt jelző biomarkerek lehetnek.

11 References

1. Blumenkranz MS. (2014) The Evolution of Laser Therapy in Ophthalmology: A Perspective on the Interactions Between Photons, Patients, Physicians, and Physicists: The LXX Edward Jackson Memorial Lecture. Am. J. Ophthalmol., 158: 12-25.e1.

2. Townes CH. (2002)How the Laser Happened: Adventures of a Scientist. Oxford University Press; 2002.

3. Gordon JP, Zeiger HJ, Townes CH. (1954) Molecular microwave oscillator and new hyperfine structure in the microwave spectrum of NH3 [7]. Phys. Rev., 95: 282–284.

4. Basov NG, Prokhorov A. (1954) Application of molecular beams to the radio spectroscopic study of the rotation spectra of molecules. Zh Eksp Theo Fiz, 27: 431.

5. Maiman TH. (1960) Stimulated Optical Radiation in Ruby. Nature, 187: 493–494.

6. Hall RN, Fenner GE, Kingsley JD, Soltys TJ, Carlson RO. (1962) Coherent Light Emission From GaAs Junctions. Phys. Rev. Lett., 9: 366–368.

7. Einstein A. (1917) Zur Quantentheorie der Strahlung. Phys.Z., 18: 121–128.

8. Jelínková H. (2013) Introduction: the history of lasers in medicine. In: Jelínková H (ed). Lasers for Medical Applications. Woodhead Publishing Series in Electronic and Optical Materials. Woodhead Publishing; 2013. pp. 1–13.

9. Palanker D, Blumenkranz M. (2012) Retinal laser therapy: biophysical basis and applications. Chapter 39. In: Ryan S (ed). RETINA.Vol 3. 5th edition. St Louis, MO: Mosby Inc,; 2012.

10. Steiner R. (2011) Laser-Tissue Interactions. In: Raulin C, Karsai S (eds). Laser and IPL Technology in Dermatology and Aesthetic Medicine.Vol 117. Berlin Heidelberg: Springer-Verlag; 2011. pp. 23–36.

11. Schmidt-Erfurth U, Hasan T. (2000) Mechanisms of Action of Photodynamic Therapy with Verteporfin for the Treatment of Age-Related Macular Degeneration. Surv. Ophthalmol., 45: 195–214.

12. O'Brart DPS. (2017) Corneal Collagen Crosslinking for Corneal Ectasias: A Review. Eur. J. Ophthalmol., 27: 253–269.

13. Paulus YM, Jain A, Gariano RF, Stanzel BV, Marmor M, Blumenkranz MS, Palanker D. (2008) Healing of retinal photocoagulation lesions. Invest Ophthalmol Vis Sci, 49: 5540–5.

14. Meyer-Schwickerath G. (1965) [Light coagulation]. Ber. Uber Zusammenkunft Dtsch. Ophthalmol. Ges., 66: 313–325.

15. Meyer-Schwickerath G. (1954) [Light coagulation; a method for treatment and prevention of the retinal detachment]. Albrecht Von Graefes Arch. Ophthalmol., 156: 2–34.

16. Gerabek WE, Gerabek W. (2005)Enzyklopädie Medizingeschichte. Walter de Gruyter; 2005. Available at: https://books.google.de/books?id=LLoOUP-y54YC.

17. Kettesy A. (1956) Közvetlen napfénnyel (solaris coagulatióval) meggyógyított ideghártya-leválás. Orv. Hetil., 15: 408–411.

18. Campbell CJ, Rittler MC, Koester CJ. (1966) Photocoagulation of the retina. Int. Ophthalmol. Clin., 6: 293–318.

19. Fankhauser F, Lotmar W. (1968) Methods of photocoagulation through the Goldmann contact glass. Bibl. Ophthalmol. Suppl. Ad Ophthalmol., 75: 256–272.

20. Gass JD. (1971) Photocoagulation of macular lesions. Trans. - Am. Acad. Ophthalmol. Otolaryngol. Am. Acad. Ophthalmol. Otolaryngol., 75: 580–608.

21. Beetham WP, Aiello LM, Balodimos MC, Koncz L. (1969) Ruby-laser photocoagulation of early diabetic neovascular retinopathy: preliminary report of a long-term controlled study. Trans. Am. Ophthalmol. Soc., 67: 39–67.

22. Diabetic Retinopathy Study Research Group. (1987) Indications for photocoagulation treatment of diabetic retinopathy: Diabetic Retinopathy Study Report no. 14. The Diabetic Retinopathy Study Research Group. Int. Ophthalmol. Clin., 27: 239–253.

23. Anon. (1991) Classification of diabetic retinopathy from fluorescein angiograms. ETDRS report number 11. Early Treatment Diabetic Retinopathy Study Research Group. Ophthalmology, 98: 807–22.

24. Anon. (1991) Grading diabetic retinopathy from stereoscopic color fundus photographs--an extension of the modified Airlie House classification. ETDRS report number 10. Early Treatment Diabetic Retinopathy Study Research Group. Ophthalmology, 98: 786–806.

25. Early Treatment Diabetic Retinopathy Study Group. (1987) Treatment Techniques and Clinical Guidelines for Photocoagulation of Diabetic Macular Edema: Early Treatment Diabetic Retinopathy Study Report Number 2. Ophthalmology, 94: 761–774.

26. Early Treatment Diabetic Retinopathy Study Research Group. (1991) Early photocoagulation for diabetic retinopathy. ETDRS report number 9. Early Treatment Diabetic Retinopathy Study Research Group. Ophthalmology, 98: 766–85.

27. The Branch Vein Occlusion Study Group. (1984) Argon Laser Photocoagulation for Macular Edema in Branch Vein Occlusion. Am. J. Ophthalmol., 98: 271–282.

28. Branch Vein Occlusion Study Goup. (1986) Argon Laser Scatter Photocoagulation for Prevention of Neovascularization and Vitreous Hemorrhage in Branch Vein Occlusion: A Randomized Clinical Trial. Arch. Ophthalmol., 104: 34–41.

29. Central Vein Occlusion Study Group. (1997) Natural history and clinical management of central retinal vein occlusion. The Central Vein Occlusion Study Group. Arch. Ophthalmol. Chic. Ill 1960, 115: 486–491.

30. Macular Photocoagulation Study Group. (1991) Argon Laser Photocoagulation for Neovascular Maculopathy: Five-Year Results From Randomized Clinical Trials. Arch. Ophthalmol., 109: 1109–1114.

31. Seres A, Papp A, Süveges I. (2000) A maculopathia diabetica lézerkezeléséről. Szemészet, 137: 163–171.

32. Nguyen QD, Brown DM, Marcus DM, Boyer DS, Patel S, Feiner L, Gibson A, Sy J, Rundle AC, Hopkins JJ, Rubio RG, Ehrlich JS. (2012) Ranibizumab for Diabetic Macular Edema: Results from 2 Phase III Randomized Trials: RISE and RIDE. Ophthalmology, 119: 789–801.

33. Mitchell P, Bandello F, Schmidt-Erfurth U, Lang GE, Massin P, Schlingemann RO, Sutter F, Simader C, Burian G, Gerstner O, Weichselberger A. (2011) The RESTORE Study: Ranibizumab Monotherapy or Combined with Laser versus Laser Monotherapy for Diabetic Macular Edema. Ophthalmology, 118: 615–625.

34. Korobelnik J-F, Do DV, Schmidt-Erfurth U, Boyer DS, Holz FG, Heier JS, Midena E, Kaiser PK, Terasaki H, Marcus DM, Nguyen QD, Jaffe GJ, Slakter JS, Simader C, Soo Y, Schmelter T, Yancopoulos GD, Stahl N, Vitti R, Berliner AJ, Zeitz O, Metzig C, Brown DM. (2014) Intravitreal Aflibercept for Diabetic Macular Edema. Ophthalmology, 121: 2247–2254.

35. Gross JG, Glassman AR, Jampol LM, Inusah S, Aiello LP, Antoszyk AN, Baker CW, Berger BB, Bressler NM, Browning D, Elman MJ, Ferris FL, Friedman SM, Marcus DM, Melia M, Stockdale CR, Sun JK, Beck RW. (2015) Panretinal Photocoagulation vs Intravitreous Ranibizumab for Proliferative Diabetic Retinopathy: A Randomized Clinical Trial. JAMA, 314: 2137–2146.

36. Gross JG, Glassman AR, Liu D, Sun JK, Antoszyk AN, Baker CW, Bressler NM, Elman MJ, Ferris FL, Gardner TW, Jampol LM, Martin DF, Melia M, Stockdale CR, Beck RW. (2018) Five-Year Outcomes of Panretinal Photocoagulation vs Intravitreous Ranibizumab for Proliferative Diabetic Retinopathy. JAMA Ophthalmol., 136: 1138–1148.

37. Fong DS, Girach A, Boney A. (2007) Visual side effects of successful scatter laser photocoagulation surgery for proliferative diabetic retinopathy: a literature review. Retina, 27: 816–24.

38. Patel JI, Jenkins L, Benjamin L, Webber S. (2002) Dilated pupils and loss of accommodation following diode panretinal photocoagulation with sub-tenon local anaesthetic in four cases. Eye, 16: 628–632.

39. Ebrahim B, Frohman L, Zarbin M, Bhagat N. (2009) Tonic Pupil Following Pars Plana Vitrectomy and Endolaser. Case Rep. Med., 2009. Available at: https://www.ncbi.nlm.nih.gov/pmc/articles/PMC2728613/ [Accessed December 13, 2019].

40. Lin J, Chang JS, Smiddy WE. (2016) Cost Evaluation of Panretinal Photocoagulation versus Intravitreal Ranibizumab for Proliferative Diabetic Retinopathy. Ophthalmology, 123: 1912–1918.

41. Flaxel CJ, Adelman RA, Bailey ST, Fawzi A, Lim JI, Vemulakonda GA, Ying G. (2019) Diabetic Retinopathy Preferred Practice Pattern®. Ophthalmology,. Available at: http://www.sciencedirect.com/science/article/pii/S0161642019320925 (in Press).

42. Schmidt-Erfurth U, Garcia-Arumi J, Bandello F, Berg K, Chakravarthy U, Gerendas BS, Jonas J, Larsen M, Tadayoni R, Loewenstein A. (2017) Guidelines for the Management of Diabetic Macular Edema by the European Society of Retina Specialists (EURETINA). Ophthalmologica, 237: 185–222.

43. Obeid A, Gao X, Ali FS, Talcott KE, Aderman CM, Hyman L, Ho AC, Hsu J. (2018) Loss to Follow-Up in Patients with Proliferative Diabetic Retinopathy after Panretinal Photocoagulation or Intravitreal Anti-VEGF Injections. Ophthalmology, 125: 1386–1392.

44. Jain At, Blumenkranz MS, Paulus Y, Wiltberger MW, Andersen DE, Huie P, Palanker D. (2008) Effect of Pulse Duration on Size and Character of the Lesion in Retinal Photocoagulation. Arch. Ophthalmol., 126: 78–85.

45. Sher A, Jones BW, Huie P, Paulus YM, Lavinsky D, Leung L-SS, Nomoto H, Beier C, Marc RE, Palanker D. (2013) Restoration of Retinal Structure and Function after Selective Photocoagulation. J. Neurosci., 33: 6800–6808.

46. Dorin G. (2003) Subthreshold and micropulse diode laser photocoagulation. Semin. Ophthalmol., 18: 147–153.

47. Dorin G. (2004) Evolution of retinal laser therapy: minimum intensity photocoagulation (MIP). Can the laser heal the retina without harming it? Semin. Ophthalmol., 19: 62–68.

48. Lanzetta P, Dorin G, Pirracchio A, Bandello F. (2001) Theoretical bases of non-ophthalmoscopically visible endpoint photocoagulation. Semin. Ophthalmol., 16: 8–11.

49. Lavinsky D, Cardillo JA, Melo LAS, Dare A, Farah ME, Belfort R. (2011) Randomized Clinical Trial Evaluating mETDRS versus Normal or High-Density Micropulse Photocoagulation for Diabetic Macular Edema. Invest. Ophthalmol. Vis. Sci., 52: 4314–4323.

50. Vujosevic S, Bottega E, Casciano M, Pilotto E, Convento E, Midena E. (2010) Microperimetry and fundus autofluorescence in diabetic macular edema: subthreshold micropulse diode laser versus modified early treatment diabetic retinopathy study laser photocoagulation. Retina, 30: 908–916.

51. Kumar V, Ghosh B, Mehta DK, Goel N. (2010) Functional outcome of subthreshold versus threshold diode laser photocoagulation in diabetic macular oedema. Eye, 24: 1459–1465.

52. Figueira J, Khan J, Nunes S, Sivaprasad S, Rosa A, de Abreu JF, Cunha-Vaz JG, Chong NV. (2009) Prospective randomised controlled trial comparing sub-threshold micropulse diode laser photocoagulation and conventional green laser for clinically significant diabetic macular oedema. Br J Ophthalmol, 93: 1341–4.

53. Akhlaghi M, Dehghani A, Pourmohammadi R, Asadpour L, Pourazizi M. (2018) Effects of subthreshold diode micropulse laser photocoagulation on treating patients with refractory diabetic macular edema. J. Curr. Ophthalmol., 31: 157–160.

54. Lois N, Gardner E, Waugh N, Azuara-Blanco A, Mistry H, McAuley D, Acharya N, Aslam TM, Bailey C, Chong V, Downey L, Eleftheriadis H, Fatum S, George S, Ghanchi F, Groppe M, Hamilton R, Menon G, Saad A, Sivaprasad S, Shiew M, Steel DH, Talks

JS, Adams C, Campbell C, Mills M, Clarke M. (2019) Diabetic macular oedema and diode subthreshold micropulse laser (DIAMONDS): study protocol for a randomised controlled trial. Trials, 20. Available at: https://www.ncbi.nlm.nih.gov/pmc/articles/PMC6373040/ (in Press).

55. van Dijk EHC, Fauser S, Breukink MB, Blanco-Garavito R, Groenewoud JMM, Keunen JEE, Peters PJH, Dijkman G, Souied EH, MacLaren RE, Querques G, Downes SM, Hoyng CB, Boon CJF. (2018) Half-Dose Photodynamic Therapy versus High-Density Subthreshold Micropulse Laser Treatment in Patients with Chronic Central Serous Chorioretinopathy: The PLACE Trial. Ophthalmology, 125: 1547–1555.

56. Battaglia Parodi M, Iacono P. (2019) Re: van Dijk et al.: Half-dose photodynamic therapy versus high-density subthreshold micropulse laser treatment in patients with chronic central serous chorioretinopathy: the PLACE trial (Ophthalmology. 2018;125:1547-1555). Ophthalmology, 126: e29–e30.

57. Kernt M, Ulbig M, Kampik A, Neubauer AS. (2014) Navigated Laser Therapy for Diabetic Macular Oedema. Eur. Endocrinol., 10: 66–69.

58. Bressler SB, Glassman AR, Almukhtar T, Bressler NM, Ferris FL, Googe JM, Gupta SK, Jampol LM, Melia M, Wells JA. (2016) Five-Year Outcomes of Ranibizumab With Prompt or Deferred Laser Versus Laser or Triamcinolone Plus Deferred Ranibizumab for Diabetic Macular Edema. Am. J. Ophthalmol., 164: 57–68.

59. Blindbæk SL, Peto T, Grauslund J. Aflibercept and navigated versus conventional laser in diabetic macular oedema: a 12-month randomized clinical trial. Acta Ophthalmol. (Copenh.), n/a. Available at: https://onlinelibrary.wiley.com/doi/abs/10.1111/aos.14266 (ahead of Print) [Accessed December 14, 2019].

60. Payne JF, Wykoff CC, Clark WL, Bruce BB, Boyer DS, Brown DM, Payne JF, Clark WL, Wells JA, Johnson DL, Wykoff CC, Brown DM, Benz M, Chen E, Fish RH, Kim RY, Major JC, O'Malley RE, Schefler AC, Shah AR, Wong TP, Boyer DS, Novack RL, Chu TG, Rahhal F, Tabandeh H, Roe RH, Dayani PN, Liao D, et al. (2019) Randomized Trial of Treat and Extend Ranibizumab With and Without Navigated Laser Versus

Monthly Dosing for Diabetic Macular Edema: TREX-DME 2-Year Outcomes. Am. J. Ophthalmol., 202: 91–99.

61. Fujimoto J, Swanson E. (2016) The Development, Commercialization, and Impact of Optical Coherence Tomography. Invest. Ophthalmol. Vis. Sci., 57: OCT1–OCT13.

62. Michelson AA, Pease FG. (1921) Measurement of the Diameter of Alpha-Orionis by the Interferometer. Proc. Natl. Acad. Sci. U. S. A., 7: 143–146.

63. Fercher AF, Mengedoht K, Werner W. (1988) Eye-length measurement by interferometry with partially coherent light. Opt. Lett., 13: 186–188.

64. Huang D, Swanson EA, Lin CP, Schuman JS, Stinson WG, Chang W, Hee MR, Flotte T, Gregory K, Puliafito CA, Fujimoto JG. (1991) Optical coherence tomography. Science, 254: 1178–1181.

65. Fercher AF, Hitzenberger CK, Drexler W, Kamp G, Sattmann H. (1993) In Vivo Optical Coherence Tomography. Am. J. Ophthalmol., 116: 113–114.

66. Swanson EA, Izatt JA, Hee MR, Huang D, Lin CP, Schuman JS, Puliafito CA, Fujimoto JG. (1993) In vivo retinal imaging by optical coherence tomography. Opt. Lett., 18: 1864–1866.

67. Békési L, Bíró A, Berta A. (1998) Az optikai koherencia tomográfia szemészeti alkalmazásáról. Szemészet, 135: 173–177.

68. Győri J, Pados K, Salacz G. (2002) Optikai koherencia tomográffal szerzett gyakorlati tapasztalataink a retina vizsgálatában. Szemészet, 139: 251–256.

69. Nemes J, Somfai G, Hargitai J. (2004) Optikai koherencia tomográffal észlelt strukturális változások diabeteses maculopathia miatt végzett fotokoaguláció után. Szemészet, 141: 41–44.

70. Reumueller A, Schmidt-Erfurth U, Salas M, Sacu S, Drexler W, Pircher M, Pollreisz A. (2019) Three-Dimensional Adaptive Optics-Assisted Visualization of Photoreceptors in Healthy and Pathologically Aged Eyes. Invest. Ophthalmol. Vis. Sci., 60: 1144–1155.

71. Drexler W, Sattmann H, Hermann B, Ko TH, Stur M, Unterhuber A, Scholda C, Findl O, Wirtitsch M, Fujimoto JG, Fercher AF. (2003) Enhanced Visualization of Macular Pathology With the Use of Ultrahigh-Resolution Optical Coherence Tomography. Arch. Ophthalmol., 121: 695–706.

72. Ergun E, Hermann B, Wirtitsch M, Unterhuber A, Ko TH, Sattmann H, Scholda C, Fujimoto JG, Stur M, Drexler W. (2005) Assessment of Central Visual Function in Stargardt's Disease/Fundus Flavimaculatus with Ultrahigh-Resolution Optical Coherence Tomography. Invest. Ophthalmol. Vis. Sci., 46: 310–316.

73. Mylonas G, Ahlers C, Malamos P, Golbaz I, Deak G, Schuetze C, Sacu S, Schmidt-Erfurth U. (2009) Comparison of retinal thickness measurements and segmentation performance of four different spectral and time domain OCT devices in neovascular age-related macular degeneration. Br. J. Ophthalmol., 93: 1453–1460.

74. Malamos P, Ahlers C, Mylonas G, Schütze C, Deak G, Ritter M, Sacu S, Schmidt-erfurth U. (2011) Evaluation Of Segmentation Procedures Using Spectral Domain Optical Coherence Tomography In Exudative Age-related Macular Degeneration. Retina, 31: 453–463.

75. Spaide RF, Koizumi H, Pozonni MC. (2008) Enhanced Depth Imaging Spectral-Domain Optical Coherence Tomography. Am. J. Ophthalmol., 146: 496–500.

76. Boer JF de, Leitgeb R, Wojtkowski M. (2017) Twenty-five years of optical coherence tomography: the paradigm shift in sensitivity and speed provided by Fourier domain OCT [Invited]. Biomed. Opt. Express, 8: 3248–3280.

77. Klein T, Wieser W, Reznicek L, Neubauer A, Kampik A, Huber R. (2013) Multi-MHz retinal OCT. Biomed. Opt. Express, 4: 1890–1908.

78. Jia Y, Tan O, Tokayer J, Potsaid B, Wang Y, Liu JJ, Kraus MF, Subhash H, Fujimoto JG, Hornegger J, Huang D. (2012) Split-spectrum amplitude-decorrelation angiography with optical coherence tomography. Opt. Express, 20: 4710–4725.

79. Fingler J, Schwartz D, Yang C, Fraser SE. (2007) Mobility and transverse flow visualization using phase variance contrast with spectral domain optical coherence tomography. Opt. Express, 15: 12636–12653.

80. Chen X, Rahimy E, Sergott RC, Nunes RP, Souza EC, Choudhry N, Cutler NE, Houston SKS, Munk MR, Fawzi AA, Mehta S, Hubschman J-P, Ho AC, Sarraf D. (2015) Spectrum of Retinal Vascular Diseases Associated With Paracentral Acute Middle Maculopathy. Am. J. Ophthalmol., 160: 26-34.e1.

81. Dansingani KK, Inoue M, Engelbert M, Freund KB. (2015) Optical coherence tomographic angiography shows reduced deep capillary flow in paracentral acute middle maculopathy. Eye, 29: 1620–1624.

82. Kim AY, Rodger DC, Shahidzadeh A, Chu Z, Koulisis N, Burkemper B, Jiang X, Pepple KL, Wang RK, Puliafito CA, Rao NA, Kashani AH. (2016) Quantifying retinal microvascular changes in uveitis using spectral domain optical coherence tomography angiography (SD-OCTA). Am. J. Ophthalmol., 171: 101–112.

83. Zhang M, Hwang TS, Campbell JP, Bailey ST, Wilson DJ, Huang D, Jia Y. (2016) Projection-resolved optical coherence tomographic angiography. Biomed. Opt. Express, 7: 816–828.

84. Hwang TS, Zhang M, Bhavsar K, Zhang X, Campbell JP, Lin P, Bailey ST, Flaxel CJ, Lauer AK, Wilson DJ, Huang D, Jia Y. (2016) Visualization of 3 Distinct Retinal Plexuses by Projection-Resolved Optical Coherence Tomography Angiography in Diabetic Retinopathy. JAMA Ophthalmol., 134: 1411–1419.

85. American Diabetes Association. (2010) Diagnosis and Classification of Diabetes Mellitus. Diabetes Care, 33: S62–S69.

86. Shaw JE, Sicree RA, Zimmet PZ. (2010) Global estimates of the prevalence of diabetes for 2010 and 2030. Diabetes Res. Clin. Pract., 87: 4–14.

87. Cowie CC, Rust KF, Byrd-Holt DD, Eberhardt MS, Flegal KM, Engelgau MM, Saydah SH, Williams DE, Geiss LS, Gregg EW. (2006) Prevalence of Diabetes and

Impaired Fasting Glucose in Adults in the U.S. Population: National Health and Nutrition Examination Survey 1999–2002. Diabetes Care, 29: 1263–1268.

88. Danaei G, Finucane MM, Lu Y, Singh GM, Cowan MJ, Paciorek CJ, Lin JK, Farzadfar F, Khang Y-H, Stevens GA, Rao M, Ali MK, Riley LM, Robinson CA, Ezzati M, Global Burden of Metabolic Risk Factors of Chronic Diseases Collaborating Group (Blood Glucose). (2011) National, regional, and global trends in fasting plasma glucose and diabetes prevalence since 1980: systematic analysis of health examination surveys and epidemiological studies with 370 country-years and 2·7 million participants. Lancet Lond. Engl., 378: 31–40.

89. Klein BEK. (2007) Overview of Epidemiologic Studies of Diabetic Retinopathy. Ophthalmic Epidemiol., 14: 179–183.

90. Schneider M, Süveges I. (2004) Retinopathia diabetica: magyarországi epidemiológiai adatok. Szemészet, 141: 449–452.

91. Szabó D, Sándor GL, Tóth G, Pék A, Lukács R, Szalai I, Tóth GZ, Papp A, Nagy ZZ, Limburg H, Németh J. (2018) Visual impairment and blindness in Hungary. Acta Ophthalmol. (Copenh.), 96: 168–173.

92. Szabó D, Tóth G, Sándor GL, Pék A, Lukács R, Szalai I, Tóth GZ, Papp A, Nagy ZZ, Limburg H, Németh J. (2017) A vakság okai Magyarországon. A RAAB-metodika első hazai megvalósítása. Szemészet, 154: 119–126.

93. Kiss H, Németh J. (2013) A vakság okai Magyarországon. Szemészet, 150: 103–111.

94. Tóth G, Szabó D, Sándor GL, Pék A, Szalai I, Papp A, Nagy ZZ, Limburg H, Németh J. (2018) A cukorbetegség és a diabéteszes retinopathia hazánkban a RAAB+ DRM-vizsgálat eredményei szerint. Szemészet, 155: 82–90.

95. Zhang X, Saaddine JB, Chou C-F, Cotch MF, Cheng YJ, Geiss LS, Gregg EW, Albright AL, Klein BEK, Klein R. (2010) Prevalence of Diabetic Retinopathy in the United States, 2005-2008. JAMA, 304: 649–656.

96. Chua J, Lim C, Wong T, Sabanayagam C. (2018) Diabetic Retinopathy in the Asia-Pacific. Asia-Pac. J. Ophthalmol., 7: 3–16.

97. Klein R, Klein BEK, Moss SE, Davis MD, DeMets DL. (1984) The Wisconsin Epidemiologic Study of Diabetic Retinopathy: III. Prevalence and Risk of Diabetic Retinopathy When Age at Diagnosis Is 30 or More Years. Arch. Ophthalmol., 102: 527–532.

98. Klein R, Klein BE, Moss SE, Cruickshanks KJ. (1995) The Wisconsin Epidemiologic Study of Diabetic Retinopathy. XV. The long-term incidence of macular edema. Ophthalmology, 102: 7–16.

99. Eppens MC, Craig ME, Cusumano J, Hing S, Chan AKF, Howard NJ, Silink M, Donaghue KC. (2006) Prevalence of Diabetes Complications in Adolescents With Type 2 Compared With Type 1 Diabetes. Diabetes Care, 29: 1300–1306.

100. Tóth G, Szabó D, Sándor GL, Szalai I, Lukács R, Pék A, Tóth GZ, Papp A, Nagy ZZ, Limburg H, Németh J. (2017) Diabetes and diabetic retinopathy in people aged 50 years and older in Hungary. Br. J. Ophthalmol., 101: 965–969.

101. Diabetes Control and Complications Trial Research Group. (1995) Progression of Retinopathy with Intensive versus Conventional Treatment in the Diabetes Control and Complications Trial. Ophthalmology, 102: 647–661.

102. Diabetes Control and Complications Trial/Epidemiology of Diabetes Interventions and Complications Research Group, Lachin JM, Genuth S, Cleary P, Davis MD, Nathan DM. (2000) Retinopathy and nephropathy in patients with type 1 diabetes four years after a trial of intensive therapy. N. Engl. J. Med., 342: 381–389.

103. UK Prospective Diabetes Study Group. (1998) Tight blood pressure control and risk of macrovascular and microvascular complications in type 2 diabetes: UKPDS 38. BMJ, 317: 703–713.

104. Leiden HA van, Dekker JM, Moll AC, Nijpels G, Heine RJ, Bouter LM, Stehouwer CDA, Polak BCP. (2002) Blood Pressure, Lipids, and Obesity Are Associated With Retinopathy: The Hoorn Study. Diabetes Care, 25: 1320–1325.

105. Stitt AW, Gardiner TA, Archer DB. (1995) Histological and ultrastructural investigation of retinal microaneurysm development in diabetic patients. Br. J. Ophthalmol., 79: 362–367.

106. Hammes H-P, Lin J, Renner O, Shani M, Lundqvist A, Betsholtz C, Brownlee M, Deutsch U. (2002) Pericytes and the Pathogenesis of Diabetic Retinopathy. Diabetes, 51: 3107–3112.

107. Garcia-Martin E, Cipres M, Melchor I, Gil-Arribas L, Vilades E, Polo V, Rodrigo MJ, Satue M. (2019) Neurodegeneration in Patients with Type 2 Diabetes Mellitus without Diabetic Retinopathy. J. Ophthalmol., 2019. Available at: https://www.ncbi.nlm.nih.gov/pmc/articles/PMC6702840/ [Accessed February 22, 2020].

108. Toprak I, Fenkci SM, Yaylali GF, Martin C, Yaylali V. (2019) Early retinal neurodegeneration in preclinical diabetic retinopathy: a multifactorial investigation. Eye,: 1–8.

109. Milibák T. (2012) A diabéteszes maculopathia diagnosztikája és kezelése. Szemészet,: 243–259.

110. Deák GG, Schmidt-Erfurth UM, Jampol LM. (2018) Correlation of Central Retinal Thickness and Visual Acuity in Diabetic Macular Edema. JAMA Ophthalmol., 136: 1215–1216.

111. Schmidt-Erfurth U, Lang GE, Holz FG, Schlingemann RO, Lanzetta P, Massin P, Gerstner O, Bouazza AS, Shen H, Osborne A, Mitchell P. (2014) Three-Year Outcomes of Individualized Ranibizumab Treatment in Patients with Diabetic Macular Edema: The RESTORE Extension Study. Ophthalmology, 121: 1045–1053.

112. Brown DM, Nguyen QD, Marcus DM, Boyer DS, Patel S, Feiner L, Schlottmann PG, Rundle AC, Zhang J, Rubio RG, Adamis AP, Ehrlich JS, Hopkins JJ. (2013) Long-term Outcomes of Ranibizumab Therapy for Diabetic Macular Edema: The 36-Month Results from Two Phase III Trials: RISE and RIDE. Ophthalmology, 120: 2013–2022.

113. Sun JK, Glassman AR, Beaulieu WT, Stockdale CR, Bressler NM, Flaxel C, Gross JG, Shami M, Jampol LM, Diabetic Retinopathy Clinical Research Network. (2019) Rationale and Application of the Protocol S Anti-Vascular Endothelial Growth Factor Algorithm for Proliferative Diabetic Retinopathy. Ophthalmology, 126: 87–95.

114. Papp A. (2016) A diabéteszes makulaödéma korszerű kezelése. Szemészet, 153: 160–174.

115. Somfai G, Ferencz M, Fiedler O, Varga T, Somogyi A, Németh J. (2007) Diabéteszes retinopathia a XXI. század elején: prevenció, diagnosztika és terápia. Magy. Belorvosi Arch., 60: 123–127.

116. Moutray T, Evans JR, Lois N, Armstrong DJ, Peto T, Azuara-Blanco A. (2018) Different lasers and techniques for proliferative diabetic retinopathy. Cochrane Database Syst. Rev., 2018. Available at: https://www.ncbi.nlm.nih.gov/pmc/articles/PMC6494342/ (in Press) [Accessed December 5, 2019].

117. Blumenkranz M, Yellachich D, Andersen D, Wiltberger M, Mordaunt D, Marcellino G, Palanker D. (2006) SEMIAUTOMATED PATTERNED SCANNING LASER FOR RETINAL PHOTOCOAGULATION. Retina, 26: 370–376.

118. Anon. (1987) Techniques for scatter and local photocoagulation treatment of diabetic retinopathy: Early Treatment Diabetic Retinopathy Study Report no. 3. The Early Treatment Diabetic Retinopathy Study Research Group. Int Ophthalmol Clin, 27: 254–64.

119. Diabetic Retinopathy Clinical Research Network. (2007) Comparison of Modified-ETDRS and Mild Macular Grid Laser Photocoagulation Strategies for Diabetic Macular Edema. Arch. Ophthalmol., 125: 469–480.

120. Polito A, Polini G, Chiodini RG, Isola M, Soldano F, Bandello F. (2007) Effect of Posture on the Diurnal Variation in Clinically Significant Diabetic Macular Edema. Invest. Ophthalmol. Vis. Sci., 48: 3318–3323.

121. Kriechbaum K, Bolz M, Deak GG, Prager S, Scholda C, Schmidt-Erfurth U. (2010) High-resolution imaging of the human retina in vivo after scatter photocoagulation treatment using a semiautomated laser system. Ophthalmology, 117: 545–51.

122. Bolz M, Ritter M, Schneider M, Simader C, Scholda C, Schmidt-Erfurth U. (2009) A Systematic Correlation of Angiography and High-Resolution Optical Coherence Tomography in Diabetic Macular Edema. Ophthalmology, 116: 66–72.

123. Bolz M, Kriechbaum K, Simader C, Deak G, Lammer J, Treu C, Scholda C, Prünte C, Schmidt-Erfurth U. (2010) In Vivo Retinal Morphology after Grid Laser Treatment in Diabetic Macular Edema. Ophthalmology, 117: 538–544.

124. Deák GG, Bolz M, Prager S, Ritter M, Kriechbaum K, Scholda C, Schmidt-Erfurth U. (2012) Photoreceptor Layer Regeneration is Detectable in the Human Retina Imaged by SD-OCT after Laser Treatment Using Subthreshold Laser Power. Invest. Ophthalmol. Vis. Sci., 53: 7019–7025.

125. Deák GG, Bolz M, Kriechbaum K, Prager S, Mylonas G, Scholda C, Schmidt-Erfurth U. (2010) Effect of Retinal Photocoagulation on Intraretinal Lipid Exudates in Diabetic Macular Edema Documented by Optical Coherence Tomography. Ophthalmology, 117: 773–779.

126. Muqit MMK, Marcellino GR, Henson DB, Young LB, Turner GS, Stanga PE. (2011) Pascal panretinal laser ablation and regression analysis in proliferative diabetic retinopathy: Manchester Pascal Study Report 4. Eye Lond. Engl., 25: 1447–1456.

127. Wang Y, Muqit MMK, Stanga PE, Young LB, Henson DB. (2014) Spatial changes of central field loss in diabetic retinopathy after laser. Optom. Vis. Sci. Off. Publ. Am. Acad. Optom., 91: 111–120.

128. Muqit MMK, Young LB, McKenzie R, John B, Marcellino GR, Henson DB, Turner GS, Stanga PE. (2013) Pilot randomised clinical trial of Pascal TargETEd Retinal versus variable fluence PANretinal 20 ms laser in diabetic retinopathy: PETER PAN study. Br. J. Ophthalmol., 97: 220–227.

129. Al-Hussainy S, Dodson PM, Gibson JM. (2008) Pain response and follow-up of patients undergoing panretinal laser photocoagulation with reduced exposure times. Eye, 22: 96–99.

130. Lanzetta P, Polito A, Veritti D. (2008) Subthreshold laser. Ophthalmology, 115: 216-216 e1.

131. Thomas EL, Apple DJ, Swartz M, Kavka-Van Norman D. (1984) Histopathology and ultrastructure of krypton and argon laser lesions in a human retina-choroid. Retina Phila. Pa, 4: 22–39.

132. Framme C, Alt C, Schnell S, Sherwood M, Brinkmann R, Lin CP. (2007) Selective Targeting of the Retinal Pigment Epithelium in Rabbit Eyes with a Scanning Laser Beam. Invest. Ophthalmol. Vis. Sci., 48: 1782–1792.

133. Lanzetta P, Ortolani F, Petrelli L, Cugini U, Bandello F, Marchini M. (2005) ULTRASTRUCTURAL ANALYSIS OF RABBIT RETINA IRRADIATED WITH A NEW 670-NM DIODE RED LASER AT DIFFERENT POWERS. Retina, 25: 1039–1045.

134. Toth CA, Birngruber R, Boppart SA, Hee MR, Fujimoto JG, Dicarlo CD, Swanson EA, Cain CP, Narayan DG, Noojin GD, Roach WP. (1997) Argon Laser Retinal Lesions Evaluated In Vivo by Optical Coherence Tomography. Am. J. Ophthalmol., 123: 188–198.

135. Jang SY, Cho IH, Yang JY, Park HY, Woo SE, Madrakhimov SB, Chang HS, Lyu J, Park TK. (2019) The retinal pigment epithelial response after retinal laser photocoagulation in diabetic mice. Lasers Med. Sci., 34: 179–190.

136. Podoleanu A, Charalambous I, Plesea L, Dogariu A, Rosen R. (2004) Correction of distortions in optical coherence tomography imaging of the eye. Phys. Med. Biol., 49: 1277–1294.

137. Roider J, Hillenkamp F, Flotte T, Birngruber R. (1993) Microphotocoagulation: selective effects of repetitive short laser pulses. Proc Natl Acad Sci U A, 90: 8643–7.

138. Marshall J. (1970) Thermal and mechanical mechanisms in laser damage to the retina. Invest. Ophthalmol. Vis. Sci., 9: 97–115.

139. Muqit MM, Denniss J, Nourrit V, Marcellino GR, Henson DB, Schiessl I, Stanga PE. (2011) Spatial and spectral imaging of retinal laser photocoagulation burns. Invest Ophthalmol Vis Sci, 52: 994–1002.

140. Inagaki K, Ohkoshi K, Ohde S. (2012) Spectral-Domain Optical Coherence Tomography Imaging of Retinal Changes After Conventional Multicolor Laser, Subthreshold Micropulse Diode Laser, or Pattern Scanning Laser Therapy in Japanese With Macular Edema. Retina, 32: 1592–1600.

141. Lanzetta P, Furlan F, Morgante L, Veritti D, Bandello F. (2008) Nonvisible subthreshold micropulse diode laser (810 nm) treatment of central serous chorioretinopathy. A pilot study. Eur J Ophthalmol, 18: 934–40.

142. Luttrull JK, Musch DC, Spink CA. (2008) Subthreshold diode micropulse panretinal photocoagulation for proliferative diabetic retinopathy. Eye Lond, 22: 607–12.

143. Parodi MB, Spasse S, Iacono P, Di Stefano G, Canziani T, Ravalico G. (2006) Subthreshold grid laser treatment of macular edema secondary to branch retinal vein occlusion with micropulse infrared (810 nanometer) diode laser. Ophthalmology, 113: 2237–42.

144. Sivaprasad S, Elagouz M, McHugh D, Shona O, Dorin G. (2010) Micropulsed Diode Laser Therapy: Evolution and Clinical Applications. Surv. Ophthalmol., 55: 516–530.

145. Bandello F, Brancato R, Menchini U, Virgili G, Lanzetta P, Ferrari E, Incorvaia C. (2001) Light panretinal photocoagulation (LPRP) versus classic panretinal photocoagulation (CPRP) in proliferative diabetic retinopathy. Semin Ophthalmol, 16: 12–8.

146. Glaser BM, Campochiaro PA, Davis JL, Jerdan JA. (1987) Retinal pigment epithelial cells release inhibitors of neovascularization. Ophthalmology, 94: 780–4.

147. Miller H, Miller B, Ryan SJ. (1986) The role of retinal pigment epithelium in the involution of subretinal neovascularization. Invest Ophthalmol Vis Sci, 27: 1644–52.

148. Ogata N, Tombran-Tink J, Jo N, Mrazek D, Matsumura M. (2001) Upregulation of pigment epithelium-derived factor after laser photocoagulation. Am J Ophthalmol, 132: 427–9.

149. Chew EY, Klein ML, Ferris FL, Remaley NA, Murphy RP, Chantry K, Hoogwerf BJ, Miller D. (1996) Association of elevated serum lipid levels with retinal hard exudate in diabetic retinopathy. Early Treatment Diabetic Retinopathy Study (ETDRS) Report 22. Arch Ophthalmol, 114: 1079–84.

150. Kremser BG, Falk M, Kieselbach GF. (1995) Influence of Serum Lipid Fractions on the Course of Diabetic Macular Edema after Photocoagulation. Ophthalmologica, 209: 60–63.

151. Anon. (2000) Joint British recommendations on prevention of coronary heart disease in clinical practice: summary. British Cardiac Society, British Hyperlipidaemia Association, British Hypertension Society, British Diabetic Association. BMJ, 320: 705–8.

152. Verges B. (2006) Fenofibrate therapy and cardiovascular protection in diabetes: recommendations after FIELD. Curr Opin Lipidol, 17: 653–8.

153. Duncan LJ, Cullen JF, Ireland JT, Nolan J, Clarke BF, Oliver MF. (1968) A three-year trial of atromid therapy in exudative diabetic retinopathy. Diabetes, 17: 458–67.

154. Freyberger H, Schifferdecker E, Schatz H. (1994) [Regression of hard exudates in diabetic background retinopathy in therapy with etofibrate antilipemic agent]. Med Klin Munich, 89: 594–7, 633.

155. Gordon B, Chang S, Kavanagh M, Berrocal M, Yannuzzi L, Robertson C, Drexler A. (1991) The effects of lipid lowering on diabetic retinopathy. Am J Ophthalmol, 112: 385–91.

156. Keech AC, Mitchell P, Summanen PA, O'Day J, Davis TM, Moffitt MS, Taskinen MR, Simes RJ, Tse D, Williamson E, Merrifield A, Laatikainen LT, d'Emden MC, Crimet DC, O'Connell RL, Colman PG. (2007) Effect of fenofibrate on the need for laser treatment for diabetic retinopathy (FIELD study): a randomised controlled trial. Lancet, 370: 1687–97.

12 List of Publications

12.1 List of Publications related to the topic of the dissertation

1. Kriechbaum K, Bolz M, **Deak GG**, Prager S, Scholda C, Schmidt-Erfurth U. (2010) High-Resolution Imaging of the Human Retina In Vivo after Scatter Photocoagulation Treatment Using a Semiautomated Laser System. Ophthalmology, 117: 545–551. **IF: 5,017**

2. Bolz M, Kriechbaum K, Simader C, **Deak G**, Lammer J, Treu C, Scholda C, Prünte C, Schmidt-Erfurth U. (2010) In Vivo Retinal Morphology after Grid Laser Treatment in Diabetic Macular Edema. Ophthalmology, 117: 538–544. **IF: 5,017**

3. **Deák GG**, Bolz M, Prager S, Ritter M, Kriechbaum K, Scholda C, Schmidt-Erfurth U. (2012) Photoreceptor Layer Regeneration is Detectable in the Human Retina Imaged by SD-OCT after Laser Treatment Using Subthreshold Laser Power. Invest. Ophthalmol. Vis. Sci., 53: 7019–7025. **IF: 3,441**

4. **Deák GG**, Bolz M, Kriechbaum K, Prager S, Mylonas G, Scholda C, Schmidt-Erfurth U. (2010) Effect of Retinal Photocoagulation on Intraretinal Lipid Exudates in Diabetic Macular Edema Documented by Optical Coherence Tomography. Ophthalmology, 117: 773–779. **IF: 5,017**

12.2 List of Publications not related to the topic of the dissertation

Deák GG, Lammer J, Prager S, Mylonas G, Bolz M, Schmidt-Erfurth U. (2014) Refractive Changes after Pharmacologic Resolution of Diabetic Macular Edema. Ophthalmology, 121: 1054–1058. **IF: 6,135**

Deák GG, Schmidt WM, Bittner RE, Mylonas G, Roberts PK, Zotter S, Baumann B, Pircher M, Hitzenberger CK, Schmidt-erfurth UM, Ritter M. (2019) Imaging Of Vitelliform Macular Lesions Using Polarization-sensitive Optical Coherence Tomography. Retina, 39: 558–569. **IF: 4,013**

Deák GG, Goldstein DA, Zhou M, Fawzi AA, Jampol LM. (2019) Vertical Hyperreflective Lesions on Optical Coherence Tomography in Vitreoretinal Lymphoma. JAMA Ophthalmol, 137: 194–198. **IF: 6,669**

Deák GG, Schmidt-Erfurth UM, Jampol LM. (2018) Correlation of Central Retinal Thickness and Visual Acuity in Diabetic Macular Edema. JAMA Ophthalmol, 136: 1215–1216.

Deák GG, Bolz M, Ritter M, Prager S, Benesch T, Schmidt-Erfurth U. (2010) A Systematic Correlation between Morphology and Functional Alterations in Diabetic Macular Edema. Invest. Ophthalmol. Vis. Sci., 51: 6710–6714. **IF: 3,466**

Deák GG, Schmidt-Erfurth U. (2013) Imaging of the Parafoveal Capillary Network in Diabetes. Curr Diab Rep, 13: 469–475.

Deák G, Pulido J, Jampol L. (2019) Segmental Diffuse Vascular Leakage. Retinal Cases & Brief Reports, Publish Ahead of Print. Available at: insights.ovid.com [Accessed April 28, 2019].

Deák G, Sneed S, Jampol L. (2018) Cystoid Macular Edema In The Setting Of Primary Vitreoretinal Lymphoma. Retinal Cases & Brief Reports, Publish Ahead of Print. Available at: insights.ovid.com [Accessed February 24, 2019].

Bolz M, Lammer J, **Deak G**, Pollreisz A, Mitsch C, Scholda C, Kundi M, Schmidt-Erfurth U, Vienna for the DRRG. (2014) SAVE: a grading protocol for clinically significant diabetic macular oedema based on optical coherence tomography and fluorescein angiography. British Journal of Ophthalmology, 98: 1612–1617. **IF: 2,976**

Bolz M, Schmidt-Erfurth U, **Deak G**, Mylonas G, Kriechbaum K, Scholda C. (2009) Optical Coherence Tomographic Hyperreflective Foci: A Morphologic Sign of Lipid Extravasation in Diabetic Macular Edema. Ophthalmology, 116: 914–920. **IF: 7,755**

Delcourt C, Korobelnik J-F, Buitendijk GHS, Foster PJ, Hammond CJ, Piermarocchi S, Peto T, Jansonius N, Mirshahi A, Hogg RE, Bretillon L, Topouzis F, **Deak G**, Grauslund J, Broe R, Souied EH, Creuzot-Garcher C, Sahel J, Daien V, Lehtimäki T, Hense H-W, Prokofyeva E, Oexle K, Rahi JS, Cumberland PM, Schmitz-Valckenberg S, Fauser S, Bertelsen G, Hoyng C, et al. (2016) Ophthalmic epidemiology in Europe: the "European Eye Epidemiology" (E3) consortium. Eur J Epidemiol, 31: 197–210. **IF: 6,529**

Gattoussi S, Buitendijk GHS, Peto T, Leung I, Schmitz-Valckenberg S, Oishi A, Wolf S, **Deák G**, Delcourt C, Klaver CCW, Korobelnik J-F. The European Eye Epidemiology spectral-domain optical coherence tomography classification of macular diseases for epidemiological studies. Acta Ophthalmologica, 0. Available at: https://onlinelibrary.wiley.com/doi/abs/10.1111/aos.13883 [Accessed April 28, 2019]. **IF: 3,324**

Gerendas BS, Hecht A, Kundi M, Waldstein SM, **Deak G**, Simader C, Montuoro A, Schmidt-Erfurth U, Funk M. (2016) Choroidal Line Scan Measurements in Swept-Source Optical Coherence Tomography as Surrogates for Volumetric Thickness Assessment. American Journal of Ophthalmology, 162: 150-158.e1. **IF: 5,052**

Gerendas BS, Prager S, **Deak G**, Simader C, Lammer J, Waldstein SM, Guerin T, Kundi M, Schmidt-Erfurth UM. (2017) Predictive imaging biomarkers relevant for functional and anatomical outcomes during ranibizumab therapy of diabetic macular oedema. British Journal of Ophthalmology,: bjophthalmol-2017-310483. **IF: 3,384**

Gerendas BS, Waldstein SM, Simader C, **Deak G**, Hajnajeeb B, Zhang L, Bogunovic H, Abramoff MD, Kundi M, Sonka M, Schmidt-Erfurth U. (2014) Three-Dimensional Automated Choroidal Volume Assessment on Standard Spectral-Domain Optical Coherence Tomography and Correlation With the Level of Diabetic Macular Edema. American Journal of Ophthalmology, 158: 1039-1048.e1. **IF: 3,871**

Karst SG, **Deak GG**, Gerendas BS, Waldstein SM, Lammer J, Simader C, Guerin T, Schmidt-Erfurth UM. (2018) Association of Changes in Macular Perfusion With Ranibizumab Treatment for Diabetic Macular Edema: A Subanalysis of the RESTORE (Extension) Study. JAMA Ophthalmol,. Available at: https://jamanetwork.com/journals/jamaophthalmology/fullarticle/2673569 [Accessed March 28, 2018]. **IF: 6,669**

Malamos P, Ahlers C, Mylonas G, Schütze C, **Deak G**, Ritter M, Sacu S, Schmidt-erfurth U. (2011) Evaluation Of Segmentation Procedures Using Spectral Domain Optical Coherence Tomography In Exudative Age-related Macular Degeneration. Retina, 31: 453–463. **IF:2,812**

Mylonas G, Ahlers C, Malamos P, Golbaz I, **Deak G**, Schuetze C, Sacu S, Schmidt-Erfurth U. (2009) Comparison of retinal thickness measurements and segmentation performance of four different spectral and time domain OCT devices in neovascular age-related macular degeneration. British Journal of Ophthalmology, 93: 1453–1460. **IF:2,917**

Mylonas G, Bolz M, Kriechbaum K, Treu C, **Deak G**, Lammer J, Scholda C, Schmidt-erfurth U. (2013) Retinal Architecture Recovery After Grid Photocoagulation In Diabetic Macular Edema Observed In Vivo By Spectral Domain Optical Coherence Tomography. Retina, 33: 717–725. **IF: 3,177**

Mylonas G, Prager F, Wetzel B, Malamos P, **Deak G**, Amon M. (2017) Anti-vascular endothelial growth factor for unilateral acute idiopathic maculopathy. Eur J Ophthalmol,: 0.

Mylonas G, Sacu S, **Deák G**, Dunavoelgyi R, Buehl W, Georgopoulos M, Schmidt-Erfurth U. (2013) Macular Edema Following Cataract Surgery in Eyes With Previous 23-Gauge Vitrectomy and Peeling of the Internal Limiting Membrane. American Journal of Ophthalmology, 155: 253-259.e2. **IF:4,021**

Najeeb BH, Simader C, **Deak G**, Vass C, Gamper J, Montuoro A, Gerendas BS, Schmidt-Erfurth U. (2017) The Distribution of Leakage on Fluorescein Angiography in Diabetic

Macular Edema: A New Approach to Its Etiology. Invest. Ophthalmol. Vis. Sci., 58: 3986–3990. **IF: 3,388**

Pemp B, **Deák G**, Prager S, Mitsch C, Lammer J, Schmidinger G, Scholda C, Schmidt-erfurth U, Bolz M. (2014) Distribution Of Intraretinal Exudates In Diabetic Macular Edema During Anti-vascular Endothelial Growth Factor Therapy Observed By Spectral Domain Optical Coherence Tomography And Fundus Photography. Retina, 34: 2407–2415. **IF: 3,243**

Resch H, **Deak G**, Pereira I, Vass C. (2012) Comparison of optic disc parameters using spectral domain cirrus high-definition optical coherence tomography and confocal scanning laser ophthalmoscopy in normal eyes. Acta Ophthalmologica, 90: e225–e229. **IF: 2,345**

Resch H, **Deak G**, Vass C. (2010) Influence of optic-disc size on parameters of retinal nerve fibre analysis as measured using GDx VCC and ECC in healthy subjects. British Journal of Ophthalmology, 94: 424–427. **IF:2,934**

Resch, MD., Balogh A, **Deák GG**, Nagy ZZ, Papp A. (2020). Vascular Density in Age-Related Macular Degeneration after One Year of AntiVEGF Treatment with Treat-and-Extend and Fixed Regimens. PloS One 15 (2): e0229388.

Ritter M, Bolz M, Sacu S, **Deák GG**, Kiss C, Pruente C, Schmidt-Erfurth UM. (2009) Effect of intravitreal ranibizumab in avascular pigment epithelial detachment. Eye, 24: eye2009265. **IF:1,974**

Ritter M, Elledge J, Simader C, **Deak GG**, Benesch T, Blodi BA, Schmidt-Erfurth UM. (2011) Evaluation of optical coherence tomography findings in age-related macular degeneration: a reproducibility study of two independent reading centres. British Journal of Ophthalmology, 95: 381–385. **IF: 2,902**

Ritter M, Sacu S, **Deák GG**, Kircher K, Sayegh RG, Pruente C, Schmidt-Erfurth UM. (2012) In vivo identification of alteration of inner neurosensory layers in branch retinal artery occlusion. British Journal of Ophthalmology, 96: 201–207. **IF: 2,425**

Ritter M, Simader C, Bolz M, **Deák GG**, Mayr-Sponer U, Sayegh R, Kundi M, Schmidt-Erfurth UM. (2014) Intraretinal cysts are the most relevant prognostic biomarker in neovascular age-related macular degeneration independent of the therapeutic strategy. British Journal of Ophthalmology, 98: 1629–1635. **IF: 2,976**

Ritter M, Zotter S, Schmidt WM, Bittner RE, **Deak GG**, Pircher M, Sacu S, Hitzenberger CK, Schmidt-Erfurth UM. (2013) Characterization of Stargardt Disease Using Polarization-Sensitive Optical Coherence Tomography and Fundus Autofluorescence Imaging. Invest. Ophthalmol. Vis. Sci., 54: 6416–6425. **IF:3,661**

Roberts P, Sugita M, **Deák G**, Baumann B, Zotter S, Pircher M, Sacu S, Hitzenberger CK, Schmidt-Erfurth U. (2016) Automated Identification and Quantification of Subretinal Fibrosis in Neovascular Age-Related Macular Degeneration Using Polarization-Sensitive OCT. Invest. Ophthalmol. Vis. Sci., 57: 1699–1705.

IF: 3,303

Schmidt-Erfurth U, Waldstein SM, **Deak G-G**, Kundi M, Simader C. (2015) Pigment Epithelial Detachment Followed by Retinal Cystoid Degeneration Leads to Vision Loss in Treatment of Neovascular Age-Related Macular Degeneration. Ophthalmology, 122: 822–832. **IF: 6,750**

Simader C, Ritter M, Bolz M, **Deák GG**, Mayr-Sponer U, Golbaz I, Kundi M, Schmidt-Erfurth UM. (2014) Morphologic Parameters Relevant for Visual Outcome During Anti-Angiogenic Therapy of Neovascular Age-Related Macular Degeneration. Ophthalmology, 121: 1237–1245. **IF: 6,135**

Sulzbacher F, Kiss C, Munk M, **Deak G**, Sacu S, Schmidt-Erfurth U. (2011) Diagnostic Evaluation of Type 2 (Classic) Choroidal Neovascularization: Optical Coherence Tomography, Indocyanine Green Angiography, and Fluorescein Angiography. American Journal of Ophthalmology, 152: 799-806.e1. **IF: 4,223**

13 Acknowledgement

Elsősorban köszönettel tartozom szüleimnek, akik mindig mindenben támogattak, és minden lehetőséget megteremtettek, hogy fejlődhessek mind a privát mind a szakmai életben. Különös köszönettel tartozom édesapámnak Dr. Deák Györgynek, akihez mindig fordulhattam szakmai tanácsért, és akinek munkássága, és a szakmánk iránt tanúsított szeretete és alázata mindig iránymutatásként szolgált számomra.

Szintén nagy köszönettel tartozom feleségemnek Dr. Róna Zsófiának, aki megmutatta hogyan lehet nagy lelkesedéssel és szorgalommal egy PhD fokozatszerzéshez hozzáfogni, és gyermekeimnek, Lilinek és Daninak, akik nagy türelemmel voltak irántam, és elnézték nekem, hogy nem tudtam annyit velük foglalkozni az utóbbi időben mint amennyit megérdemeltek volna.

I can't thank myself enough to Professor Ursula Schmidt-Erfurth the chair of the Department of Ophthalmology at the Medical University of Vienna for her continuous support and guidance both clinical and academic throughout the last thirteen years.

I would like to thank my former research group (Diabetic Retinopathy Research Group Vienna) and my co-authors, Prof. Matthias Bolz, Assoc. Prof. Katharina Kriechbaum, aoUniv. Prof Christoph Scholda, Dr. Sonja Karst (Prager), Assoc. Prof. Markus Ritter and Dr. Jan Lammer for their help and inspiration in performing the research that serves as basis for this thesis.

Szeretnék köszönetet mondani Süveges Ildikó professzorasszonynak a sok segítségért és tanításért, amit karrierem kezdetén rezidensként illetve később mind PhD hallgató kaptam.

Szintén szeretnék köszönetet mondani Németh János és Nagy Zoltán Zsolt professzoroknak, akiktől szintén sokat tanulhattam rezidens éveim alatt, illetve akik intézetvezetőként megteremtették a lehetőségét, hogy PhD fokozatot szerezhessek.

Külön szeretnék köszönetet mondani Dr. Resch Miklós egyetemi docens Úrnak amiért elvállalta a PhD-m témavezetői feladatát, és a rengeteg segítségért és jó tanácsért amit kaptam tőle.